M.Sc. Thesis

An alternative method for estimating the porosity and the permeability of (potential) geothermal reservoirs using magnetotelluric data;

A case study of the Sherwood Sandstone Group in the Lough Neagh Basin, Northern Ireland

Author:
Merijn de Block

Supervision by:
dr. C.J. Peach, Utrecht University, the Netherlands
dr. M. Muller, Dublin Institute for Advanced Studies, Ireland
W. van Leeuwen, IF Technology, the Netherlands

March 5, 2013

Department of Earth Sciences
Utrecht University
Utrecht, The Netherlands

School of Cosmic Physics
Dublin Institute for Advanced Studies
Dublin, Ireland

IF Technology BV
Arnhem, The Netherlands

Abstract

Since traditional methods for estimating the hydraulic properties of reservoir rocks, such as laboratory analysis of core samples and pumping tests, are time-consuming, invasive and expensive, a method for the reliable estimation of reservoir rock properties from surface measurements would be beneficial. In this thesis an alternative method is introduced for the estimation of the porosity and the permeability of a (potential) geothermal reservoir. In this method, the electrical resistivity of the reservoir rock is determined based on magnetotelluric (MT) data. Then, petrophysical relations (i.e. Archie's first law and the RGPZ model) are used in to derive values for the porosity and the permeability from the resistivity values predicted by the MT models. A case study is carried out of the Sherwood Sandstone Group in the Lough Neagh Basin, Northern Ireland, utilizing this alternative approach. For this purpose, wireline logging data and core sample data from three boreholes are utilized in conjunction with MT data from five sites located close to the boreholes. The results are used to advance the assessment of the geothermal energy potential of the Sherwood Sandstone Group.

The wireline logging data are evaluated and modeled using Interactive Petrophysics software and a porosity-permeability relationship is derived from core sample measurements. The results are used to determine average values for the resistivity, porosity and permeability of the upper part of the Sherwood Sandstone Group. The MT data are analyzed and processed, before being used for extensive 1D resistivity modeling. For this, three different inversion codes are used: Occam, the WinGLink sharp boundary code and Minim. The Minim models are used to determine the resistivity of the upper part of the Sherwood Sandstone Group. From the resistivity values the porosity and permeability are derived using Archie's first law and the RGPZ model respectively. The values of the parameters of Archie's first law and the RGPZ model are defined based on wireline logging data and core sample data from the boreholes.

Comparing the results of the MT and petrophysical modeling, it is concluded that accurate estimates of the porosity and the permeability can be obtained using the method introduced here, provided that the resistivity determined based on the MT models does not deviate from the actual average resistivity of the target formation by more than 1 Ωm. Additional geological data are essential for calibration of Archie's first law and the RGPZ model. Therefore, this method is best utilized in combination with additional geological data from a reference site, allowing calibration of the petrophysical models. After calibration the petrophysical models can be applied to the entire MT survey area.

From the borehole data analysis porosity and permeability values for the upper part of the Sherwood Sandstone Group are obtained, with the porosity varying between 18 and 21 % and the permeability varying between 83 and 723 mD. These values indicate a good to excellent quality of the Sherwood Sandstone Group as a geothermal reservoir. Future work on the geothermal energy exploration of the Sherwood Sandstone Group in the Lough Neagh Basin should focus on identifying the areas in the basin with the highest geothermal potential.

Assertion

I herewith ensure that this thesis has been written self-dependently. Only the mentioned references were used.

Merijn de Block

Utrecht, March 5, 2013

Acknowledgements

I would like to thank my supervisors: Dr. Colin Peach for giving me the opportunity to realize this M.Sc. thesis outside of the university; Wouter van Leeuwen for supervising my work at IF Technology and for his guidance and advice; and Dr. Mark Muller for supervising my work at DIAS, his invaluable support and guidance and his constructive and thorough comments on the first version of this thesis.

Furthermore, I am grateful to Guus Willemsen for giving me the opportunity to conduct my research during an internship at IF Technology, and of course the people at IF Technology who have been very supporting and created a great working environment.

I would also like to thank Prof. Alan Jones for making it possible to conduct part of the research at DIAS in Dublin. Many thanks to all the people at 5 Merrion Square, whose support and hospitality made my stay in Dublin a great experience.

Thanks to Peter Betts who thoroughly evaluated my work in IP, and to Martin van Drongelen for his help with Matlab. Last but not least, I would like to thank my family and friends for their support, and of course my parents for making this all possible.

Contents

List of Figures

List of Tables

1 Introduction

1.1 Background

In today's search for increasing energy sustainability and greater independence from fossil fuels, geothermal energy is gaining more recognition as a technically and economically viable renewable energy source. Geothermal energy, in the form of natural steam or hot water, can be exploited for different applications and currently is used in more than 50 countries worldwide for different purposes, including electricity generation, heat pumps, space-heating, greenhouse heating and industrial processes (Lund & Freeston 2000, Barbier 2002). Commonly, geothermal resources are classified according to their energy content and in modern literature a distinction often is made between low-enthalpy (temperatures lower than 150 °C) and high-enthalpy (temperatures higher than 150 °C) resources. Low-enthalpy resources have traditionally been viewed as less favorable for electricity generation and instead are often used for space-heating and greenhouse heating. However, due to improving drilling methods and the development of binary power plants, electricity can now be generated from low-enthalpy recourses with reservoir temperatures as low as 73 °C (Erkan et al. 2008).

In Ireland the usage of geothermal energy is mainly restricted to exploration of shallow geothermal resources (< 100 m), consisting of ground source heat exchangers in private homes and a number of larger units operating in office blocks, university buildings, etc. (Goodman et al. 2004). Currently, the IRETHERM project is being undertaken, in which the geothermal energy potential of deeper geothermal resources (> 1000 m) in Ireland is assessed. For this purpose a comprehensive program of electromagnetic field surveys is combined with 3D modeling of Ireland's crustal heat production, in order to identify the geological settings and localities with the highest potential for geothermal energy provision. One of the geothermal targets of the IRETHERM project is the Sherwood Sandstone Group in the Lough Neagh Basin, which is a sedimentary basin located in Northern Ireland. The infill of the basin consists mainly of Permian and Triassic clastic rocks, including the Sherwood Sandstone Group. In a previous study temperatures were modeled for the Lough Neagh Basin, resulting in temperatures between 40 °C and 85 °C for the depth range between 1000 m and 2500 m, which corresponds to a geothermal gradient of approximately 30 °C/km (Pasquali et al. 2010). In another study the electrical conductivity structure of the basin was analyzed, showing that the Sherwood Sandstone Group is the main conductive feature (Loewer

2011). Also, the total energy stored in the Sherwood Sandstone Group was estimated (Pasquali et al. 2010). It was concluded that the Sherwood Sandstone Group forms a low-enthalpy geothermal resource with a high potential for geothermal energy exploitation (Pasquali et al. 2010, Loewer 2011). However, this potential only exists in the case of adequate hydraulic properties of the reservoir. Therefore, the next step in assessing the geothermal potential of the Sherwood Sandstone Group in the Lough Neagh Basin is to determine the hydraulic properties.

Successful geothermal energy exploitation depends on the availability of a suitable reservoir, a sufficient temperature associated with the reservoir and adequate hydraulic properties of the reservoir rocks. Reservoir characterization, therefore, is a critical part of geothermal energy exploration. In reservoir characterization, porosity and permeability are essential parameters as they are two of the most important hydraulic properties involved in the storage and movement of fluids in rocks and sediments. The hydraulic properties of reservoir rocks and aquifers can be accurately measured through laboratory analysis of core samples. Other commonly applied methods for measuring these properties include pumping tests and slug tests. However, these approaches are time-consuming, invasive and expensive. Therefore, extensive research has been done on developing alternative methods for estimating the hydraulic properties of rocks. It was recognized that relating the hydraulic properties to the electrical conductivity of the rock can be highly effective, since the hydraulic conductivity and the electrical conductivity of rocks mainly depend on the same parameters (e.g. porosity, permeability, tortuosity, pore geometry). The electrical conductivity of reservoir rocks and aquifers can be measured in boreholes using wireline logging tools or at the surface using geophysical survey methods. A more detailed overview of the research on relating hydraulic properties to the electrical conductivity can be found in many publications, e.g. Niwas & Singhal (1985), Friedman (2005), Lesmes & Friedman (2005).

A method for reliably estimating hydraulic properties from surface electrical conductivity measurements would be beneficial. Through time many researchers have developed methods for this purpose, e.g. Niwas & Singhal (1985), Soupios et al. (2007), Chandra et al. (2008). In these studies it was recognized that combining surface measurements with borehole data or pumping test data can be very useful. This way correlations can be established at a reference point between the electrical conductivity and the hydraulic properties of the rocks. Using these correlations the hydraulic properties of the reservoir rocks or the aquifer can be estimated from surface measurements for the entire investigation area (Niwas & Sing-

hal 1985, Soupios et al. 2007). However, most of these studies utilized controlled source electromagnetic imaging methods, which have a limited depth range. Although it is not impossible for controlled source electromagnetic surveys to penetrate deeper than 1 km, this would require, for example, very large transmitter loops (in the case of time domain electromagnetic (TDEM) methods) or very large dipole lengths, transmitter power and source-transmitter distances (in the case of controlled source audio-frequency magnetotellurics (CSAMT)). The only electromagnetic imaging method that easily reaches depths of penetration greater than 1 km is magnetotellurics (MT), provided the cultural noise levels are not high. MT is a passive electromagnetic geophysical survey technique that can be used for imaging the conductivity structure of the subsurface by measuring the Earth's electric and magnetic fields at the surface. The MT method is commonly used in geothermal exploration, as it is a very useful tool for imaging and determining the depths, geometry and geological characteristics of electrically conductive features that are typically associated with geothermal resources. However, MT is not frequently used for investigating the hydraulic properties of reservoir rocks and/or aquifers. An exception is a study performed by Unsworth et al. (2005), who combined MT data with Archie's first law in order to determine porosity values for an aquifer system.

It should be noted that it is impossible to determine exactly the hydraulic properties of rocks from surface electrical conductivity measurements. This is due to the many, extremely variable, rock properties involved in the hydraulic and electrical conductivity and the inverse problems inherent in deriving the electrical conductivity from surface measurements (Niwas & de Lima 2003, Soupios et al. 2007). Nevertheless, keeping this in mind reliable estimates of the hydraulic properties can be obtained using these methods. The fact that the hydraulic properties of rocks can be more accurately measured using other methods (e.g. analysis of core samples and pumping tests) is adequately compensated by the advantages of surface measurements (i.e. the low costs, the noninvasive nature and the time-saving) combined with the amount or spatial extent of information obtained by applying this method.

1.2 Research outline and objectives

In this thesis an alternative method or approach is introduced for estimating the porosity and the permeability of (potential) geothermal reservoirs. In this method, processing and modeling of MT data is used to determine the electrical resistivity of the reservoir rocks. Then, petrophysical relations (i.e. Archie's first

law and the RGPZ model) are used in order to derive values for the porosity and the permeability from the resistivity values determined by the MT models. In this study, this approach is applied to a case study of the Sherwood Sandstone Group in the Lough Neagh Basin, Northern Ireland. For this purpose, MT data from five sites are utilized in conjunction with wireline logging data and core sample data of three boreholes located in the Lough Neagh Basin. The main objective of this research is to introduce and verify an alternative method for estimating the porosity and the permeability based on MT measurements. As a secondary objective, the results are used to advance the assessment of the geothermal energy potential of the Sherwood Sandstone Group. For the sake of clarity the research is subdivided into three different parts:

- **Part 1) Borehole data analysis.** In the first part, wireline logging data and core sample data from the three boreholes are evaluated using Interactive Petrophysics software in order to determine average values for the electrical resistivity, porosity and permeability of the upper part of the Sherwood Sandstone Group.
- **Part 2) Processing and modeling of MT data.** In the second part, MT data from five sites located close to one of the three boreholes are processed and used for extensive 1D modeling in order to determine the electrical resistivity of the Sherwood Sandstone Group.
- **Part 3) Petrophysical modeling.** In the last part of the research, Archie's first law and the RGPZ model are calibrated using wireline logging data and core sample data and used to derive values for the porosity and the permeability of the Sherwood Sandstone Group from the resistivity values determined in the MT models.

For all resistivity, porosity and permeability values determined in this research the associated uncertainty ranges are calculated, in order to assess the confidence in the results and the reliability of the applied methods. Finally, a comparison is made between the results of the MT and petrophysical modeling and the results the borehole data analysis. Note that the available core sample data only comprises the upper part of the Sherwood Sandstone Group (or the Toomebridge Sandstone Formation). Additionally, preliminary studies show that the upper part of the Sherwood Sandstone Group is more favorable for geothermal exploitation than the lower part, which is compositionally different (Naylor et al. 2003). Therefore, in this research the focus lies on the upper part of the Sherwood Sandstone Group. To ensure that the effects of

lateral variation in the basin are minimized, MT data are only used from sites that are located close to one of the three boreholes.

1.3 Thesis outline

The first part of this thesis contains the theory and background information necessary for this research. It is subdivided into three different chapters: the first chapter is concerned with the MT method, the second chapter with the petrophysical relations between resistivity, porosity and permeability and the third chapter introduces the geological and geothermal aspects of the Lough Neagh Basin relevant to this study.

The second part of this thesis contains the methods and results of the three different parts of the research as outlined above. At the end a summary of the results is given and the results of the different parts of the research are compared with each other.

In the third part of the thesis the quality of the data, the effectiveness and limitations of the applied methods and the results are discussed. Furthermore, the results are used in order to verify the method for porosity and permeability estimation introduced in this thesis and to continue the assessment of the geothermal energy potential of the Sherwood Sandstone Group. Finally, the research is summarized and an overview of the main conclusions is given.

PART 1

THEORY AND BACKGROUND INFORMATION

2 The magnetotelluric method

In this chapter the magnetotelluric method is introduced by first explaining the theory underlying magnetotellurics and secondly discussing the different steps involved in producing models from magnetotelluric measurements (i.e. the processing, analysis and modeling of magnetotelluric data). Also, all magnetotelluric related concepts, methods and models used in this study are introduced.

Magnetotellurics (MT) is a passive electromagnetic geophysical survey technique that can be used for imaging the Earth's subsurface, by measuring the time-varying components of the electric and magnetic fields at the Earth's surface over a broad range of frequencies. It is passive in the sense that it utilizes naturally occurring electromagnetic (EM) fields generated by different inductive sources which penetrate the Earth, a process that is controlled by the Earth's conductivity structure and the frequency of the EM fields. As the EM fields penetrate the Earth, the conductivity structure and heterogeneities in the subsurface produce an electromagnetic response, distorting the EM fields. By simultaneously measuring the time-varying components of the electric field and magnetic field at the Earth's surface, complex ratios (impedances) can be derived, which describe the penetration of the EM fields into the Earth and from which the conductivity structure of the Earth can be determined. During penetration into the Earth the electromagnetic waves are attenuated. This attenuation depends on the frequency of the waves, as longer period fluctuations are attenuated more slowly and therefore penetrate deeper into the Earth. This is an important property used in MT, since it means that by increasing the sounding period of an MT sounding the penetration depth of the measured EM fields increases.

2.1 History and development

The development of the MT method started in the 1950's, when Tikhonov (1950) and Cagniard (1953) designed MT sounding as a method for studying the vertical variations in the electrical conductivity of the Earth. In their initial studies they did not go beyond the 1D model, but soon it became apparent that horizontal conductive inhomogeneities in the Earth could significantly distort the results of an MT sounding. Therefore, a theory was needed to consider the electric and magnetic fields within a horizontal inhomogeneous Earth, capable of studying the conductivity variations in the Earth in two and three dimensions. The first papers concerning imaging the conductivity structures of the Earth in 2D and 3D were pub-

lished in the 1960's and since then considerable progress has been made in the 2D and 3D interpretation of MT sounding data, helped by rapid advances in the fields of mathematics and increasing computing power. Nowadays, magnetotelluric models can deal with 1D), 2D and 3D structures and heterogeneities, as well as combinations of 1D, 2D and/or 3D structures. Multiple forward modeling and inversion codes are available for 1D and 2D cases. For 3D cases, however, inversion is computationally very demanding and the number of available inversion codes is limited.

2.2 Inductive sources of MT fields

While the magnetic field of the Earth is generated by processes in the Earth's outer core, MT seeks to exploit the superimposed electromagnetic fields (or magnetotelluric fields or MT fields) that induce large-scale, naturally occurring electric currents in the conductive Earth, also known as telluric currents. There are multiple inductive sources that contribute to these MT fields and as a result the MT fields occur in a broad range of frequencies (Simpson & Bahr 2005).

MT fields with frequencies lower than 1 Hz have their origin in interactions of the solar wind with the Earth's magnetic field and the ionosphere. The solar wind consists of a continuous stream of charged particles (mainly protons and electrons) and as it reaches the Earth it reacts with the Earth's magnetic field and the ionosphere. During this interaction, protons and electrons are deflected in opposite directions by the magnetosphere, establishing an electric field, while simultaneously large-scale electric currents are created in the ionosphere. These electric currents produce electromagnetic fields which penetrate the Earth (MT fields) and in turn induce telluric currents in the Earth. The telluric currents flow within the Earth in large circular patterns that stay fixed with respect to the sun and normally flow in sheets parallel to the surface (Telford et al. 1990, Kearey et al. 2002). Variations in the density, velocity and intensity of the solar wind cause oscillations of the magnetosphere and therefore variations in the MT fields. These variations are complexly modified by inductive and magnetohydrodynamic interactions between the magnetosphere and the ionosphere. The largest fluctuations are caused by solar storms (Simpson & Bahr 2005).

MT fields with frequencies higher than 1 Hz are due to meteorological activity such as lightning discharges, especially the large and numerous events from the highly disturbed equatorial regions. The signals discharged by lightning are known as "sferics" or "spherics" and consist of MT fields propagating

around the world within the waveguide bounded by the ionosphere and the Earth's surface, while inducing telluric currents in the Earth (Simpson & Bahr 2005, Telford et al. 1990).

Due to amplitude attenuation, around 1 Hz the natural EM variations of the MT fields are of low intensity compared to other frequencies and therefore the quality of the MT data is often reduced in the frequency range from approximately 0.5 - 5 Hz. This frequency range is therefore called the dead-band (Simpson & Bahr 2005).

2.3 Assumptions and fundamental equations

2.3.1 Assumptions

As MT considers electromagnetic induction in the Earth, a number of assumptions have been made in order to simplify the interpretation and modeling of MT data. These assumptions are (modified after Simpson & Bahr (2005)):

1. Maxwell's general electromagnetic equations are obeyed.
2. The Earth does not generate electromagnetic energy, but only dissipates or absorbs it.
3. All electromagnetic fields may be treated as conservative and analytic away from their sources.
4. The natural electromagnetic fields exploited by the MT method are generated by large-scale, uniform, horizontal sheets of current in the ionosphere and thus can be treated as monochromatic electromagnetic plane waves normally incident on the surface of the Earth (also referred to as the plane wave assumption).
5. Within a 1D layered Earth no accumulation of free charges is expected to be sustained. In a multi-dimensional Earth, charges can accumulate along conductivity discontinuities.
6. Charge is conserved, obeying the equation: $\mathbf{j} = \sigma\mathbf{E}$, in which $\mathbf{j}$ is the total electric current density (in Am^{-2}), σ is the conductivity of the sounding medium (in Sm^{-1}) and $\mathbf{E}$ is the electric field (in Vm^{-1}).
7. Time-varying displacement currents are negligible compared to the time-varying conduction currents. Therefore, the electromagnetic induction in the Earth can be treated as a pure diffusion process.

8. Variations in the electrical permittivity and magnetic permeability of rocks are negligible compared with variations in the bulk rock conductivity.

Due to the plane wave assumption (assumption 4) time invariance of the exciting source is implied. As a consequence the impedance tensor (section 2.4) should be constant regardless of when the measurements were made. The plane wave assumption however does not hold in equatorial and auroral zones (Simpson & Bahr 2005, Berdichevsky & Dmitriev 2008).

2.3.2 Maxwell's equations

Maxwell's general electromagnetic equations (assumption 1) are a set of partial differential equations that describe the relationships between electric and magnetic fields and electric charges and currents and can be used to describe the behavior of electromagnetic fields at any frequency. For a polarizable, magnetizable medium containing no electric and magnetic sources Maxwell's equations are given by (Simpson & Bahr 2005):

- Faraday's law: The induced electromotive force in a closed circuit is equal to the time rate of change of the magnetic flux through the circuit (i.e. time variations in a magnetic field that passes through a closed circuit induce corresponding fluctuations in the electric field within the closed circuit with its axis oriented in the direction of the inducing field):

$$\nabla \times \mathbf{E} = -\frac{\partial \mathbf{B}}{\partial t}. \tag{1}$$

- Ampère's law: Any closed loop of electrical current has an associated magnetic field and has a magnitude proportional to the total current flow. The magnetic field along the edges of a surface is equal to the sum of the electric currents and the time variations of the current displacement through the surface:

$$\nabla \times \mathbf{H} = \mathbf{j} - \frac{\partial \mathbf{D}}{\partial t}. \tag{2}$$

- Gauss's law: The magnetic field is source free and there are no free magnetic charges (i.e. no magnetic monopoles exist):

$$\nabla \times \mathbf{B} = 0. \tag{3}$$

- Gauss's law for the electric field: The electric field is a field with the charge density as its source. The electric flux through a closed surface of a volume is proportional to the electric charge enclosed by the volume:

$$\nabla \times \mathbf{D} = \rho. \tag{4}$$

In these equations **B** is magnetic induction (in T), **H** is the magnetic intensity (in Am^{-1}), **D** is electric displacement (in Cm^{-2}), ρ is the electric charge density (in Cm^{-3}) and t is time (in s).

For a linear, isotropic medium it has been showed that the following equations hold (Simpson & Bahr 2005):

$$\mathbf{B} = \mu\mathbf{H}, \tag{5}$$

$$\mathbf{D} = \varepsilon\mathbf{E}, \tag{6}$$

in which μ is the magnetic permeability and ε the electrical permittivity. Based on assumption 8., free-space values are assumed ($\mu = 1.2566 \times 10^{-6}$ Hm^{-1} and $\varepsilon = 8.85 \times 10^{-12}$ Fm^{-1}). Taking into account that time-varying displacement currents are negligible ($\frac{\partial \mathbf{D}}{\partial t} = 0$, assumption 7.) and that charge is conserved ($\mathbf{j} = \sigma\mathbf{E}$, assumption 6.), Maxwell's equations can be rewritten as:

$$\nabla \times \mathbf{E} = -\frac{\partial \mathbf{B}}{\partial t}, \tag{7}$$

$$\nabla \times \mathbf{B} = \mu\sigma\mathbf{E}, \tag{8}$$

$$\nabla \cdot \mathbf{B} = 0, \tag{9}$$

$$\nabla \cdot \mathbf{E} = \frac{\rho}{\varepsilon}. \tag{10}$$

2.3.3 Diffusion equations

Assuming a plane wave with a harmonic time dependence of the form $e^{-i\omega t}$ (in which $\omega = \pi f$, the angular frequency in Hz), equation 7 can be rewritten as:

$$\nabla \times \mathbf{E} = -\frac{\partial \mathbf{B}}{\partial t} = i\omega \mathbf{B}. \tag{11}$$

By taking the curl of equations 7 and 8 diffusion equations can be derived from which information concerning the conductivity structure of the subsurface can be extracted. In order to do this the following proven vector identities can be used:

$$\nabla \times (\nabla \times \mathbf{F}) = (\nabla \cdot \nabla \cdot \mathbf{F}) - \nabla^2 \mathbf{F}, \tag{12}$$

$$\nabla \times (\Psi \mathbf{F}) = \Psi \nabla \times \mathbf{F} - \mathbf{F} \times \nabla \Psi. \tag{13}$$

Using the vector identity given in equation 12 and equation 11 the curl of equation 7 can then be given in two different ways:

$$\nabla \times (\nabla \times \mathbf{E}) = (\nabla \cdot \nabla \cdot \mathbf{E}) - \nabla^2 \mathbf{E}, \tag{14}$$

$$\nabla \times (\nabla \times \mathbf{E}) = \nabla \times (-i\omega \mathbf{B}). \tag{15}$$

Since an isotropic and homogeneous medium is assumed $\nabla \cdot \mathbf{E} = 0$, as the conductivity is constant. Combining equations 14 and 15 then gives:

$$-\nabla^2 \mathbf{E} = \nabla \times (-i\omega \mathbf{B}). \tag{16}$$

Using the vector identity given in equation 13 and equation 8, equation 16 can be rewritten as:

$$-\nabla^2 \mathbf{E} = -i\omega \nabla \times \mathbf{B}, \tag{17}$$

$$\nabla^2 \mathbf{E} = i\omega\mu\sigma\mathbf{E}. \tag{18}$$

In the same way, using the vector identity given in equation 12 and equation 9, taking the curl of equation 8 gives:

$$-\nabla^2 \mathbf{B} = \nabla \times \mu\sigma\mathbf{E}. \tag{19}$$

Using the vector identity given in equation 13 and equation 11, equation 16 can be rewritten as:

$$-\nabla^2 \mathbf{B} = \mu\sigma(\nabla \times \mathbf{E}), \tag{20}$$

$$\nabla^2 \mathbf{B} = i\omega\mu\sigma\mathbf{B}. \tag{21}$$

Equations 18 and 21 are the diffusion equations describing the diffusion of the electric and magnetic fields through the Earth. The diffusive character of propagating EM fields is the reason why MT measurements yield volume soundings, i.e. the MT response functions (e.g. apparent resistivity, impedance phase etc.) are volumetric averages of the sampled medium (Simpson & Bahr 2005).

2.3.4 EM induction in a 1D Earth

Taking into account the plane wave assumption, in which plane waves propagate in a vertical direction perpendicular to the Earth's surface, and assuming a homogeneous half-space (with a coordinate system (x,y,z) with z being the vertical component, i.e. the depth) the following solutions can be found for the diffusion equations (equations 18 and 21):

$$\mathbf{E} = \mathbf{E}_1 e^{i\omega t - qz} + \mathbf{E}_2 e^{i\omega t + qz}, \tag{22}$$

$$\mathbf{B} = \mathbf{B}_1 e^{i\omega t - qz} + \mathbf{B}_2 e^{i\omega t + qz}. \tag{23}$$

Assumption 2. states that the Earth only dissipates or absorbs EM energy and does not generate it, implying that arbitrary large electric field amplitudes cannot be supported within the Earth. Therefore

$\mathbf{E}_2 = 0$, since $\mathbf{E}$ should diminish with increasing depth (z) (Simpson & Bahr 2005). Taking the second derivative (with respect to depth) of equation 22 then gives:

$$\frac{\partial^2 \mathbf{E}}{\partial z^2} = q^2 \mathbf{E}_1 e^{i\omega t - qz} = q^2 \mathbf{E}. \tag{24}$$

Since a homogeneous half-space is assumed, $\frac{\partial^2 \mathbf{E}}{\partial x^2} = \frac{\partial^2 \mathbf{E}}{\partial y^2} = 0$. Applying this condition and comparing equation 24 with equation 18 gives the following expressions for q:

$$q^2 = i\mu\sigma\omega, \tag{25}$$

$$q = \sqrt{i\mu\sigma\omega} = \pm\left(\sqrt{\frac{\mu\sigma\omega}{2}} + i\sqrt{\frac{\mu\sigma\omega}{2}}\right). \tag{26}$$

The inverse of the real part of q is the electromagnetic (EM) skin depth (or penetration depth) of an electric field with angular frequency ω into a half-space with conductivity σ. The equation for the EM skin depth is:

$$p = \frac{1}{\mathrm{Re}(q)} = \sqrt{\frac{2}{\mu\sigma\omega}}. \tag{27}$$

The EM skin depth gives the depth at which EM fields are attenuated to e^{-1} of their amplitudes at the surface, which depends on the conductivity of the penetrated medium. The inverse of q is referred to as the Schmucker-Weidelt transfer function and is given by the equation (Simpson & Bahr 2005):

$$C = \frac{1}{q} = \frac{p}{2} - i\frac{p}{2}. \tag{28}$$

The Schmucker-Weidelt transfer function can be calculated from the measured electric and magnetic field components according to the equation:

$$C = \frac{1}{q} = \frac{E_x}{i\omega B_y} = -\frac{E_y}{i\omega B_x}. \tag{29}$$

When C is known, the average resistivity of the homogeneous half-space can be calculated, which is referred to as the apparent resistivity (ρ_a). By combining equations 26 and 29 the apparent resistivity

can be calculated according to:

$$\rho_a = \frac{1}{\sigma} = \frac{1}{|q|^2}\mu\omega = |C|^2\mu\omega. \tag{30}$$

Since C is complex, the impedance phase can also be extracted, which describes the phase difference between the electric and the magnetic fields. The impedance phase (ϕ) can be calculated using:

$$\phi = \tan^{-1}\left(\frac{\mathrm{Im}C}{\mathrm{Re}C}\right). \tag{31}$$

The apparent resistivity and the impedance phase are two of the most commonly used response functions and frequently used for displaying MT data, usually plotted as a function of period, $T = \frac{2\pi}{\omega}$.

2.4 The impedance tensor

During an MT sounding the time-varying components of the electric and magnetic fields are measured simultaneously in orthogonal directions. Transfer functions can be derived from these measurements. Transfer functions (e.g. the impedance tensor and the geomagnetic transfer function) describe a linear system with an input and a predictable output and can thus be used to describe the response of the Earth to the time-varying electromagnetic field. In MT a transfer function can be defined as a function that relates the measured EM fields at a given frequency, and it's these transfer functions from which the conductivity structure of the Earth can be determined.

One of the most common transfer functions is the impedance tensor ($\underline{Z}$), which describes the penetration of the EM fields into the Earth, which depends on the Earth's conductivity structure, and thus can be used for imaging and interpretation of the conductivity structure of the subsurface. The impedance tensor is usually described by a 2×2 matrix and relates orthogonal components of the horizontal electric field (E_x, E_y) and magnetic field ($\frac{B_x}{\mu_0}$, $\frac{B_y}{\mu_0}$ or H_x, H_y), according to the equation (Simpson & Bahr 2005):

$$\begin{bmatrix} E_x \\ E_y \end{bmatrix} = \begin{bmatrix} Z_{xx} & Z_{xy} \\ Z_{yx} & Z_{yy} \end{bmatrix} \begin{bmatrix} \frac{B_x}{\mu_0} \\ \frac{B_y}{\mu_0} \end{bmatrix}. \tag{32}$$

Applying the relation $\mathbf{B} = \mu\mathbf{H}$, this results in the equivalent equation:

$$\begin{bmatrix} E_x \\ E_y \end{bmatrix} = \begin{bmatrix} Z_{xx} & Z_{xy} \\ Z_{yx} & Z_{yy} \end{bmatrix} \begin{bmatrix} H_x \\ H_y \end{bmatrix}, \quad \text{or} \quad \mathbf{E} = \underline{Z}\mathbf{H}. \tag{33}$$

Each component of the impedance tensor is a complex, frequency-dependent value and can be associated with a phase and a magnitude, describing the relation between two mutually perpendicular components of the horizontal electric and magnetic fields (Simpson & Bahr 2005, Caldwell et al. 2004).

2.4.1 The 1D Earth

In a 1D MT model the conductivity varies only with depth (z). For the impedance tensor this means that the following conditions apply (Simpson & Bahr 2005, Berdichevsky & Dmitriev 2008):

$$Z_{xx} = Z_{yy} = 0, \quad \text{and} \quad Z_{xy} = -Z_{yx}, \tag{34}$$

i.e., the diagonal components Z_{xx} and Z_{yy} are zero, while the off-diagonal components Z_{xy} and Z_{yx} have the same amplitude since the conductivity does not vary in lateral directions. Applying these conditions the impedance tensor assumes the form (Simpson & Bahr 2005, Berdichevsky & Dmitriev 2008):

$$\begin{bmatrix} Z \end{bmatrix} = \begin{bmatrix} 0 & Z_{xy} \\ -Z_{xy} & 0 \end{bmatrix} = \begin{bmatrix} 0 & Z \\ -Z & 0 \end{bmatrix} = Z \begin{bmatrix} 0 & 1 \\ -1 & 0 \end{bmatrix}. \tag{35}$$

Combining this with equation 32 gives:

$$\begin{bmatrix} E_x \\ E_y \end{bmatrix} = \begin{bmatrix} 0 & Z_{xy} \\ -Z_{xy} & 0 \end{bmatrix} \begin{bmatrix} \frac{B_x}{\mu_0} \\ \frac{B_y}{\mu_0} \end{bmatrix}, \tag{36}$$

or written as components:

$$E_x = \frac{1}{\mu_0} Z_{xy} B_y \quad \text{and} \quad E_y = -\frac{1}{\mu_0} Z_{xy} B_x. \tag{37}$$

Solving these equations gives:

$$Z_{xy} = \mu_o \frac{E_x}{B_y} = -\mu_0 \frac{E_y}{B_x}. \tag{38}$$

This result is analogous to the Schmucker-Weidelt transfer function (equation 29), with the only difference being the definition of the transfer function itself. In case of the Schmucker-Weidelt transfer function $C = \frac{1}{q} = \frac{E_x}{i\omega B_y} = -\frac{E_y}{i\omega B_x}$, while the impedance tensor is defined as $Z = \mu_0 \frac{E_x}{B_y} = -\mu_0 \frac{E_y}{B_x}$. Therefore, these two transfer functions are related by:

$$Z = i\omega\mu_0 C. \tag{39}$$

This implies that equation 38 can be derived from Maxwell's equations for the 1D case (and also for 2D along strike). Also, equations for the apparent resistivity and the impedance phase analogous to equations 30 and 31 can be derived:

$$\rho_a = \frac{1}{\mu_o \omega}|Z|^2, \quad \text{and} \quad \phi = \tan^{-1}\left(\frac{\mathrm{Im}Z}{\mathrm{Re}Z}\right). \tag{40}$$

2.4.2 The 2D Earth

In a 2D model the conductivity varies vertically (in the z-direction) and in one horizontal (the x- or y-) direction, perpendicular to the strike of the conductive anomaly (also referred to as the electromagnetic (EM) strike). In an ideal situation one of the associated fields (**E** or **B**) is parallel to the strike, so that $Z_{xx} = Z_{yy} = 0$, since an electric field parallel to the strike induces magnetic fields only perpendicular to strike and vice versa. In the case of a 2D along strike case, the impedance tensor then becomes (Simpson & Bahr 2005):

$$\left[Z\right] = \begin{bmatrix} 0 & Z_{xy} \\ Z_{yx} & 0 \end{bmatrix}. \tag{41}$$

When this condition holds, the EM field can be decoupled into two modes: the E-polarization mode (or transverse electric mode, or TE mode), which describes currents flowing parallel to the strike direction, and the B-polarization mode (or transverse magnetic mode, or TM mode), which describes the currents flowing perpendicular to the strike direction. Assuming the strike direction is along the x-axis, this gives:

$$TEmodel \begin{cases} \frac{\partial E_x}{\partial y} = i\omega B_z \\ \frac{\partial E_x}{\partial z} = -i\omega B_y \\ \frac{\partial B_z}{\partial y} - \frac{\partial B_y}{\partial z} = \mu_0 \sigma E_x \end{cases} \qquad TMmodel \begin{cases} \frac{\partial B_x}{\partial y} = \mu_0 \sigma E_z \\ -\frac{\partial B_x}{\partial z} = \mu_0 \sigma E_y \\ \frac{\partial E_z}{\partial y} - \frac{\partial E_y}{\partial z} = -i\omega B_x \end{cases}. \tag{42}$$

This decoupling of the EM field into two modes is called polarization. Z_{xy} and Z_{yx} then are the different impedances of the two polarization modes, Z_{xy} being the impedance of the E-polarization mode and Z_{yx} being the impedance of the B-polarization mode (Simpson & Bahr 2005, Berdichevsky & Dmitriev 2008). Because of the plane wave assumption (section 2.3.1), which implies that the EM fields penetrating the Earth propagate in the vertical direction, the polarization directions are in the xy-plane, parallel to the Earth's surface (Telford et al. 1990).

Note that an ideal situation has been assumed, in which one of the incorporating fields is parallel to the strike. However, for most recorded MT data this is not the case, since the strike direction often is not precisely known at the time of the MT survey. In this case the diagonal components Z_{xx} and Z_{yy} will not be zero and the TE and TM modes will be mixed in the impedance tensor. When an ideal 2D structure and noise-free data are assumed, it is possible to rotate the observed impedance tensor ($\underline{Z}_{obs}$) by an angle θ around a vertical axis, until the 2D impedance tensor ($\underline{Z}_{2D}$) is in strike coordinates and the diagonal components are zero. Using the Cartesian rotation matrix $\underline{R}_\theta$ with rotation angle θ, the 2D impedance tensor can be calculated as:

$$\underline{Z}_{2D} = \underline{R}_\theta \underline{Z}_{obs} \underline{R}_\theta^T , \tag{43}$$

where

$$\underline{R}_\theta = \begin{pmatrix} \cos\theta & \sin\theta \\ -\sin\theta & \cos\theta \end{pmatrix} \quad \text{and} \quad \underline{R}_\theta^T = \begin{pmatrix} \cos\theta & -\sin\theta \\ \sin\theta & \cos\theta \end{pmatrix} . \tag{44}$$

However, in the case of a non-ideal 2D structure and/or noisy data it will be impossible to find a rotation angle in which the diagonal elements are zero.

2.4.3 The 3D Earth

In 3D models, the conductivity varies with depth (the z-direction) and both lateral directions (the y- and x-directions). The impedance tensor then assumes the form (Berdichevsky & Dmitriev 2008):

$$\left[Z\right] = \begin{bmatrix} Z_{xx} & Z_{xy} \\ Z_{yx} & Z_{yy} \end{bmatrix} = \begin{bmatrix} \mathrm{Re}Z_{xx} & \mathrm{Re}Z_{xy} \\ \mathrm{Re}Z_{yx} & \mathrm{Re}Z_{yy} \end{bmatrix} + i \begin{bmatrix} \mathrm{Im}Z_{xx} & \mathrm{Im}Z_{xy} \\ \mathrm{Im}Z_{yx} & \mathrm{Im}Z_{yy} \end{bmatrix} . \tag{45}$$

In this case no rotation angle can be found for which the diagonal elements of the impedance tensor are zero, and thus the decoupling into two modes is not valid anymore. Instead, in a 3D earth, the impedance

tensor is characterized by four non-zero complex elements.

2.4.4 Dimensionality

The general properties of the impedance tensor depend on the dimensionality of the conductivity structures and heterogeneities in the subsurface. It must be emphasized that the dimensionality of a structure depends on the EM skin depth of an MT sounding. A 3D body with a different conductivity than the half-space that surrounds it induces a 1D response for MT sounding periods that are sufficiently short, so that the EM skin depths are small compared to the shortest dimensions of the body. As the sounding period increases, the EM skin depth will eventually extend sufficiently to encompass at least one edge of the anomaly and the impedance tensor will appear multi-dimensional. Increasing the sounding period even further, such that the EM skin depth is much greater than the dimensions of the anomaly, the inductive response of the anomaly becomes weak, while the galvanic response (section 2.5) remains (fig. 2.1) (Simpson & Bahr 2005).

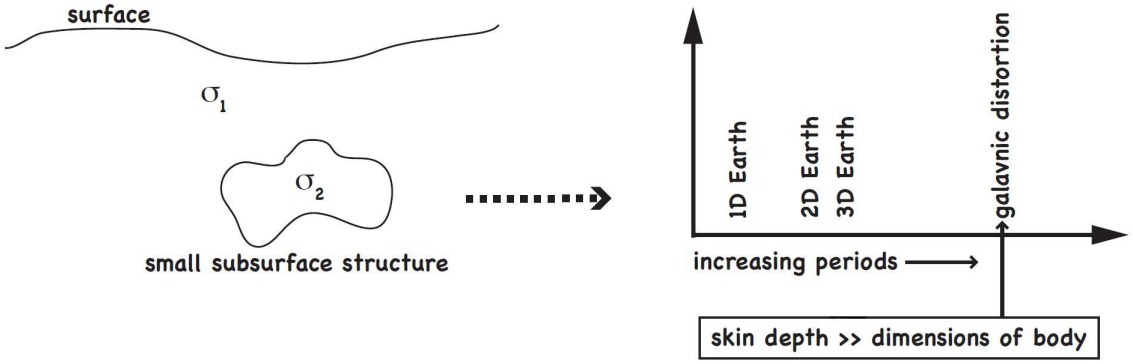

Figure 2.1: Sketch illustrating the dependence of dimensionality on scale. A 3D body with conductivity σ_2 is embedded in homogenous half space with conductivity σ_1. Depending on the EM skin depth compared to the dimensions of the body, the MT response will be 1D, 2D or 3D and for an EM skin depth much greater than the dimensions of the body only the galvanic response will remain. Modified from Simpson & Bahr (2005).

2.5 Distortion effects

Local, near-surface, conductive heterogeneities in the subsurface that cannot be resolved within the conductivity model can still act as a source for biasing effects, distorting the data. In these distortion effects a distinction can be made between inductive effects (frequency-dependent) and galvanic effects (frequency-independent). These effects can significantly distort the determination of the dimensionality and therefore need to be considered when processing and interpreting MT data.

Inductive effects are caused by excessive currents at conductive boundaries (either distinct boundaries or continuous transitions). Following Faraday's law (equation 1), variations through time in the primary magnetic field induce corresponding variations in the electric field and thus induce excessive currents which flow in closed loops. These currents produce secondary magnetic fields, which add vectorially to the primary magnetic field and hence produce inductive effects (Berdichevsky & Dmitriev 2008). The magnitude of the induction (and thus the inductive response) depends on the scale of the conductive structure that causes it, i.e. a larger conductive structure causes a larger inductive response. Inductive distortion effects manifest themselves at high frequencies, since at lower frequencies the EM skin depths exceeds the depth and dimensions of near-surface conductive heterogeneities and the induction effects vanish (Simpson & Bahr 2005, Berdichevsky & Dmitriev 2008).

Galvanic effects are caused by excessive charges at conductive boundaries. At these boundaries electrical charges build up, caused by the primary electric field. These excess charges cause secondary electric fields which add vectorially to the primary electric field and hence produce galvanic effects (Simpson & Bahr 2005). As galvanic effects are caused by conductive heterogeneities, a distinction can be made between heterogeneities with a higher conductivity than the surrounding material and heterogeneities with a lower conductivity than the surrounding material. A volume with a higher conductivity attracts the passing electric currents and thus causes an increase of electrical current in the body (current channeling). Resistive heterogeneities, however, deflect the passing electrical currents and cause them to flow around the resistive body (current deflection) (Simpson & Bahr 2005). Jiracek (1990) showed that galvanic effects can also be produced by topography (referred to as galvanic topographic distortion), when the primary electric field is perpendicular to the trend of the topography. The main difference between galvanic effects caused by conductive heterogeneities and galvanic effects caused by topography is that for the latter no conductivity heterogeneities are necessary. In contrast to the inductive effects, the galvanic effects are most pronounced at low frequencies, when the EM skin depth far exceeds the depths and dimensions of near-surface conductive heterogeneities (Berdichevsky & Dmitriev 2008).

The extent to which these inductive and galvanic effects affect the data is thus closely related to the EM skin depth of the MT sounding. At higher frequencies (i.e. lower EM skin depths) the data are affected by inductive effects due to near-surface conductive heterogeneities. However, at lower frequencies, when the EM skin depth exceeds the depth and the dimensions of near-surface conductive heterogeneities, the

inductive effects becomes negligible, while the galvanic effects due to the near-surface conductive heterogeneities remain. These galvanic effects are manifested as static shift, which is a subset of the galvanic effects (and thus frequency-independent) and is characterized by a shift of the apparent resistivity curves. The corresponding parts of the impedance phase curves are not affected by this shift (Simpson & Bahr 2005, Berdichevsky & Dmitriev 2008).

2.6 Processing, analysis and modeling of MT data

During an MT recording, the time-varying electric and magnetic fields are measured simultaneously through time in two orthogonal directions at the Earth's surface. The resulting time series are data sets consisting of recorded values of the components of the magnetic field (H_x, H_y and H_z) and components the electric field (E_x and E_y), sampled at sequential (and usually fixed) time intervals. From these time series transfer functions are derived, which describe the response of the Earth to the time-varying electromagnetic field and from which the Earth's conductivity structure is derived. The process of deriving the transfer functions from the time series is called data processing, and this process usually involves pre-conditioning of the time series, transformation of the time series into the frequency domain and noise reduction (by minimizing statistical and bias errors). After processing, the transfer functions are analyzed, which includes distortion analysis and removal (including rotation of the impedance tensor to the EM strike direction) and possibly smoothing of the response functions. After the MT data are processed and analyzed the MT responses are ready for 1D, 2D or 3D modeling as appropriate.

2.6.1 Time series to transfer functions

Pre-conditioning of the time series is done in order to correct for the effect of trends, layout errors and bad records within the data sets (e.g. spikes, null-records). Also, in the pre-conditioning, the full record of a time series is divided into a number of segments (also called 'windows'). The effects of bad records in the time series are in many cases automatically removed during the processing. However, when the number of good records is sparse, pre-conditioning can increase the number of usable segments and thus enhance the quality of the obtained information.

The time series recorded during an MT survey are commonly transformed into the frequency domain using a Fourier transformation (or alternatively, by using a wavelet-transformation). Fourier transfor-

mations are performed for the segments of the time series instead of the full record. The time length of the segments determines the maximum wavelength (i.e. minimum frequency) that is analyzed, since a shorter measurement period yields shorter wavelengths. Obviously, the greater the number of segments, the shorter their time lengths will be. Usually, the window length is chosen to be as short as possible for a given frequency in order to increase the number of estimates and the more segments that are used the better the statistical result will be. Increasing the window length, however, increases reliability of each estimate but yields a smaller number of estimates. Once the data are transformed into the frequency domain, the raw power spectra for each time segment for each channel are used to calculate auto and cross spectra (i.e. the products of the field components and their complex conjugate), from which the transfer function is calculated.

Aside from certain types of instrumentation error, there are two types of error inherent in the estimation of transfer functions: statistical error and bias error (Jones et al., 1989). The latter is caused by noise in the magnetic and electric fields and contains three types of sources (Simpson & Bahr 2005):

- cultural (e.g. electricity power lines, generators, railways, electric fences),
- meteorological (e.g. wind, lightning), and
- sensor.

To avoid these biased errors, remote reference processing was introduced by Goubau et al. (1978) and Gamble et al. (1979). In this processing method components of the magnetic and/or electric field are measured at a remote site which are correlated with the components measured at the local MT site. Often several MT sites, which are measured simultaneously during an MT survey, are used as remote references for each other. However, it must be noted that correlated noise components between the local and the remote fields are not removed by remote reference processing and can cause bias effects. Also, remote reference processing results always have larger associated statistical noise than the standard single station methods (Jones et al. 1989). Statistical error is generally reduced by stacking of the spectra calculated for the different segments of the time series or by using robust processing techniques. A processing method is considered robust when it is relatively insensitive to the presence of a moderate amount of bad data (Jones et al. 1989) and thus is able to produce a superior set of estimates from a data set affected by errors. Jones et al. (1989) concluded that (1) in order to minimize bias errors, remote reference processing

should be applied whenever possible, and that (2) robust processing techniques give superior results to spectral stacking.

2.6.2 Distortion removal

As explained in section 2.5, inductive and galvanic distortion cause biasing of MT data due to local, near-surface, conductive heterogeneities. Over time, a number of methods have been proposed to correct for the effects of distortion, e.g. Swift (1967), Bahr (1988), Weaver et al. (2000), Caldwell et al. (2004). One of the most commonly used methods used is decomposition, in which the impedance tensor is decomposed into a galvanic response due to local 3D conductive heterogeneities and an inductive response due to an underlying 2D regional structure. In this method the observed impedance tensor ($\underline{Z}_{obs}$) is separated into a tensor that describes the response to the underlying 2D structure ($\underline{Z}_{2D}$) and a tensor that describes the response to the local 3D structures (distortion matrix $\underline{C}$). The basic requirement is that the components of the distortion matrix must be real and frequency independent (Simpson & Bahr 2005, Berdichevsky & Dmitriev 2008). A widely used technique for decomposition was proposed by Groom & Bailey (1989), in which they present a method to divide the distortion matrix ($\underline{C}$), describing the relationship between the distorted impedance ($\underline{Z}_{obs}$) and the regional impedance ($\underline{Z}_{2D}$), into four parameters representing different aspects of distortion (Groom & Bailey 1989):

$$\underline{Z}_{obs} = \underline{C}\underline{Z}_{2D} = g\underline{TSA}\underline{Z}_{2D}. \tag{46}$$

The four parameters used to describe the distortion are the scaling or site gain factor (g), the twist tensor ($\underline{T}$), the shear tensor ($\underline{S}$) and the anisotropy tensor ($\underline{A}$), which can all can be expressed in terms of real values. The gain factor at a station scales the regional electric field without causing any directional change. The twist tensor rotates the regional electric field clockwise towards the local strike, which affects both amplitude and phase of the impedance. The shear tensor causes rotating of a vector clockwise on the x-axis of a coordinate system, not coinciding with the regional principle axis system, whereas a vector on the y-axis is rotated anticlockwise. This also affects both amplitude and phase of the impedance. The anisotropy tensor scales the electric field on the two axes coinciding with the regional EM strike by a different factor, both indistinguishable from the regional structure without independent information (fig. 2.2).

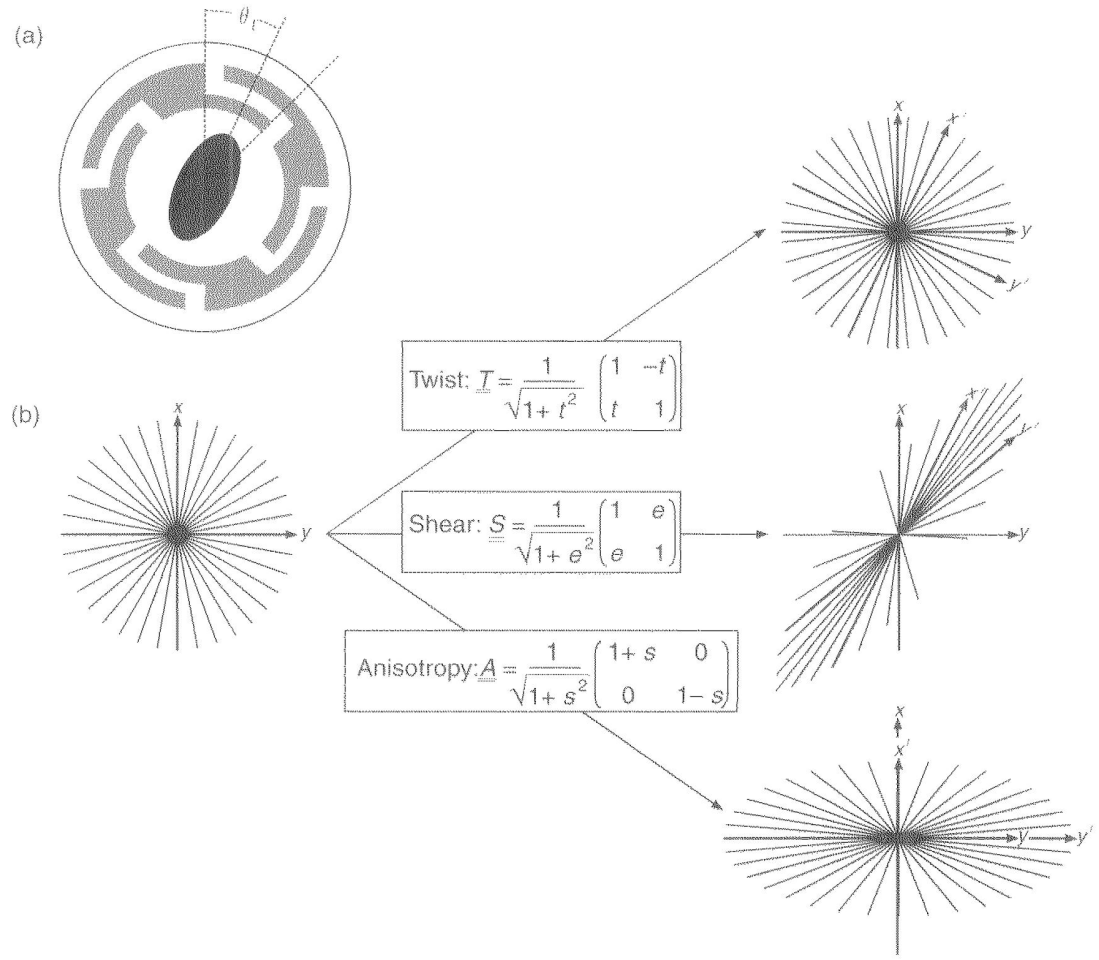

Figure 2.2: Visual representation of the Groom and Bailey method for decomposition. (a) The idealized physical model consists of a highly conductive swamp (black), encompassed by a moderately conductive region (gray) and an insulator (white). The MT data are collected at the centre of the swamp and θ_t denotes the local strike of the swamp. (b) Distortion of a set of unit vectors by twist $\underline{T}$, shear $\underline{S}$ and anisotropy $\underline{A}$, which are expressed in terms of the real values t, e and s. Taken from Simpson & Bahr (2005).

Note that for the Groom and Bailey decomposition method, a 2D regional structure is assumed and that for the method to provide useful results the EM strike direction must be known in order to rotate the observed impedance tensor (section 2.4.2). McNeice & Jones (2001) proposed an extension to the Groom-Bailey decomposition method in which a global minimum is sought to determine the most appropriate strike direction and distortion parameters for a range of frequencies and a set of MT sites. This is done by using the following equation:

$$\underline{Z}_{obs} = \underline{C}_\theta \underline{C}\underline{Z}_{2D}\underline{R}_\theta^T. \tag{47}$$

McNeice & Jones (2001) developed a freely available computer program called STRIKE, in which this

extended Groom-Bailey approach is used to decompose data. The program can be used to find an appropriate strike direction over the whole length of a profile (or segments of it) and at all frequencies. The most recent version of STRIKE also allows an analysis of a depth band using the Niblett-Bostick depth approximation (Niblett 1960, Bostick 1977).

It must be emphasized that decomposition to strike is not equivalent to rotation of the observed impedance tensor into that direction. When applying a decomposition, the impedance elements are recalculated, most distortion effects are removed and only static shift remains. Spratt et al. (2009) use the maximum phase difference between the Z_{xy} (TE) and Z_{yx} (TM) modes in decomposed data as an indication of dimensionality, stating that data can be treated as 1D if the maximum phase difference is well below 10 ° over a broad period band.

2.6.3 D+ and ρ+

The D+ approach, published by Parker (1980), Parker & Whaler (1981) and Parker (1982), is a method to test for consistency of complex admittance data with the assumption that the data are 1D. It is based on the fact that the discrete MT response of any 1D conductivity profile can be matched arbitrarily well by the response of a model consisting of a finite system of delta functions. Data sets for which this is true are said to be D+ consistent. Parker & Booker (1996) proposed an extension to the D+ approach, called ρ+, in which they use the logarithm of the admittance rather than the admittance itself. The admittance is related to the apparent resistivity (ρ_a) and the impedance phase (ϕ) by:

$$\rho_a = \mu_0 \omega |c|^2 \quad textrmand \quad c = |c| e^{i(\phi - \pi/2)}. \tag{48}$$

The 1D code by Parker & Booker (1996) can thus be used to calculate a conductivity model from either apparent resistivities or impedance phases or both. This can be used as a consistency check of measured data in order to produce improved, smoothed MT response functions.

2.6.4 Modeling

After transformation into the frequency domain, minimizing the errors, distortion removal and smoothing, the MT data can be used for modeling. Modeling is used to produce 1D, 2D or 3D models based on the measured data in order to determine the subsurface conductivity structure and a distinction can be made

between two methods: forward modeling and inversion. Forward modeling is an iterative procedure in which the electromagnetic induction process is simulated to obtain synthetic data responses for an input model, consisting of a conductivity structure. The results are compared with the measured data and the model can be modified where the data are poorly fitted, until a set of model parameters is found that satisfactory fits the measured data. Inversion methods can be divided into three categories according to their approach: direct methods, iterative methods and stochastic methods. Direct inversion aims to directly derive the model parameters from the observed data, while iterative and stochastic inversion is similar to the 'trial and error' process in which one or more starting models are created and their responses are calculated. Model parameters are automatically adapted during the inversion process in order to minimize the difference between the calculated responses and the measured data, usually presented by an RMS misfit.

An important feature of inversion is its non-uniqueness, i.e. a range of models fit the measured data equally well (except for ideal observations with a 1D subsurface and noise-free data). Rough models usually fit the measured data better, but often contain resistivity distributions that are not in agreement with plausible geological scenarios, e.g. unrealistically high conductivity and/or resistivity values. Therefore, during modeling often constraints are imposed on the models, such as a restriction on the number of possible layers, a limited parameter range or the so-called smoothness of the model. A higher degree of smoothing is generally desirable as it usually yields models with less structure, meaning that the persisting structures are more reliable. However, due to the additional constraints on the model parameters a trade-off between smoothness of the model and data misfit is commonly observed.

In this study, three 1D inversion codes are used: Occam (Constable et al. 1987), a 1D inversion code generating sharp boundary models implemented in WinGLink, and Minim (Fischer et al. 1981). The Occam code is proposed by Constable et al. (1987), who argue that seeking the smoothest possible model reduces the temptation of overinterpreting the data and eliminates arbitrary discontinuities in layered models. Therefore the Occam code seeks the smoothest model which fits the data to within an expected tolerance, rather than fitting the data as well as possible, which maximizes the roughness of the model. In contrast, the WinGLink 1D inversion code produces sharp boundary models that are derived initially from a smooth model (either Occam or Bostick models). The Minim code is proposed by Fischer et al. (1981) and tries to minimize the standard deviation between the measured and calculated impedances. The code

first analyzes the shortest periods of the data and tries to explain the observed response, specifically the apparent resistivity and the impedance phase, in terms of a two-layer structure. Shifting successively to longer periods, discrete new layers are introduced at progressively greater depth. Stabilizing features keep the inversion process from diverging and hold the necessary number of layers to a minimum.

3 Petrophysical models

This chapter is concerned with the petrophysical link between the resistivity, the porosity and the permeability of rocks. While there are many different models available for porosity estimation and especially for permeability estimation, this chapter focuses on the models that are relevant to this thesis.

In sedimentary rock formations fluids saturating the pores form the path of least resistance for electric current, as the electrical conductivity of the fluids is significantly higher than the electrical conductivity of the rock matrix. Therefore the path of electrical conductance through a rock is similar to the path of hydraulic conductance and thus is highly related to the porosity and permeability (Khalil & Santos 2009). The electrical conductivity of a rock formation is therefore primary a function of the degree of saturation, the conductivity of the saturating fluid and the rock properties that influence the pore geometry, as these determine the path of hydraulic and thus electrical flow (Salem & Chillingarian 1999, Lesmes & Friedman 2005). This explains why the bulk effective conductivity of a saturated rock formation is relatively insensitive to the electrical conductivity of the host rock, but that variations in porosity and permeability of the rock can significantly influence the bulk effective conductivity (Simpson & Bahr 2005). Due to the complexity of the pore geometry of sedimentary rocks it has proven to be impossible to derive theoretical models that relate the electrical conductivity of a rock formation to other rock properties (including porosity and permeability). Therefore, in practice commonly (semi-)empirical petrophysical models are used for porosity and permeability estimation. These models are based on combining hydrological, geophysical and/or core sample data with theoretical models. However, as empirical models are based on observation these models and derived values of their parameters can be very site and lithology specific.

3.1 Porosity estimation

Porosity is a measure of the amount of void space in a porous medium. It is defined as the ratio of the pore volume to the total volume of the sample and thus has no unit. When a medium contains isolated pores the effective porosity (commonly considered to represent the pore space available for fluid flow) is less than the total porosity.

The foundation for porosity estimation from electrical conductivity measurements of rock formations was laid by Archie (1942), when he developed an empirical equation for porosity determination from elec-

trical conductivity for a fully saturated, clean (i.e. clay-free) medium with one conducting phase, i.e. the water saturating the pores. Since then numerous variations and modifications of Archie's equation have been published in order to improve the equation and correct for the assumptions made by Archie. It's these models that are commonly applied for porosity determination from electrical conductivity measurements in scientific and commercial applications.

3.1.1 Archie's laws

Archie (1942) developed an empirical equation that relates the porosity to the electrical conductivity. For his equation Archie assumed (1) a clean (i.e. clay-free) medium, and (2) a sufficient salinity of the water saturating the pores. His equation became known as Archie's first law:

$$F = \frac{\sigma_w}{\sigma_0} = \frac{1}{\phi^m}, \tag{49}$$

in which F is the formation factor, which is the ratio of the electrical conductivity of the water (σ_w) to the bulk effective conductivity of the saturated rock (σ_0), ϕ is the porosity and m is the cementation exponent. Archie (1942) postulated that the formation factor is an intrinsic property of the rock. This implies that the formation factor solely depends on the rock properties that affect electrical conductivity through the rock (i.e. the properties that influence the saturated pores) and is independent of the water resistivity. The term formation factor was used because it was approximately constant for any given formation. When the water resistivity is equal to the bulk resistivity (i.e. when the porosity is 1), the formation factor is 1. As the porosity decreases, the formation factor increases, with the formation factor going to infinity as the porosity approaches 0. The formation factor can be less than 1, but only when the rock matrix is less resistive than the water resistivity, which is extremely rare (Glover 2009, Khalil & Santos 2009). The cementation exponent is a variable, for which Archie (1942) found that it increased with degree of cementation, from 1.3 for unconsolidated sands to 2.0 for consolidated sandstones, and therefore naming it the cementation exponent (Lesmes & Friedman 2005). Later research showed that the cementation exponent depends on all factors that influence the pore geometry or that influence the electrical conductive properties of the rock. This includes shape, size and type of grains and pores as well as the size and number of dead-end pores (Salem & Chillingarian 1999). Theoretically the cementation exponent can vary between 1 and infinity, with a value of 1 representing a porous medium in which the

porosity occurs as capillary tubes of a constant radius which cross through the sample in a straight line. In practice, however, a value of 1 is not observed, but values commonly lie between just over 1 and 5. Most porous, arenaceous rocks have values between 1.5 and 2.5, while values higher than 2.5 and up to 5 are generally found in carbonates with less well connected pore space (Salem & Chillingarian 1999, Glover 2009).

In 1952, Winsauer et al. proposed a modified version of Archie's first law, in which they added the tortuosity factor (a):

$$F = \frac{a}{\phi^m}. \tag{50}$$

The tortuosity factor, like the cementation exponent, is not a constant but varies largely according to many parameters that influence the electrical conductivity properties of the rock. When the water saturating the pores is the dominant electrical conductivity mechanism, as in the case of clean, well-sorted sandstones, the tortuosity factor can be assumed to be 1, because as the porosity approaches 1 the conductivity of the rock is equal to the conductivity of the water (Worthington 1993, Mavko et al. 1998). Note that the tortuosity factor is not the same as the tortuosity, which is defined as the ratio between the effective length of the flow paths and the length of the sample of porous material (Lesmes & Friedman 2005).

As the degree of water saturation is an important factor for the bulk effective conductivity, Archie (1942) developed a second empirical equation (Archie's second law) that the describes how the resistivity of a partially saturated rock varies with water saturation:

$$F = a\phi^{-m} S_w^{-n}, \tag{51}$$

where S_w is the water saturation and n is the saturation exponent. The saturation exponent describes the effect of water saturation on the bulk effective conductivity of a rock formation and usually equals 2 (Khalil & Santos 2009). Archie's second law holds for saturations as low as 0.15 or 0.20. At lower water saturations the surface conductivity becomes dominant (Lesmes & Friedman 2005).

Archie's laws, as developed by Archie (1942), are empirical relations. However, Sen et al. (1981) showed that Archie's first law can be theoretically derived using the mean field theory (sometimes referred to as the self-consistent field theory). The mean field theory describes the electrical conductivity of many-body systems, consisting of interacting spheroids with random orientations. It considers the three-

dimensional structure of the medium or its idealized geometrical description and accounts for the strong interactions between the bodies (Friedman 2005, Lesmes & Friedman 2005). Building on the work of Bruggeman (1935) and Hanai (1960, 1961), Sen et al. (1981) showed that by modeling the dielectric and conductive responses of a composite porous medium composed of two constituents, Archie's laws can be theoretically obtained.

3.1.2 Two-phase models

For his first and second law Archie (1942) assumed a clay-free medium, in which the electrical conductivity depends solely on the fluid saturating the pores. However, it has been recognized that when a rock contains conductive minerals (i.e. clay minerals) the surface conductivity, which is an additional conductivity at the grain-fluid interface, becomes significant, causing the bulk effective conductivity to be the result of more than one conducting phase (Lesmes & Friedman 2005, Glover 2010). This surface conductivity is caused by excess charges at the clay mineral surfaces due to imperfections in the lattices of the clay minerals, creating a thin "electrical double layer" at the grain-fluid interface which is capable of conducting electrical currents (Devarajan et al. 2006). In cases where the rock contains conductive clay minerals (i.e. shaly rock formations) and the surface conductivity plays a significant role in the electrical conductivity through the rock, the ratio between the water resistivity and the bulk resistivity of the rock represents the apparent formation factor (F_a) (Worthington 1993):

$$F_a = \frac{\sigma_w}{\sigma_0}. \tag{52}$$

The apparent formation factor, in contrast to the formation factor, is not an intrinsic property of the rock but also depends on properties of the water, implying that it cannot be determined from Archie's laws (Devarajan et al. 2006). However, for applying Archie's laws on clay-containing rocks, different models (e.g. Waxman & Smits (1968), Clavier et al. (1977), Bussian (1983)) are available in order to correct for this and to derive the formation factor from the apparent formation factor.

3.2 Permeability estimation

The permeability is a measure of the ability of a porous medium, such as sedimentary rocks, to allow fluids to pass through and is commonly measured in millidarcy (mD). The variation of the permeability is

very large for any given rock type and can vary between several orders of magnitude. As the permeability is measured in dimensions of area it may be thought of as representing the cross section of an effective channel for fluid flow through the pore space.

There are numerous methods available for permeability estimation from electrical. One of the most well-known permeability models is the Kozeny-Carman equation (Kozeny 1927, Carman 1937). This model was developed by comparing Darcy's law with the Poiseuille equation and originally relates permeability to pore properties, but several authors have modified the equation to relate permeability to resistivity. Other models that relate permeability to resistivity, based on different theories, are proposed by Berg (1970, 1975), Johnson et al. (1986), Katz & Thompson (1986), Friedman & Seaton (1998). In this thesis the RGPZ model (Glover et al. 2006) is used.

3.2.1 The RGPZ model

The RGPZ model was proposed by Glover et al. (2006) and originates from a previously unpublished paper by Revil, Glover, Pezard and Zamora. The model is based on the work done by Bruggeman (1935), Hanai (1960, 1961), Sen et al. (1981), Bussian (1983) and follows out of their work combined with an equation from the SSJ model (Johnson et al. 1986, Johnson & Sen 1988). It considers the electrokinetic link between fluid flow and electrical flow in porous media and contains a parameter that gives the relevant grain size, which can be transformed into an effective length scale (which represents the aperture available for fluid flow) by using electrokinetic arguments. Theoretically, the model is valid providing that (1) the range of grain sizes in the rock is large compared to the difference between the mean maximum and minimum effective grain radii, (2) the values for the formation factor and the cementation exponent are derived from saline water bearing rock, (3) the rock is unfractured such that the formation factor is much larger than 1, and (4) the model is not used in the limit $\phi \to 1$ (i.e. 100 % porosity) (Glover et al. 2006). The permeability equation of the RPGZ model is given by (Glover et al. 2006):

$$k = \frac{d^2 \phi^{3m}}{4pm^2}, \tag{53}$$

where k is the permeability, d is the effective grain diameter, ϕ is the porosity, m is the cementation exponent from Archie's first law and p is the packing parameter. The model proves to be insensitive to changes in the packing parameter and therefore a value of $p = 8/3$ is assumed for 3D arrangements of

quasi-spherical grains, which is valid for most sedimentary rocks (Glover et al. 2006). Testing of the RGPZ model using theoretical and experimental data shows that the quality of the prediction provided by the RGPZ model depends critically upon the choice of the effective grain diameter (Glover et al. 2006, Walker & Glover 2010).

4 The Lough Neagh Basin

In the first part of this chapter a geological history of the Lough Neagh Basin is given. In the second part all aspects of the Lough Neagh Basin relevant to this study are introduced, i.e. the stratigraphy, a history of the geophysical exploration of the basin and an overview of the previous research on the geothermal potential of the Sherwood Sandstone Group.

The Lough Neagh Basin is a NE-SW trending basin located in County Antrim in Northern Ireland. The basin lies within the Midland Valley Terrane and in the northwest is bounded by the Fair Head-Clew Bay Line, which is an extension of the Highland Boundary Fault. Here, adjacent to the basin, lies the Highland Border Ridge. In the southeast the Lough Neagh Basin is bounded by the Southern Upland Fault and adjacent to the basin lies the Longford-Down Massif (fig. 4.1) (Illing & Griffith 1986, Naylor et al. 2003, Johnston 2004). Although developed simultaneously, an area of Permo-Triassic sedimentary thinning separates the Lough Neagh Basin from the Larne Basin, possibly controlled by a basement high (Shelton 1997).

The development of the Lough Neagh Basin commenced in the Permian and was predominantly controlled by pre-existing structures and reactivation of (major) faults during regional tectonic events, following a Caledonian NE-SW trend (Johnston 2004, Mitchell 2004g). The basin initially subsided along these faults, following their NE-SW orientation. However, later subsidence was influenced primarily by NNW-SSE trending normal faults (McCaffrey & McCann 1992, Naylor et al. 2003, Johnston 2004). The stratigraphic sequences of the basin comprise Paleozoic (Carboniferous and Permian), Mesozoic and Tertiary rocks. Sedimentation took place mainly in the Permian and the Triassic and was influenced by the timing of the regional tectonic events and eustatic sea level variations. These sea-level changes, together with the climate, controlled the depositional facies present in the basin (McCann 1991, Illing & Griffith 1986, Johnston 2004). While the overall stratigraphy is relatively constant throughout the basin, faults that were active during and after deposition have strongly influenced the stratigraphic sequences, causing considerable lateral variations in thickness and lithology of the Paleozoic sequences across many of the faults (McCann 1990, McCaffrey & McCann 1992, Naylor et al. 2003). This may have significantly affected the preservation of the Carboniferous sequences and caused the Permo-Triassic sequences to have been broken up into a series of tilted blocks (Illing & Griffith 1986, Naylor et al. 2003).

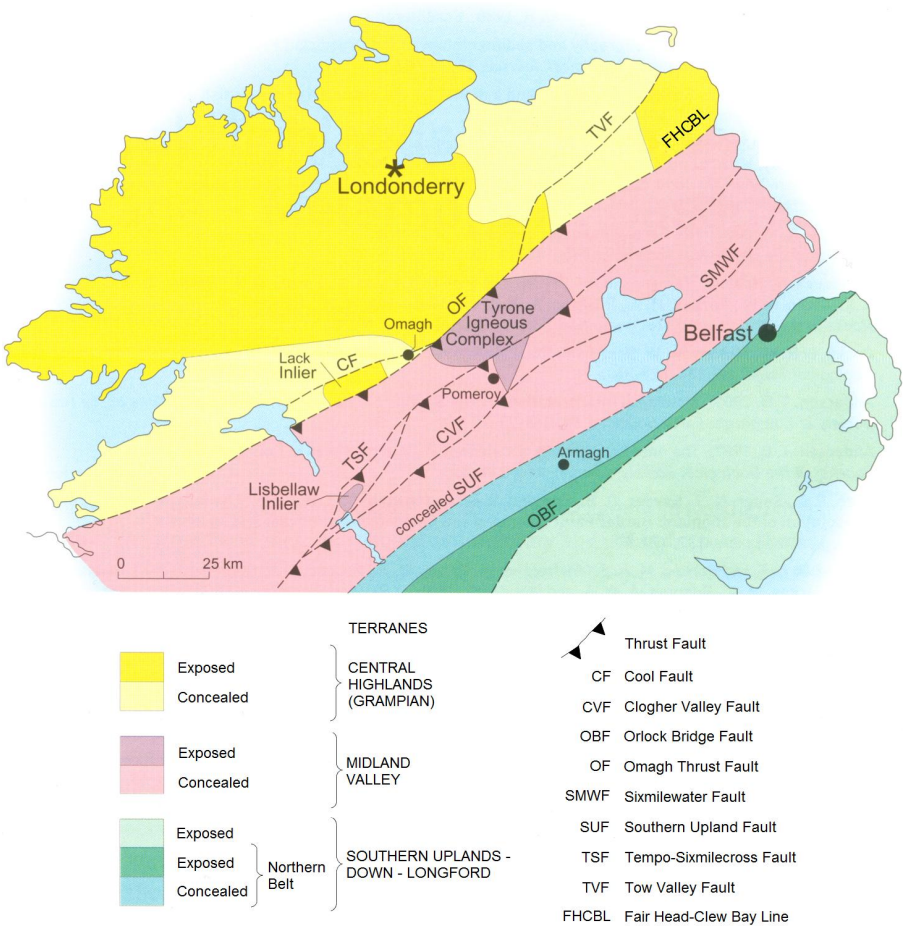

Figure 4.1: Basement terranes of Northern Ireland, modified from Anderson et al. (2004). The Lough Neagh Basin is located west of Belfast, largely underlying Lough Neagh.

4.1 Early tectonic history of Northern Ireland

The geological basement of Northern Ireland was assembled during the Caledonian Orogeny, which commenced in the Ordovician and continued until the Early Devonian. During the Caledonian Orogeny the continents Laurentia, Avalonia and Baltica collided as a consequence of the closing of the Iapetus Ocean, forming minor supercontinent Euramerica (or Laurussia) and the Caledonides mountain range. The Caledonides can be divided into seven terranes that share an internal continuity of geology. Three of these terranes make up the Irish part of the Caledonides and form the entire basement of Northern Ireland: the Central Highlands (or Grampian) Terrane, the Midland Valley Terrane and the Southern Uplands-Down-Longford Terrane (Anderson et al. 2004). During the Caledonian Orogeny the Central Highlands Terrane was sutured to the Midland Valley Terrane along the Highland Boundary Fault, while the Southern Uplands Terrane was sutured to the Midland Valley Terrane along the Southern Upland Fault (fig. 4.1) (McCaffrey & McCann 1992, Anderson et al. 2004).

At the end of the Devonian, Ireland was located on the southern margin of Euramerica (Mitchell 2004e). From the Late Devonian, throughout the Carboniferous until the Early Permian the Variscan (or Hercynian) Orogeny took place, resulting from the formation of the supercontinent Pangaea due to the collision between Gondwana and Euramerica. In this period, major faults were formed in Northern Ireland due to reactivation of Caledonian basement structures, primarily following a NE-SW trend (Mitchell 2004f). In the Early Carboniferous, during the Variscan Orogeny, a transgression to marine conditions reached Northern Ireland. However, Variscan movements in the Late Carboniferous caused compression and were accompanied by a period of erosion. Subsequently, by the end of the Carboniferous all of Ireland was land and the Variscan mountains stretched across the northern part of the country (Mitchell 2004e,f).

4.2 Permian

After the Variscan Orogeny, during the Permian and the Triassic, northwest Europe was located in equatorial latitudes within the Pangaean supercontinent. In the Early Permian the North Atlantic rifting first affected Northern Ireland. Opening of the North Atlantic resulted in tensional stresses, causing crustal subsidence which was responsible for the development of fault-bounded sedimentary basins (including the Lough Neagh Basin) due to reactivation of existing structures and faults, following a NE-SW (Caledonian) trend (McCann 1991, McCaffrey & McCann 1992, Mitchell 2004g). The Lough Neagh Basin developed due to a gradual down-throw by a series of faults, instead of one single major controlling fault, producing half-grabens (Shelton 1997, Johnston 2004). The development of the basin caused rapid burial throughout the Permian, which took place in continental conditions and was affected by eustatic sea-level variations (Illing & Griffith 1986, Shelton 1997, Mitchell 2004f,g).

In the Early Permian, sedimentation in the basins occurred primarily in an arid, hot, desert environment by rivers depositing clastic sediment on alluvial fans. In this environment the Enler Group was deposited, which consists of coarse, clastic rocks (Mitchell 2004g). In the Late Permian a southwards migrating transgression reached Northern Ireland, which marks the end of a long period of Variscan Mountain erosion. During this transgression the Belfast Harbour Evaporite Formation was deposited, consisting of a calcareous unit (often referred to as Magnesian Limestone) and locally a unit of fine-grained sandstone with evaporites (mainly anhydrite). This formation is succeeded by units of fine-grained, clastic rock that, together with the Belfast Harbour Evaporite Formation, make up the Belfast Group (Naylor et al. 2003,

Mitchell 2004g).

4.3 Triassic

The supercontinent of Pangaea continued to exist until its breakup in the Late Triassic. This brought an end to a long period of predominantly continental conditions that had influenced the climate of Ireland since the end of the Carboniferous and was the start of a period of marine conditions in Northern Ireland (Mitchell 2004b). Subsidence of the Lough Neagh Basin continued in the Early Triassic during which the basin depocentre initiated in the Permian did not change location and sedimentation appears to have been continuous across the Permo-Triassic boundary (Shelton 1997, Mitchell 2004a). The start of the Triassic is marked by a return to continental conditions and the Triassic stratigraphic sequences represent a transgression that re-established marine environments before the end of the Triassic period (Sleeman et al. 2004).

The Triassic sequence starts with the sandstones of the Sherwood Sandstone Group (equivalent to the Bunter Sandstone), which consists predominantly of sandstone with minor mud- and siltstone (McCann 1990, Cowan 1993, Naylor et al. 2003). The Sherwood Sandstone Group was deposited in continental conditions in a braided fluviatile setting, which resulted in a variety of different depositional facies, such as channel fill (both from a high and low flow regime), floodplain deposits, sheetflood deposits and aeolian facies (Cowan 1993, Mitchell 2004a). The depositional environment gradually changed from a fluviatile depositional setting into a semi-arid, lacustrine environment in which the Mercia Mudstone Group (equivalent to the Keuper Marl) was deposited. This group consists mainly of interbedded mudstone, silty mudstone and siltstone with minor amounts of gypsum and sandstone (McCann 1990, Naylor et al. 2003). Locally, the Mercia Mudstone Group contains thick halite beds, formed due to the evaporation of shallow bodies of saline water that were trapped in restricted basins and underwent continuous replenishment from the marine water of the Tethys ocean (Mitchell 2004a, Sleeman et al. 2004). The Penarth Group (formerly the Rhaetic), consisting mainly of mudstone, was deposited on top of the Mercia Mudstone Group. However, this formation was strongly eroded during the Jurassic and is absent in the boreholes of the Lough Neagh Basin (Mitchell 2004a, Loewer 2011).

4.4 Post-Triassic

The breakup of Pangaea continued throughout the Jurassic and Early Cretaceous, causing extension in Northern Ireland throughout the Early Jurassic during which the mudstones of the Lias were deposited (Mitchell 2004a,c). However, during the Jurassic-Early Cretaceous a ESE-WNW compressive regime affected Northern Ireland and caused a period of minor subsidence and subsequently a period of prolonged uplift and corresponding non-deposition, resulting in an erosional unconformity in the stratigraphic sequences of Lough Neagh Basin (Shelton 1997, Mitchell 2004c). From the Early Cretaceous onwards regional thermal subsidence occurred until the Tertiary (Naylor & Shannon 1999, McCaffrey & McCann 1992, Mitchell 2004c). In the Late Cretaceous a widespread rise in sea level (the Cenomanian transgression) occurred, during which the Ulster White Limestone Formation was deposited, consisting mainly of micrite and chalk. After this transgression Ireland was covered by seas (McCaffrey & McCann 1992, Naylor et al. 2003, Mitchell 2004c).

Another period of uplift occurred in the early Tertiary (Paleocene), followed by NE-SW extension and rifting due to the spreading between Greenland and Eurasia. This rifting resulted in a period of magmatism in Northern Ireland during which the basalt flows of the Antrim Lava Group were deposited (McCaffrey & McCann 1992, Shelton 1997, Cooper 2004). Also associated with this period are intrusions of dolerite in the form of sills and dykes (McCann 1990, McKinley et al. 2001). After the period of magmatism in the Late Paleocene and Eocene, northeast Ireland and the lava plateau were affected by a post-magmatic extensional stress system. In the Oligocene, and subsidence along NNW-SSE trending faults resulted in the deposition of the clays and lignites of the Lough Neagh Group in the Lough Neagh Basin (McCann 1990, Shelton 1997, Mitchell 2004d). During the Miocene, the basin experienced a phase of compression, leading to uplift and erosion (Shelton 1997, Naylor et al. 2003).

4.5 Boreholes and MT survey

In the mid-1950's a period of extensive exploration began in Northern Ireland in search for, amongst others, coal, salt, oil and gas. Exploration included the drilling of boreholes and geophysical surveying and resulted in a number of boreholes in the Lough Neagh and the Larne basins (McCann 1990, Naylor et al. 2003). In this study, data from three deep exploration boreholes located in the north of the Lough Neagh Basin are used: Annaghmore, Ballynamullan and Ballymacilroy (fig. 4.2). Besides the borehole

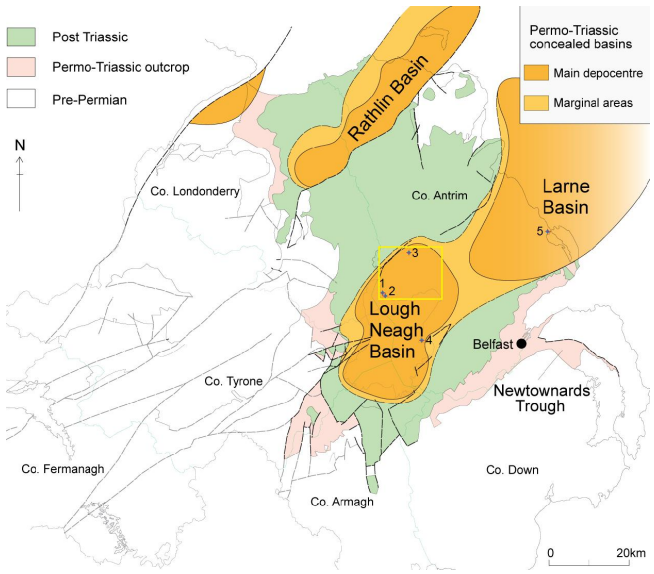

Figure 4.2: Location of sedimentary basins in Northern Ireland, modified from Johnston (2004). The main depocentres of the Lough Neagh Basin and the Larne Basin are separated by an area of sedimentary thinning. Three boreholes (1=Annaghmore, 2=Ballynamullan, 3=Ballymacilroy) are located in the MT survey area (yellow rectangle). For a more detailed overview of the MT survey area see fig. 4.3.

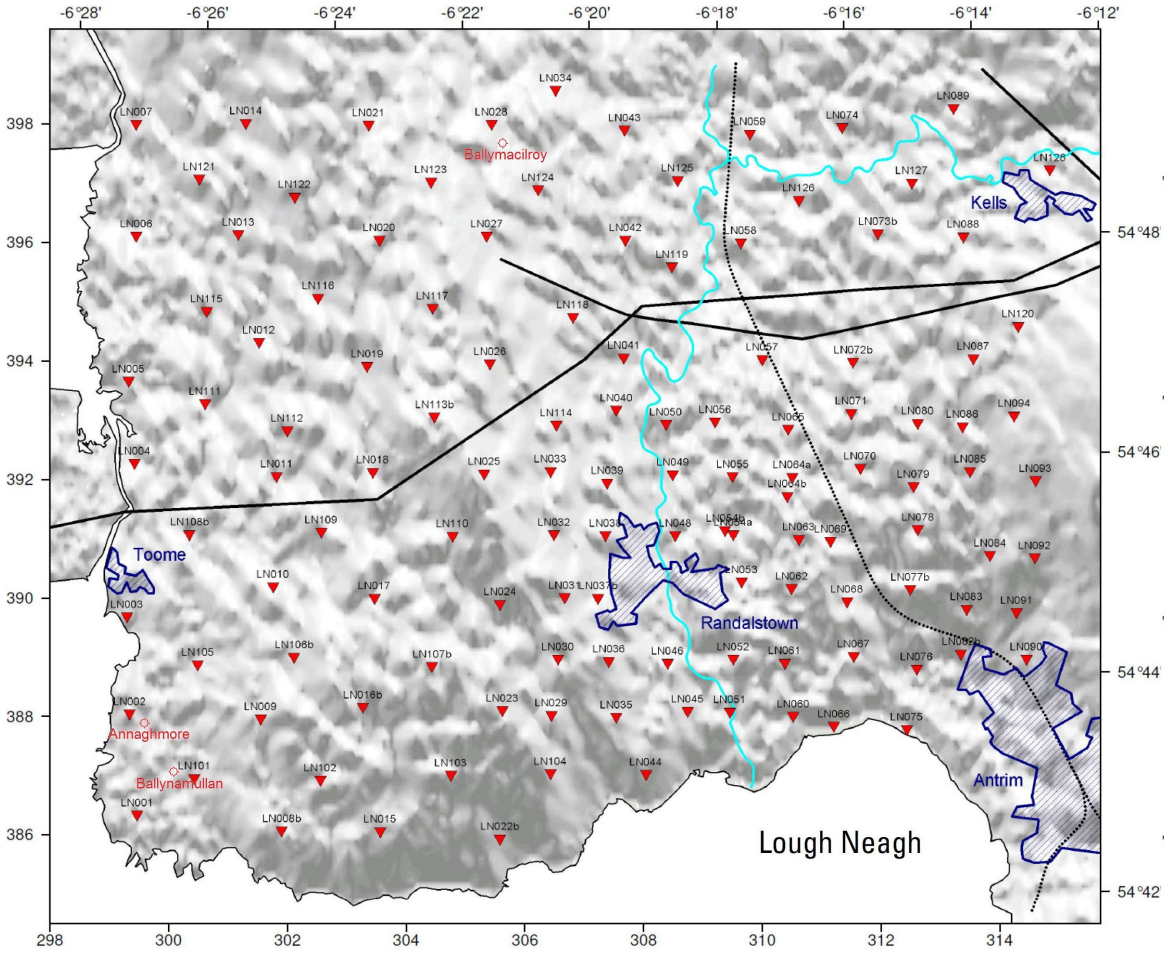

Figure 4.3: MT survey area map, modified from WesternGeco (2009). The map shows the location of 120 MT stations (red triangles) to the north of Lough Neagh. Settlements in the survey area are indicated by the blue areas, the black continuous lines denote power lines and the black dashed line denotes a railway track. The location of three boreholes (Annaghmore, Ballynamullan and Ballymacilroy) are indicated by red circles.

data, MT data from five MT sites are used. These measurements were part of an MT sounding survey with 120 stations located to the north of Lough Neagh. This survey was carried out in 2009 by Western Geco's Land EM group, Geosystem, on behalf of the Geological Survey of Northern Ireland. The MT stations were arranged on a rectangular grid between latitude 54° 42' and 54° 50' N and longitude 6° 12' and 6° 28' W (Loewer 2011). Data from the following stations are used: LN001, LN002, LN028, LN101 and LN124 (fig. 4.2 and fig. 4.3).

The Annaghmore (1993) and Ballynamullan (1994) boreholes were drilled in search for hydrocarbons, operated by Nuevo Energy, and are located at a distance of approximately 1 km from each other. Due to access problems, the Ballynamullan borehole was deviated near the base of the basalt (Naylor et al. 2003). The Ballymacilroy borehole (1979) was drilled to test a possible sub-basin defined by gravity data and is located at 13 km from Annaghmore (McCann 1990, Naylor et al. 2003). The wireline logging was operated by Schlumberger. The Ballymacilroy borehole terminated at a depth of 2272 m, while the Annaghmore borehole reached 1554 m and the Ballynamullan borehole reached a vertical depth (at Kelly Bushing) of 1371 m (and 1478 m measured depth) (Loewer 2011).

A detailed account of the stratigraphy encountered at Annaghmore, Ballynamullan and Ballymacilroy is given by Naylor et al. (2003), who based their account on borehole reports and wireline logs. Naylor et al. (2003) used recognized formal stratigraphical names where possible. Thus the well-established Sherwood Sandstone Group and Mercia Mudstone Group were used for the Triassic section, while the terms Belfast Group and Enler Group were used for the Permian section. However, Naylor et al. (2003) also introduced local names for some of the lower-rank units of the Annaghmore and the Ballynamullan boreholes. For the Ballymacilroy borehole the old terminology is used (fig. 4.4).

The youngest rocks observed in the boreholes are the basalts of the Antrim Lava Group, which overlie the Ulster White Limestone Formation (McCaffrey & McCann 1992, Naylor et al. 2003). This formation is followed by the mudstones of the Lias and the Penarth Group. These mudstones, however, are eroded off at several locations during uplift later in the Jurassic and therefore are locally absent (McCann 1990, Naylor et al. 2003). Next comes the Triassic Mercia Mudstone Group. Note that in the Lough Neagh Basin the thick halite zones of the Mercia Mudstone Group, encountered in the Larne Basin, are absent (McCann 1990, Naylor & Shannon 1999). Underlying the Mercia Mudstone Group is the Sherwood Sandstone Group, in which Naylor et al. (2003) distinguish between the top part (the Toomebridge Sandstone

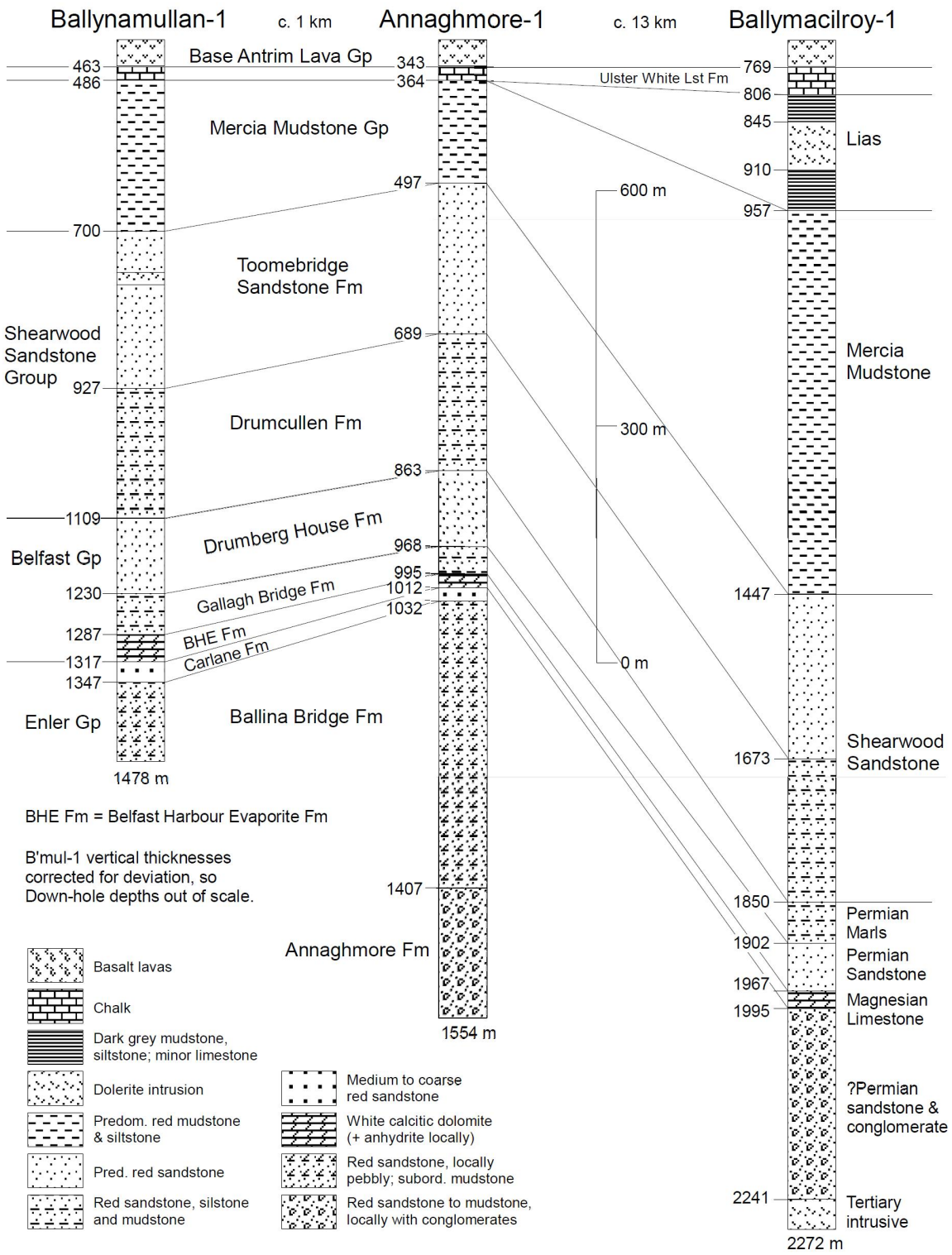

Figure 4.4: Stratigraphy and correlation of the Annaghmore, Ballynamullan and Ballymacilroy boreholes, modified from Naylor et al. (2003). The depths are in measured depth and the thicknesses in the column for the Ballynamullan borehole have been corrected for borehole deviation.

Formation) and the lower part (the Drumcullen Formation). Where the top part consists predominantly of weakly cemented sandstones, the lower part is characterized by intercalated shaly beds, has a higher mudstone content and a higher proportion of cemented sandstone. A similar distinction was noted at

Ballymacilroy (Naylor et al. 2003). Following the Sherwood Sandstone Group is the Belfast Group. The upper part of the Belfast Group consists of an argillaceous, calcareous sandstone unit (the Drumderg House Formation), which generally has been known as the Permian Marls (McCann 1990, Naylor et al. 2003). Immediately beneath this unit a sandstone formation has developed, known as the Gallagh Bridge Formation or the (Upper) Permian Sandstone, that lies on top of the Belfast Harbour Evaporite Formation, previously referred to as Magnesian Limestone (Naylor et al. 2003). The top part of the underlying Enler Group consists of a relatively clean sandstone formation (the Carlane Sandstone Formation). This formation may have a thin equivalent at Ballymacilroy and would previously have been referred to as the (Lower) Permian Sandstone (Naylor et al. 2003). The sandstones grade down into coarser material, consisting of sandstones and occasionally breccias and conglomerates (McCann 1990, Naylor et al. 2003). Annaghmore and Ballynamullan both terminate in Permian strata, while the Ballymacilroy borehole terminates in intrusive of probably Tertiary age. Since no boreholes in the Lough Neagh Basin penetrated pre-Permian rocks and obtaining high-quality seismic reflection data is difficult due to the basalts of the Antrim Lava Group that cover most of the basin, the nature and distribution of Carboniferous rocks is largely unknown (Naylor et al. 2003). However, Carboniferous rocks have been observed in boreholes in Northern Ireland and as outcrops in the Midland Valley, indicating that a thick and extensive sequence of Carboniferous rocks was deposited in the Midland Valley (Illing & Griffith 1986, McCann 1991, McCaffrey & McCann 1992, Naylor & Shannon 1999).

4.6 Geothermal potential

At first, geophysical exploration in Northern Ireland focused mainly on hydrocarbons. The Lough Neagh Basin and the Larne Basin contained a number of potential hydrocarbon plays, with the best-defined plays within the Permian and Triassic rocks. In the Triassic sequences the reservoir rocks of the Sherwood Sandstone Group are sealed by the Mercia Mudstone Group, while in the Permian play the Belfast Harbour Evaporite Group caps Enler Group reservoir rocks. Both plays rely on an underlying Carboniferous source. However, although minor gas shows have been detected in the Newmill and Larne No. 2 boreholes of the Larne Basin and oil-staining was found in the Annaghmore borehole of the Lough Neagh Basin, hydrocarbons have not been discovered in commercial quantities (Naylor & Shannon 1999, Reay 2004). Naylor & Shannon (1999) argue that this is due to unfavorable timing of hydrocarbon generation

and trap formation, combined with poor preservation of regional source rock. In the Larne Basin and the Lough Neagh Basin the main phases of hydrocarbon generation probably occurred in late Carboniferous and Early Jurassic times, possibly pre-dating the formation of some traps. Also, the distribution of Carboniferous source rocks beneath the basin is largely unknown, and the possibility that they may be limited in extent is a significant exploration risk (Naylor & Shannon 1999, Naylor et al. 2003).

Although the search for hydrocarbons proved unsuccessful, later research indicated that the Larne and Lough Neagh basins have a potential for geothermal energy exploitation, as the Permian and Triassic sandstones of the Lower Permian Sandstone and the Sherwood Sandstone Group form potential low-enthalpy geothermal reservoirs (Pasquali et al. 2010, Loewer 2011). In the Geothermal Energy Review of Northern Ireland study, which was completed in 2005, a series of temperatures were modeled for different boreholes, including the Annaghmore and Ballymacilroy boreholes. Based on the lithologies encountered in the boreholes and the temperature profiles recorded subsequent to the completion of the drilling, temperatures were modeled at depths of 1000 m, 1500 m, 2000 m and 2500 m (fig. 4.5).

BOREHOLE NAME	T (°C) at 1000m	T (°C) at 1500m	T (°C) at 2000m	T (°C) at 2500m
Annaghmore No. 1	42.33	53.33	64.33	75.33
Ballymacilroy No. 1	49.28	62.00	74.00	85.00
Ballytober No. 1	37.50	51.50	66.00	80.00
Big Dog No. 1	33.89	45.60	57.40	69.20
Glenoo No. 1	33.50	43.00	52.50	61.50
Kilcoo Cross No. 1	35.00	46.50	57.00	68.00
Killary Glebe No. 1	39.60	51.00	61.00	71.50
Langford Lodge	43.00	56.00	68.00	80.00
Larne No. 2	43.00	51.00	60.50	70.00
Newmill No. 1	31.00	34.10	50.50	59.90
Owengarr No. 1	38.00	43.50	52.50	63.00
Port More No. 1	45.50	62.80	82.00	99.50
Slisgarrow No. 1	39.00	50.00	57.80	69.50
Wind Farm No. 1	27.00	40.50	54.50	68.50

Figure 4.5: Modeled temperatures at specific depths for a number of boreholes (Pasquali et al. 2010).

From the results temperatures were predicted for the Annaghmore and Ballymacilroy boreholes that lie between 40 °C and 85 °C for the depth range between 1000 m and 2500 m. This, in combination with the geothermal gradient of approximately 30 °C/km indicates a good geothermal exploitation potential (Pasquali et al. 2010, Loewer 2011). Additionally, Pasquali et al. (2010) performed a study in which the geothermal energy potential of potential geothermal reservoirs was analyzed, focusing on the Lower Permian Sandstone and the Sherwood Sandstone Group of the sedimentary basins of Northern Ireland. Based on rock property parameters such as mean temperature, porosity and specific heat capacity, the total geothermal energy stored in the reservoirs was calculated based on the volumetric method (Muffler &

Cataldi 1978). For the purpose of this calculation, the volume of rock was assumed as being the thickness of the formation over a 22.5 km^2 area, which is considered the normal radius of influence of a geothermal well doublet of a period of 25 years of production (Pasquali et al. 2010). The results show that the total energy stored in the Sherwood Sandstone Group at Ballymacilroy is approximately 1 GWh (fig. 4.6). It is important to note that the northeastern and southwestern areas of Lough Neagh have been identified as the main depocentres in the Lough Neagh Basin. However, the boreholes of the Lough Neagh Basin are located away from the main depocentres and no additional data are available for these areas. Therefore, no temperatures and/or geothermal energy potential was modeled/calculated for the main depocentres of the Lough Neagh Basin, which are likely to contain thicker sedimentary sequences than the areas that have been tested (Pasquali et al. 2010). More recently, Loewer (2011) used MT and gravity data in order to assess the potential of the geothermal reservoirs. Loewer (2011) concluded that the Sherwood Sandstone Group is the most electrically conductive feature in the basin, implying high porosity and permeability values.

Formation Ranking	Site Location Rank	Site Location	Lithology	Reservoir Thickness (m)	Base of Geothermal Target Formation (m)	Total Energy Stored in the Reservoir (MW h)
1	1	Larne	Lwr. Permian Sandstone	900	2800	**2274.70**
	2	Ballymoney	Lwr. Permian Sandstone	500	2200	**1073.33**
	3	Magheramorne	Lwr Permian Sandstone	250	2200	**528.84**
	4	Antrim	Lwr. Permian Sandstone	200	2200	**378.22**
2	1	Port More	Sherwood Sandstone	680	1830	**1456.08**
	2	Magheramorne	Sherwood Sandstone	650	1600	**1281.96**
	3	Ballymacilroy	Sherwood Sandstone	420	1870	**983.50**
	4	Ballymoney	Sherwood Sandstone	500	1400	**951.69**
	5	Antrim	Sherwood Sandstone	400	1600	**761.35**
	6	Langford Lodge	Sherwood Sandstone	270	1515	**446.12**
	7	Larne	Sherwood Sandstone	650	1615	**439.53**
3	1	North West Basin	Carboniferous Basal Sandstone	150	2000	**318.65**

Figure 4.6: Calculated values for the total geothermal energy stored in the reservoirs per borehole (Pasquali et al. 2010). The total geothermal energy was calculated based on the volumetric method (Muffler & Cataldi 1978). The volume of rock was assumed as being the thickness of the formation over a 22.5 km^2 area.

PART 2

METHODS AND RESULTS

5 Borehole data analysis

The objective of the borehole data analysis is to determine average values for the electrical resistivity, the porosity and the permeability of the upper part of the Sherwood Sandstone Group (or Toomebridge Sandstone Formation). The borehole data are made available by the Geological Survey of Northern Ireland and comprise wireline logging data and core sample data. Wireline logging data are available from three boreholes: Annaghmore, Ballynamullan and Ballymacilroy. Core sample data, consisting of 28 effective porosity and horizontal intrinsic permeability measurements, are only available for the upper part of the Sherwood Sandstone Group in the Ballymacilroy borehole. In this borehole samples were taken between 1524 and 1548 m (measured depth) at regular three foot intervals.

The wireline logging data are evaluated and modeled using Interactive Petrophysics (IP) software in order to determine the porosity and the permeability of the rock formations. Since the formations of interest are the sand- and mudstone formations, only these are analyzed here. Evaporite formations and dolerite intrusions present in the boreholes are not included in this analysis. Standard deterministic evaluation techniques are applied using the available wireline logging data in order to produce porosity curves. For this the following logs are used: the gamma ray (GR) log, the neutron (NHPI) log, the density (RHOB) log, the deep induction resistivity (ILD) log, the caliper (CALI) log and the sonic (DT) log. Estimates of the porosity from the wireline logging data are subsequently checked against core sample measurements. Since it is not possible to determine the permeability directly from the logging data, an independent empirical porosity-permeability relationship is derived from core sample measurements in the upper part of the Sherwood Sandstone Group in the Ballymacilroy borehole. This relationship is then applied to the porosity curves in IP for the same formation in all three boreholes in order to produce permeability curves. Finally, Monte Carlo simulation is used to investigate the impact of uncertainties in the input data on the calculated results.

5.1 Available data, loading and QC

The wireline logging data comprise digitized log data in LAS format and a number of different reports containing zone tops and well deviation data. However, very limited information is available for the drilling mud properties (i.e. temperature and resistivity). For all three boreholes, the log data comprise part of the Mercia Mudstone Group, the complete Sherwood Sandstone Group and a large part of the

underlying Permian strata.

The wireline logging data are loaded into an IP database and the data from subsequent log runs are spliced together. The zone tops used are based on the stratigraphy described by Naylor et al. (2003) (fig. 4.4), who provided a detailed account of the stratigraphy of the Annaghmore, Ballynamullan and Ballymacilroy boreholes based on borehole reports and wireline logs. See appendix A for an overview of the stratigraphy of each borehole as defined in IP. As the available borehole data contain no temperature data, a temperature log is created based on Pasquali et al. (2010), who modeled a series of temperatures for a number of boreholes, including Annaghmore and Ballymacilroy, based on temperature profiles recorded subsequent to the completion of drilling (fig. 4.5). As the Ballynamullan borehole was not included in the research of Pasquali et al. (2010), the temperature log of Annaghmore is also used for Ballynamullan, since the boreholes are located less than 1 km from each other. Finally, deviation data are used to calculate a true vertical depth curve for the Ballynamullan borehole.

The Ballynamullan borehole encountered two dolerite intrusions that affect the log data: the first intrusion is located in the Sherwood Sandstone Group between 763.4 and 779.7 m and the second intrusion is located at the base of the Drumderg House Formation between 1229.2 and 1230.8 m. The logs of the Ballymacilroy borehole contain two zones where the quality of the logs is such that reliable interpretation is deemed impossible and the logs are nullified: the first zone lies in the Sherwood Sandstone Group between depths of 1474.9 and 1495.4 m and the second zone lies in the Gallagh Bridge Formation between 1912.4 and 1939.6 m. Note that all these depths are in measured depth.

5.2 Producing porosity curves

In IP, standard deterministic evaluation techniques are used to produce porosity curves based on the wireline logging data. There are, however, several formation characteristics, in addition to porosity, that affect the log responses (e.g. clay volume, formation water resistivity, clay resistivity, water saturation). In the standard deterministic evaluation approach these formation characteristics are determined beforehand and taken into account when calculating the porosity curves. This approach consists of two modules: the clay volume module and the porosity and water saturation module. Although the two modules are used separately, they are linked so that they don't function independently. This link ensures that the same zones, zone depths and zone names are used in both modules and that the parameters that occur in both

modules are linked, i.e. if a value is changed in one module it will automatically be changed in the other module.

5.2.1 Clay volume calculation

First, the clay volume module is used to calculate clay volume curves. In this module the clay volume is calculated based on two different methods, using a single clay indicator, in which a single wireline log is used to determine the clay volume, and using double clay indicators, which are cross-plot combinations of two wireline logs used to determine the clay volume.

For the single clay indicator the gamma ray log is used. The clay volume is then calculated using the following linear relationship:

$$VCLGR = \frac{Gr - GrClean}{GrClay - GrClean}, \tag{54}$$

where Gr: input from the gamma ray log, $GrClay$: gamma ray value in a 100 % clay zone, $GrClean$: gamma ray value in a clean (i.e. clay-free) zone and $VCLGR$: the gamma ray indicator clay volume. The gamma ray values for a 100 % clay zone and a clay-free zone are determined based on the wireline logging data, using the clay volume module interactive plot (fig. 5.1).

For the double clay indicators the neutron and density logs are used. The double clay indicators work on the principle of defining two clean points and a clay point, with the clean points defining the neutron and density values in a clean, clay-free zone and the clay point defining the neutron and density values in a 100 % clay zone (fig. 5.2). The clay volume then is calculated using:

$$VCLND = \frac{\begin{array}{c}(NDDenClean2 - NDDenClean1) \times (Neu - NDNeuClean1) - \\ (Den - NDDenClean1) \times (NDNeuClean2 - NDNeuClean1)\end{array}}{\begin{array}{c}(NDDenClean2 - NDDenClean1) \times (NDNeuClay - NDNeuClean1) - \\ (NDDenClay - NDDenClean1) \times (NDNeuClean2 - NDNeuClean1)\end{array}}, \tag{55}$$

where Den: input from the density log, $NDDenClay$: density value for the clay point, $NDNeuClay$: neutron value for the clay point, $NDDenClean1$ and $NDDenClean2$: density values for clean point 1 and clean point 2 respectively, $NDNeuClean1$ and $NDNeuClean2$: neutron values for clean point 1 and clean point 2 respectively, Neu: input from the neutron log and $VCLND$: the neutron-density indicators clay

volume. The density and neutron values for the clean points and the clay point are determined based on the wireline logging data, using the clay volume module interactive plot (fig. 5.1) and the neutron-density cross-plot (fig. 5.2). See appendix B for the clay volume module interactive plot of each borehole.

For a reliable clay volume calculation it is expected that the clay volumes calculated using the single and double clay indicators are in strong agreement. However, at some places in the Drumderg House Formation in the Annaghmore well the clay volume calculated using the double clay indicators differs significantly from the clay volume calculated by the single clay indicator. Additionally, the caliper log shows substantial washout in this area. Therefore, for this formation the caliper log is used as a bad hole indicator, switching off the double clay indicators for caliper log values larger than 9.5 inch.

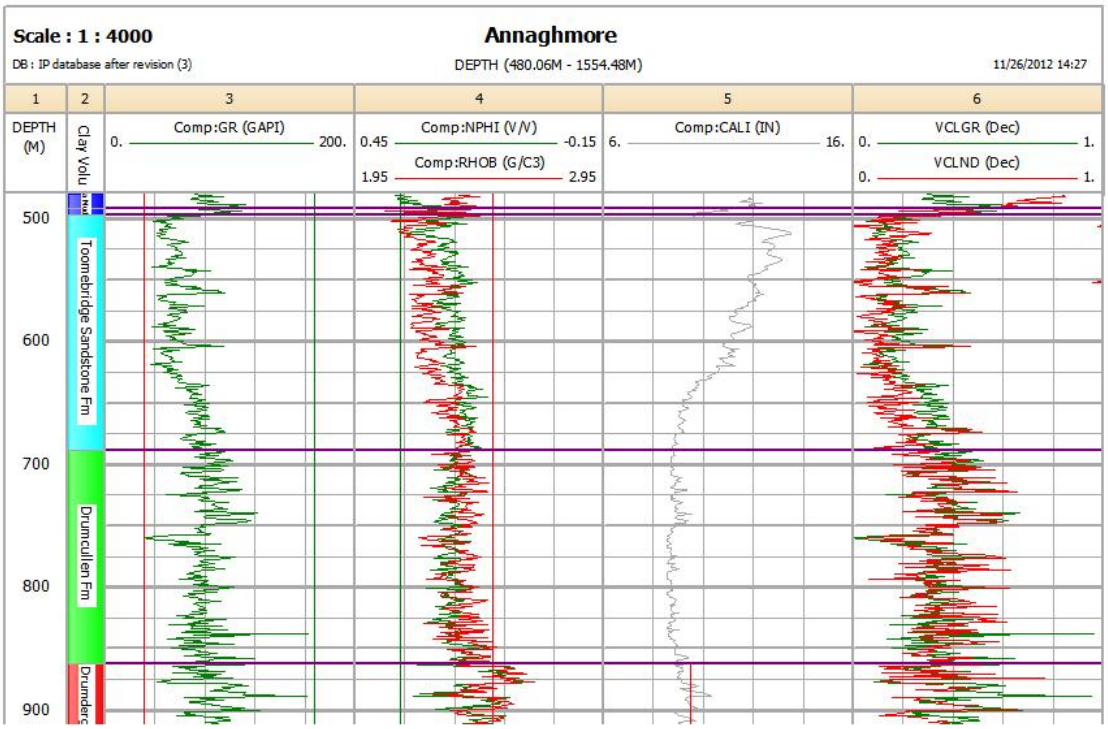

Figure 5.1: The clay volume module interactive plot for a part of the stratigraphy of the Annaghmore well. The first track shows the measured depth, the second track shows the stratigraphy, the third track is the single clay indicator track showing the gamma ray (GR) log, the fourth track is the double clay indicators track showing the neutron (NPHI) and the density (RHOB) logs, the fifth track shows the caliper (CALI) log and the sixth track shows the clay volume curves calculated from the single clay indicator ($VCLGR$; green line) and the double clay indicators ($VCLND$; red line). Note that for each log/curve the units are specified in the figure. By positioning the straight, vertical green and red lines in the single clay indicator track and the double clay indicators track the values of parameters used to calculate the clay volume are determined. In the single clay indicator track the green line defines the $GrClay$ value, while the red line defines the $GrClean$ value. In the double clay indicators track the green and red lines define the values of $NDNeuClay$ and $NDDenClay$ respectively.

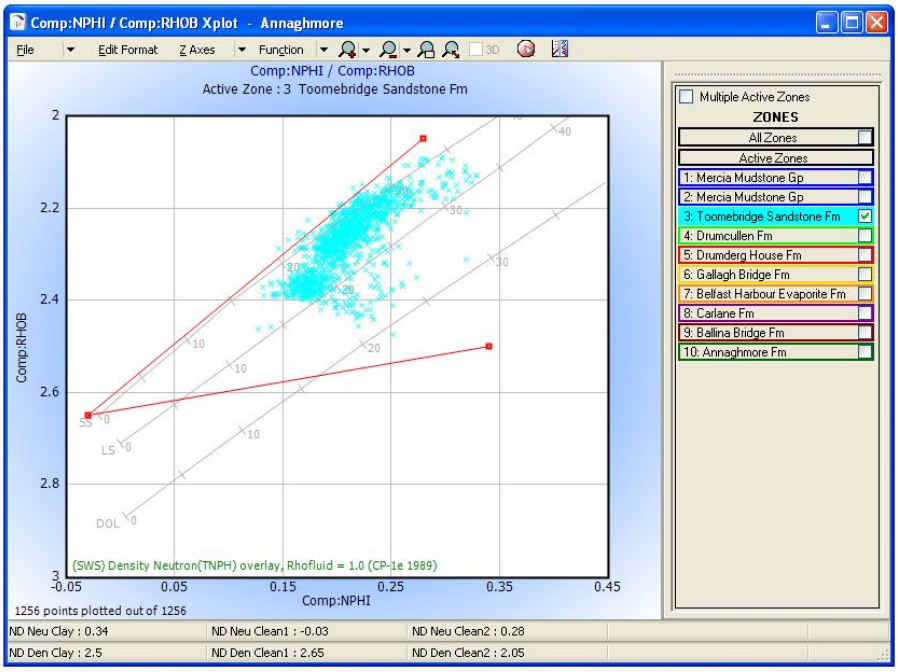

Figure 5.2: Example of the neutron (NHPI)-density (RHOB) cross-plot, with the neutron log values on the x-axis (in v/v) and the density log values on the y-axis (in g/cc). In this example the data for the Toomebridge Sandstone Formation of the Annaghmore well are shown (blue data points). The three red points in the cross-plot indicate clean point 1 (far left), clean point 2 (top) and the clay point (far right), with the red line connecting clean point 1 and clean point 2 indicating the clean formation line. By determining the positions of these three points the values of parameters used to calculate the clay volume are determined. The grey lines are empirically obtained clean formation lines for sandstone (SS), limestone (LS) and dolomite (DOL).

Next, the clay volumes determined by the single and double clay indicators are used to produce a number of final clay volume curves (i.e. minimum clay volume, average clay volume and clay volume mixed). By default, the curve used in the second module (the porosity and water saturation module) is the minimum clay volume (VCL) curve, which is determined by taking the minimum value of the two evaluation methods (i.e. the single clay indicator and the double clay indicators) at each depth and clipping the curve to be between 0 and 1. The resulting minimum clay volume curves are used in order to define the mean clay volume of the upper part of the Sherwood Sandstone Group. This gives mean clay volumes of 14 % (Annaghmore), 19 % (Ballynamullan) and 17 % (Ballymacilroy).

An overview of the clay volume module parameter values utilized for the Upper Sherwood Sandstone Group/Toomebridge Sandstone Formation is given in appendix C.

5.2.2 Porosity calculation

When the final clay volume curves are determined, the porosity and water saturation module is used to calculate the porosity. In this module values for, amongst others, the flushed zone water saturation (Sxo)

and the effective porosity ($PHIE$) are determined. Since the flushed zone water saturation is necessary to calculate the effective porosity and vice versa, an iterative process is used. The iteration loop is started by assuming a value for Sxo of 1.0 and continues until the difference between iterations in $PHIE$ is less than 0.001 and the difference between iterations in Sxo is less than 0.002.

Before the iterative process is started, the following parameters are calculated automatically: the mud filtrate salinity ($SalinSxozone$), the mud filtrate density ($RhoSxozone$), the hydrocarbon hydrogen index ($NeuHcHI$) and the apparent hydrocarbon density ($DenHcapp$). These parameters are calculated using the temperature log, the mud filtrate resistivity (Rmf) and the hydrocarbon density ($HcDen$). For Rmf the default value of 0.1 is used, as no data are available for the mud filtrate resistivity, while for $HcDen$ a standard value of 0.2 is used (IFTechnology 2012). The equations that are used in these calculations are stored in appendix D.1.

The iterative process starts with calculating the effective porosity, using the neutron-density porosity model in combination with the variable matrix grain density logic. By using the variable matrix grain density logic IP first determines, based on the matrix grain density ($RhoGD$), whether the sandstone/limestone or limestone/dolomite model is used (note that $RhoGD$ is the same as the $NDDenClean1$ parameter of the clay volume module and its value thus follows from the analysis performed in the clay volume module). If $RhoGD$ is greater than 2.71 g/cc the model will be limestone/dolomite, while if $RhoGD$ is less than 2.71 g/cc the sandstone/limestone model is selected. Here, the sandstone/limestone model is selected, since for $RhoGD$ a standard value of 2.65 g/cc is assumed (IFTechnology 2012). Next, the sandstone/limestone model is used to calculate four porosities, which are calculated by applying both the density porosity model (equation 57) and the neutron porosity model (equation 58) on the two matrices of the sandstone/limestone model. For the sandstone matrix a value for $RhoGD$ of 2.65 g/cc is utilized, while for the limestone matrix a $RhoGD$ value of 2.71 g/cc is used. From these four porosities the effective porosity ($PHIE$) is calculated as follows:

$$PHIE = \phi_{D1} + \frac{\phi_{N1} - \phi_{D1}}{1 - (\phi_{N1} - \phi_{N1})/(\phi_{D1} - \phi_{D2})}, \tag{56}$$

where ϕ_{D1} and ϕ_{D2} are the density porosities for matrix 1 and matrix 2 and ϕ_{N1} and ϕ_{N2} are the neutron porosities for matrix 1 and matrix 2, respectively. Once $PHIE$ is calculated, $RhoGD$ is recalculated using the density porosity model. Therefore, the input value for $RhoGD$ can be different than the output value.

The output value for $RhoGD$ must fall within the limits set for the matrix grain density, $RhoGDmin$ and $RhoGDmax$, with respective values of 2.6 and 2.85 g/cc (IFTechnology 2012). If not, the output value for $RhoGD$ is set to its limit and $PHIE$ is recalculated by calculating the porosity using the density porosity model and the neutron porosity model and taking the minimum porosity value of these two models.

The density porosity model calculates the porosity (ϕ) using the following equation:

$$\phi = \frac{RhoGD - Den - VCL \times (RhoGD - RhoWetClay)}{RhoGD - RhoSxozone \times Sxo - DenHcapp \times (1 - Sxo)}, \tag{57}$$

where $RhoWetClay$ is the wet clay density and VCL is the clay volume as given by the minimum clay volume curve in the clay volume module. Note that $RhoWetClay$ is the same as the $NDDenClay$ parameter of the clay volume module and its value thus follows from the analysis performed in the clay volume module.

When using the neutron porosity model the porosity is calculated as follows:

$$\phi = \frac{Neu - VCL \times NeuWetClay + Neumatrix + Exfact + NeuFormSal}{Sxo + (1 - Sxo) \times NeuHcHI}, \tag{58}$$

$$Exfact = \left(\frac{RhoGD}{2.65}\right)^2 \times (2 \times Swx \times {\phi_x}^2 + 0.04 \times \phi_x) \times (1 - Swx), \tag{59}$$

$$\phi_x = \phi + VCL \times NeuWetClay, \tag{60}$$

$$Swx = \frac{\phi \times (Sxo + (1 - Sxo) * NeuHcHI) + VCL \times NeuWetClay}{\phi_x}, \tag{61}$$

where $Exfact$: the neutron excavation factor, $NeuFormSal$: the neutron formation salinity correction, $Neumatrix$: the neutron matrix correction and $NeuWetClay$: the wet clay neutron value. The neutron formation salinity correction value is automatically calculated from the Neutron Tool look-up table that is defined for a particular neutron logging tool. Also, since a value for $RhoGD$ is given, the neutron matrix correction parameter is overridden by the $RhoGD$ value. The $NeuWetClay$ parameter is the same as the $NDNeuClay$ parameter of the clay volume module and its value thus follows from the analysis performed

in the clay volume module.

When $PHIE$ is calculated, several limitations are applied to the $PHIE$ curve. First, the density log is used as a bad hole indicator. For intervals where the value of the density log is smaller than 2.2 g/cc, the porosity is calculated using the sonic porosity model. The resulting sonic porosity then acts as the effective porosity limit, i.e. $PHIE$ is less than or equal to the porosity resulting from the sonic porosity model. See appendix D.2 for the equations and parameters used in the sonic porosity model. Secondly, for intervals where the value of the minimum clay volume curve is larger than the cutoff value of 0.4 a maximum $PHIE$ value is determined ($PHIlimit$). For these intervals $PHIE$ is less than or equal to $PHIlimit$. Also, for these intervals the cementation exponent (see equation 63) is recalculated. The equations used to calculate $PHIlimit$ and to recalculate the cementation exponent are stored in appendix D.3. After the limitations are applied to the $PHIE$ curve the total porosity ($PHIT$) is calculated as follows:

$$PHIT = PHIE + VCL \times PhiTClay, \tag{62}$$

where $PhiTClay$ is the total porosity clay, for which a standard value of 0.1 is used (IFTechnology 2012).

When the total porosity is calculated, the effective water saturation (Sw) is calculated using the Indonesian saturation equation, which is given by:

$$\frac{1}{\sqrt{Rt}} = \sqrt{\frac{PHIE^m}{a \times Rw} + \frac{VCL^{(1-VCL/2)}}{\sqrt{ResClay}}} \times Sw^{n/2}, \tag{63}$$

where a: tortuosity factor, m: cementation exponent, n: saturation exponent, $ResClay$: clay resistivity, Rt: input from the deep induction resistivity log and Rw: formation water resistivity. The tortuosity factor is assumed to be 1, following Worthington (1993) and Mavko et al. (1998), while for the saturation exponent a value of 2 is used, following Khalil & Santos (2009). The values for the cementation exponent, the formation water resistivity and the clay resistivity are based on the wireline logging data. The cementation exponent and the formation water resistivity values are determined using the deep induction resistivity-total porosity cross-plot (fig. 5.3), while the value for the clay resistivity is determined using the wet clay volume-deep induction resistivity cross-plot (fig. 5.4).

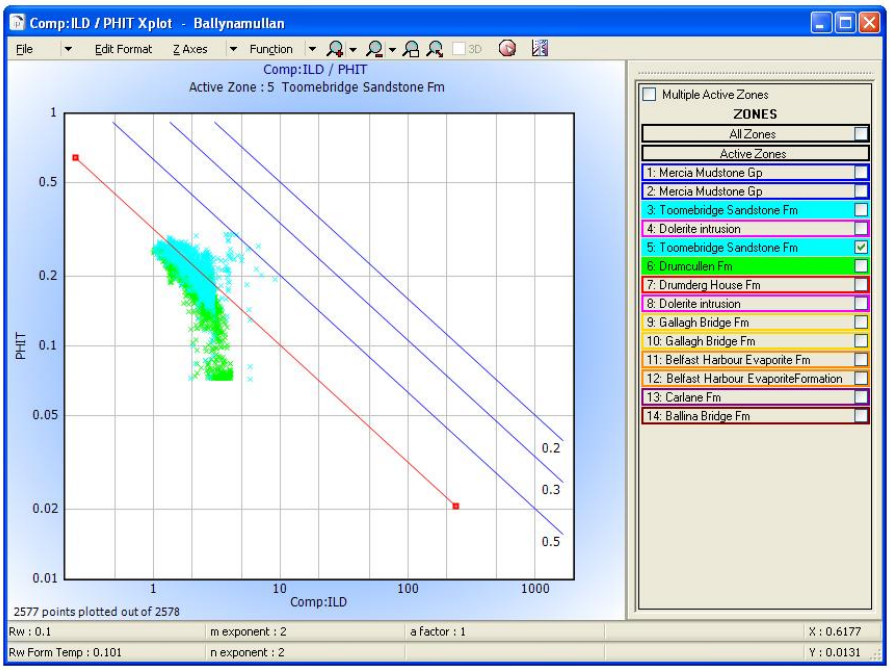

Figure 5.3: Example of the deep induction resistivity (ILD)-total porosity ($PHIT$) cross-plot (or Pickett plot), with the deep induction resistivity on the x-axis (in Ωm) and the total porosity on the y-axis (in decimals). The cross-plot shows data from the Toomebridge Sandstone Formation (blue data points) and the Drumcullen Formation (green data points) of the Ballynamullan well. By shifting the red points to match the data the formation water resistivity (Rw) and the cementation exponent (m) can be determined per stratigraphic formation, based on the selected saturation equation. The blue lines give the resistivity-total porosity relation for different degrees of water saturation (0.5 corresponds to 50 % water saturation etc.).

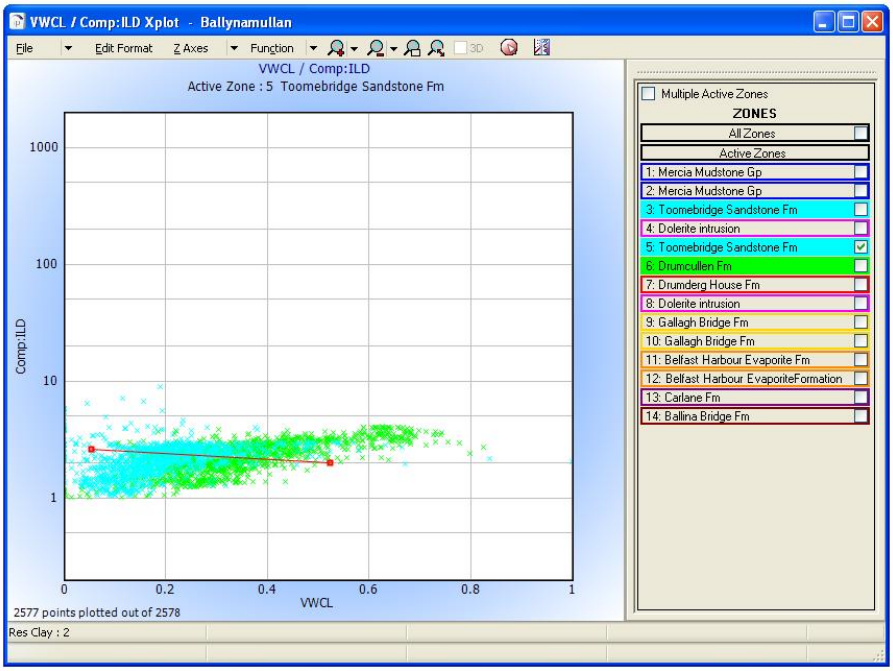

Figure 5.4: Example of the wet clay volume ($VWCL$)-deep induction resistivity (ILD) cross-plot, with the wet clay volume (in decimals) on the x-axis and the resistivity (in Ωm) on the y-axis. Note that, by default, the minimum clay volume (VCL) curve, calculated in the clay volume module, is used as the wet clay volume curve. The cross-plot shows data from the Toomebridge Sandstone Formation (blue data points) and the Drumcullen Formation (green data points) of the Ballynamullan borehole. By shifting the red points to match the data the clay resistivity ($ResClay$) can be determined per stratigraphic formation, based on the selected saturation equation.

Next, the flushed zone water saturation (Sxo) is derived from the effective water saturation, using:

$$Sxo = \frac{Sw + Invasionfactor}{1 + Invasionfactor}. \tag{64}$$

For the $Invasionfactor$ a value of 1 is used (IFTechnology 2012). For the final Sxo curve the following limit applies: $Sxo \leq Sw^{Sxolimit}$, with $Sxolimit$ having a value of 0.2.

The calculation and limitation of the Sxo curve is the final step of the iteration loop. The iteration continues until the difference between iterations in $PHIE$ is less than 0.001 and the difference between iterations in Sxo is less than 0.002. When the iteration is finished, some final calculations are made, which include calculation of the bulk volume water (BVW) curve and the silt volume ($VSILT$) curve, both of which are displayed in the porosity and water saturation interactive plot (fig. 5.5).

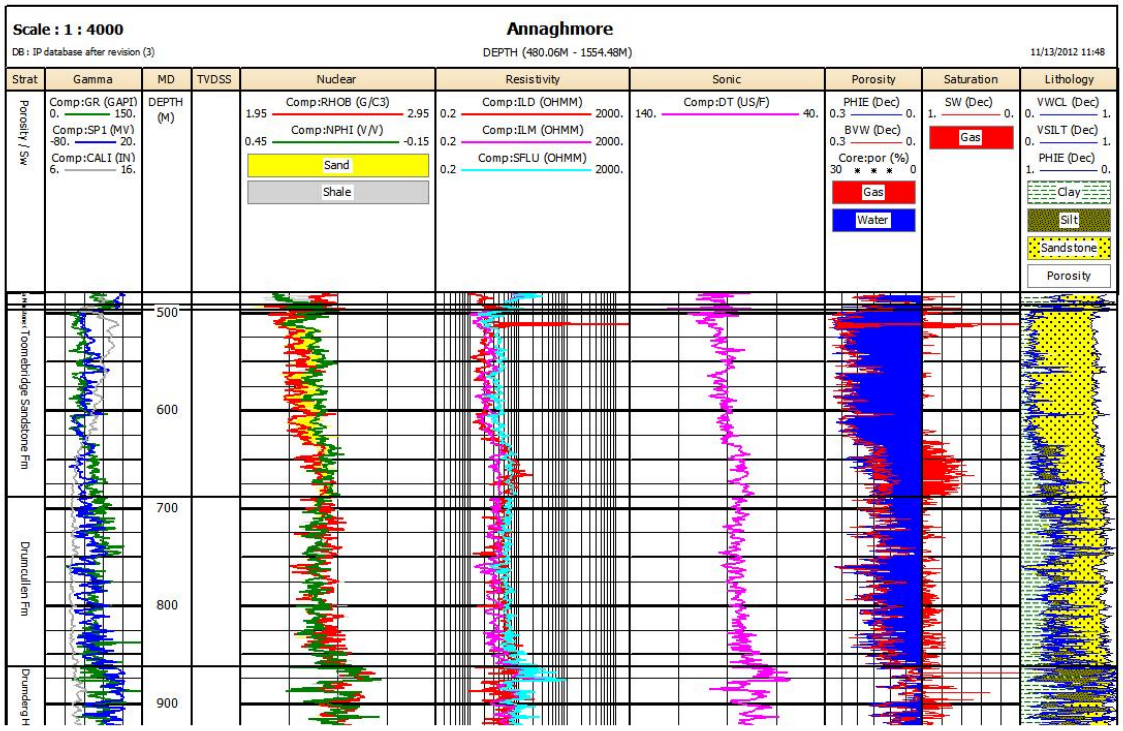

Figure 5.5: The porosity and water saturation module interactive plot for the Annaghmore well, showing the same part of the stratigraphy shown in fig. 5.1. The interactive plot displays the following wireline logs: the gamma ray (GR) log, the spontaneous potential (SP1) log, the caliper (CALI) log, the density (RHOB) log, the neutron (NPHI) log, the deep induction resistivity (ILD) log, the medium induction (ILM) log, the spherically focused resistivity (SFLU) log and the sonic (DT) log. The following output curves are displayed in the interactive plot: the effective porosity ($PHIE$) curve, the bulk volume water (BVW) curve, the effective water saturation (SW) curve, the wet clay volume ($VWCL$) curve and the silt volume ($VSILT$) curve. The output curves can be used for interpretation, as can be seen in the lithology track of the interactive plot, where the clay volume curve, the silt volume curve and the effective porosity curve are used to display the proportion of clay, silt, sandstone and porosity of the total rock.

See appendix D.4 for the equations used for calculation of the BVW and $VSILT$ curves. The porosity and water saturation interactive plot of each borehole is stored in appendix E and the porosity and water saturation module parameter values utilized for the Upper Sherwood Sandstone Group/Toomebridge Sandstone Formation are given in appendix F.

Finally a crosscheck of the porosity calculation is performed by comparing the porosity calculated from the neutron-density porosity model with that calculated only from the density porosity model or the sonic porosity model. The porosities calculated using the three different methods are in good agreement with each other, validating the resulting porosity curves.

5.3 Core sample data and permeability curves

Appendix G gives the results of the core measurements from the upper part of the Sherwood Sandstone Group in the Ballymacilroy borehole. The results show that over a depth interval of approximately 45 m the permeability values vary significantly. The core sample data are loaded into IP and corrected for the compaction effect of the overburden. A compaction factor of 0.95 is applied to the porosity measurements and the Juhasz compaction correction is applied to the permeability measurements (Juhasz 1986). After the correction for the overburden, a depth shift of approximately 1.5 m is applied to the core sample data in order to match the core measurements with the wireline logging data.

After the overburden correction and the depth shift, the core porosity measurements are used as a QC for the effective porosity curves produced in IP, by plotting the core porosity measurements against the values of the effective porosity curve at corresponding depths and determining the best-fitting relation using reduced major axis regression (RMA) (fig. 5.6). The cross-plot shows that, even though there is a degree of scatter, the best-fitting relation has a slope close to 45 °, indicating good agreement between the porosity values from the core sample data and the porosity values calculated from the wireline logging data.

Next, a porosity-permeability relation is determined, outside IP, based on the core sample data. Using RMA software (Bohonak 2004), a porosity-permeability relation is produced and values for the 95 % confidence interval are determined (fig. 5.7). The resulting porosity-permeability relation is given by:

$$Permeability(mD) = exp(-7.67 + 64.782 \times porosity(dec)). \tag{65}$$

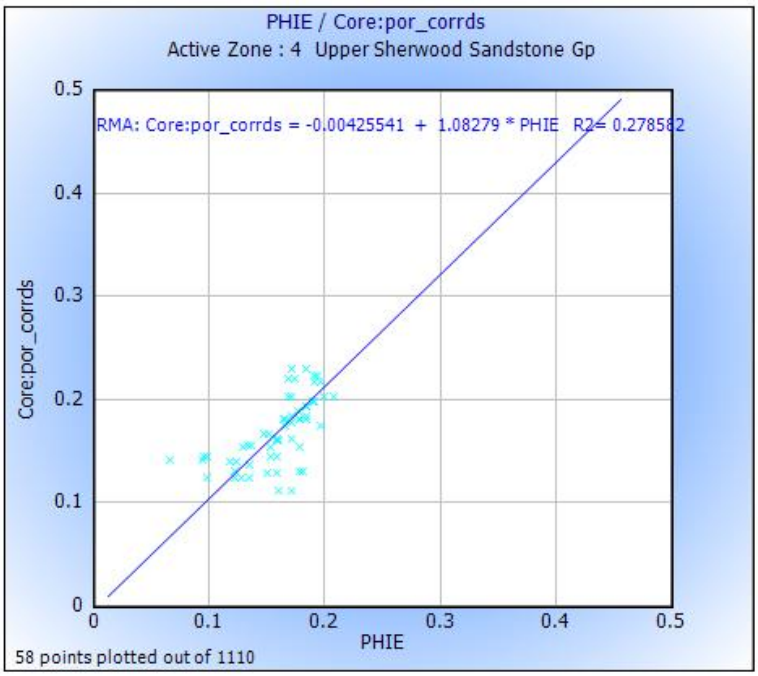

Figure 5.6: Cross-plot with the effective porosity ($PHIE$) curve calculated in IP (in decimals) on the x-axis and the porosity core sample measurements from the upper part of the Sherwood Sandstone Group in the Ballymacilroy borehole (in decimals) on the y-axis. A best-fitting relation is determined using RMA. This cross-plot is used as a QC for the effective porosity curve calculated in IP.

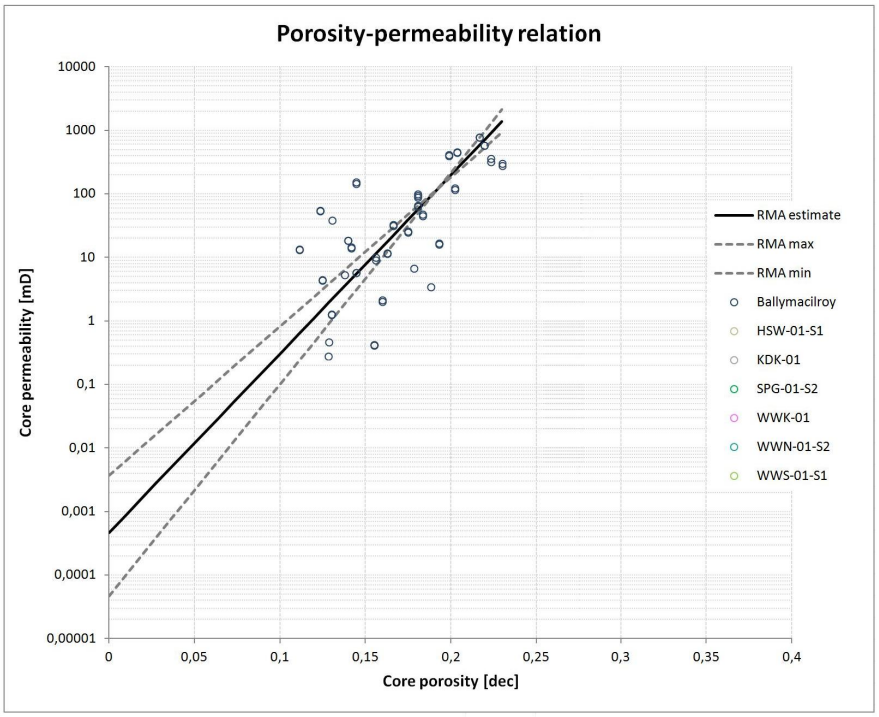

Figure 5.7: Plot of the porosity-permeability relation (indicated by the solid line) and the associated 95 % confidence interval (indicated by the dashed lines) produced using RMA. The relation is based on core sample data from the upper part of the Sherwood Sandstone Group in the Ballymacilroy borehole, indicated by the circles. The porosity-permeability relation has a RMA intercept of -7.67, an RMA slope of 64.782 and 95 % confidence intervals of (-9.969,-5,604) for the intercept and (54.058, 76.697) for the slope.

The porosity-permeability relation is then applied to the effective porosity curves in IP in order to produce permeability curves for the upper part of the Sherwood Sandstone Group (fig. 5.8). See appendix H for plots of the calculated permeability curve for each borehole. In order to apply the porosity-permeability relation to the effective porosity curves the porosity parameter in the relation is replaced with the $PHIE$ curve produced in IP. Cut-off values for the permeability curves of 0.01 and 1000 mD are used for the Ballymacilroy borehole, while cut-off values of 0.1 and 5000 mD are used for the Annaghmore and Ballynamullan boreholes. These different cut-off values are based on the minimum and maximum values of the permeability curves and are used to avoid unreasonable spikes in the permeability curves. As the Sherwood Sandstone Group is located at greater depth in the Ballymacilroy borehole than it is in the Annaghmore and Ballynamullan boreholes, porosity and permeability values tend to be lower at Ballymacilroy, explaining the lower values in the Ballymacilroy borehole.

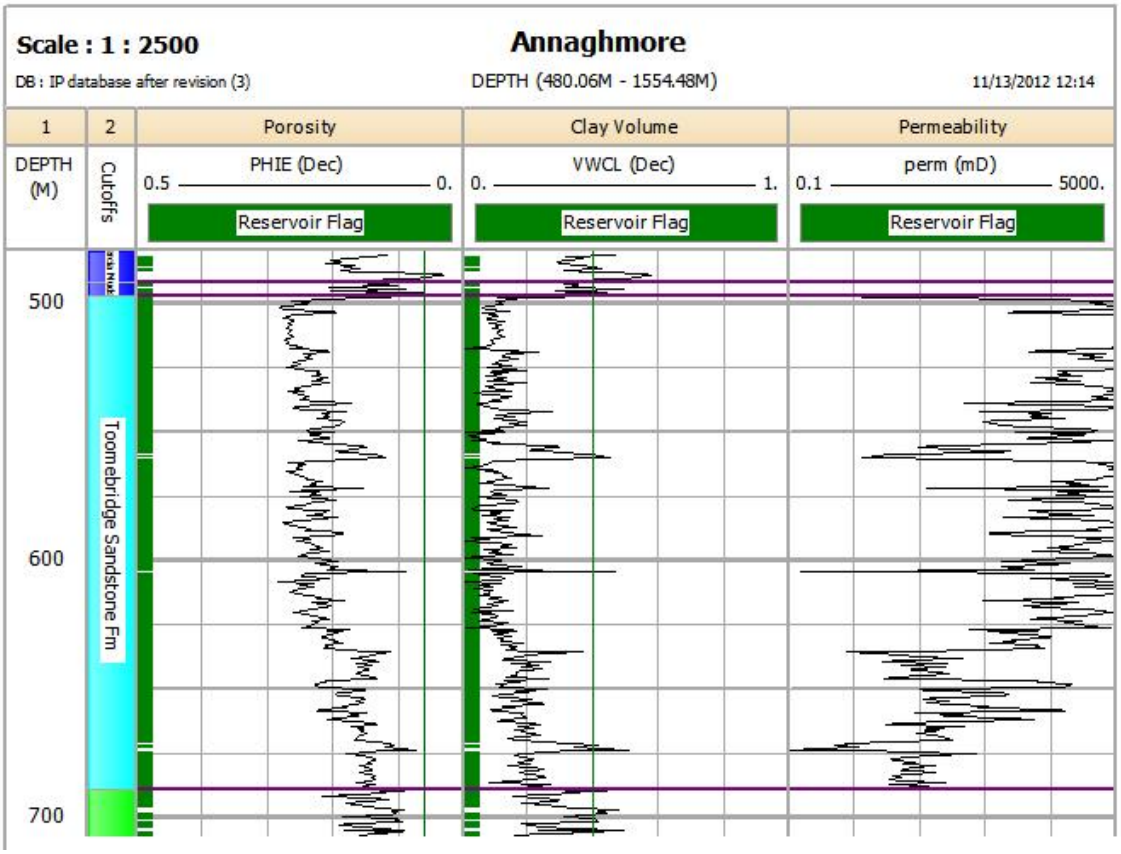

Figure 5.8: Plot showing the calculated effective porosity ($PHIE$), wet clay volume ($VWCL$) and permeability curves ($perm$) for the Annaghmore borehole. For each curve the units are specified in the figure. The plot shows the same part of the stratigraphy shown in figures 5.1 and 5.5. Note that the permeability curve is only calculated for the Toomebridge Sandstone Formation, since this was the only formation with core sample data available for calculating an effective porosity-permeability relationship

5.4 Monte Carlo uncertainty analysis

A Monte Carlo simulation is carried out in order to investigate the impact of uncertainties in the input data and various petrophysical parameters on the calculated results. For most parameters and log readings the default uncertainty ranges are assumed, except for the formation water resistivity. For this parameter the allowed variation was changed from 0.2 to 0.15 Ωm, necessary to prevent values of 0 for the formation water resistivity, which are impossible and cause an error in the Monte Carlo simulation. The permeability curve is analyzed twice, once for the arithmetic mean and once for the geometric mean. The Monte Carlo simulation is performed using 200 iterations for the whole range of the log data for each borehole. Results of the Monte Carlo simulation include computed average values and P90, P50 and P10 averages for, amongst others, the porosity, water saturation, clay volume and permeability over each of the evaluated intervals. See appendix I for a listing of the results of the Monte Carlo uncertainty analysis. The results show that the porosity is well resolved, with a maximum difference between the average value and the P10 and P90 averages of 1 % porosity for the upper part of the Sherwood Sandstone Group (or Toomebridge Sandstone Formation). The permeability values are less well resolved, with the P10 and P90 averages deviating from the average values by several orders of magnitude for the upper part of the Sherwood Sandstone Group, indicating a high sensitivity to changes in the input data and the petrophysical parameters.

5.5 Results

The borehole data analysis is used in this research to determine averages for the electrical resistivity, the porosity and the permeability for the upper part of the Sherwood Sandstone Group (or Toomebridge Sandstone Formation) of the three boreholes. Average resistivity values are determined for the upper part of the Sherwood Sandstone Group for each borehole. This is done by taking the deep induction resistivity (ILD) logs and removing those parts that would distort the averaging, i.e. the igneous intrusion in the Ballynamullan borehole and the zone with the bad data quality in the Ballymacilroy borehole. Also, spikes in the ILD logs showing unrealistically high values are removed, since these spike are not representative of the resistivity of the formation and significantly affect the average value. After the ILD logs are edited, the geometric mean is determined for the upper part of the Sherwood Sandstone Group, which gives average resistivity values of 3.1 Ωm (Annaghmore), 2.1 Ωm (Ballynamullan) and 1.1 Ωm (Ballymacilroy).

Average porosity values for the upper part of the Sherwood Sandstone Group are determined using the results of the Monte Carlo analysis. In the Monte Carlo analysis the average porosity (arithmetic mean) is calculated for each of the specified intervals using the effective porosity ($PHIE$) curve. In the cases of the Ballynamullan and the Ballymacilroy boreholes, the upper part of the Sherwood Sandstone Group is interrupted by an intrusion and a zone of bad data quality respectively. The Monte Carlo analysis then calculates the average porosity for the part of the formation above the interruption and the part below the interruption separately. In these cases the average porosity value for the entire formation is determined using:

$$\phi_{average}Total = \frac{\phi_{average}1 \times Gross1 + \phi_{average}2 \times Gross2}{Gross1 + Gross2}, \tag{66}$$

in which $\phi_{average}$ is the average porosity and $Gross$ is the thickness (corrected for the deviation of the borehole) of the intervals. This results in the following average porosity values: 21 % (Annaghmore), 20 % (Ballynamullan) and 18 % (Ballymacilroy).

In order to determine average permeability values the permeability curves produced in IP are used. When calculating average permeability values, the appropriate method for averaging needs to be determined. On a small scale (centimeters) the permeability of sedimentary rocks is related to the pore geometry and permeability values thus can vary by several orders of magnitude over small-scale distances. The pore geometry of a depositional facies is significantly affected by the depositional environment and depositional processes. Therefore, on a larger scale the average permeability mainly depends on the spatial arrangement of the different depositional facies (Herweijer 1997). Because of this, the method of averaging that is most appropriate when averaging permeability values for an entire formation depends on the nature of the formation. The three methods that traditionally have been used for averaging (i.e. harmonic, geometric and arithmetic) can be generalized using the power-average equation (Herweijer 1997):

$$k_{eff}{}^{\omega} = \frac{1}{n}\sum_{1}^{n} k_i{}^{\omega}, \tag{67}$$

in which k_{eff} is the average permeability, k_i are small-scale measurements and ω is a power-exponent in the interval [-1,1]. The value of ω depends on the nature of the formation. In the case of the Sherwood Sandstone Group, the sediments have been deposited in a braided fluviatile setting and consist of a variety of different depositional facies. Therefore, a heterogeneous character of the formation is assumed. For

a three-dimensional, heterogeneous medium it has been demonstrated that ω assumes a value of 1/3 (Noetinger 1994, Herweijer 1997). This results in average permeability values of 723 mD (Annaghmore), 303 mD (Ballynamullan) and 83 mD (Ballymacilroy).

Table 5.1 gives an overview of the average values for the resistivity, porosity and permeability of the upper part of the Sherwood Sandstone Group. The table shows that in all three boreholes the Sherwood Sandstone Group is highly conductive, with average resistivity values ranging from 1.1 Ωm to 3.1 Ωm. Porosity and permeability values are the lowest at Ballymacilroy, which is as expected since at Ballymacilroy the upper part of the Sherwood Sandstone Group is located at greater depth (1447 m) compared to Annaghmore and Ballynamullan (497 m and 685 m respectively). The Monte Carlo uncertainty analysis showed that the porosity values are well resolved and changes in the input data and the petrophysical parameters do not significantly affect the resulting porosity values. The permeability, however, is highly sensitive to changes in the input data and the petrophysical parameters, which significantly affect the resulting permeability values. Furthermore, table 5.1 shows that the upper part of the Sherwood Sandstone Group has the highest resistivity as well as the highest porosity and permeability at Annaghmore. Simultaneously, Ballymacilroy has the lowest resistivity as well as the lowest porosity and the permeability. This is contrary to expectations, as theoretically a lower resistivity would indicate higher porosity and permeability values.

Borehole	**Average resistivity (Ωm)**	**Average porosity (%)**	**Average permeability (mD)**
Annaghmore	3.1	21	723
Ballynamullan	2.1	20	303
Ballymacilroy	1.1	18	83

Table 5.1: Values for the average resistivity, average porosity and average permeability for each borehole resulting from the borehole wireline logging data and core sample data analysis.

6 Processing and modeling of MT data

The objective of the processing and modeling of the MT data is to create 1D models of the conductivity structure of the subsurface for each MT site in order to derive the electrical resistivity of the upper part of the Sherwood Sandstone Group. Since these MT models are to be compared and integrated with borehole data, MT data are required from sites that are located close to one of the three boreholes (i.e. Annaghmore, Ballynamullan or Ballymacilroy). The MT data, recorded during the 2009 survey (section 4.5), are made available by the Geological Survey of Northern Ireland (GSNI) and consists of data from five MT sites: LN002 near Annaghmore, LN001 and LN101 near Ballynamullan and LN028 and LN124 near Ballymacilroy (fig. 4.3). MT responses are provided as EDI files (with respect to a True North coordinate system), processed by Schlumberger under contract to GSNI. The data ranges from roughly 1000 Hz to 0.001 Hz for all five sites. Appendix J shows plots of the original data files, in which the response functions (apparent resistivity and impedance phase) are plotted as a function of period. An example of one of these plots is given in figure 6.1.

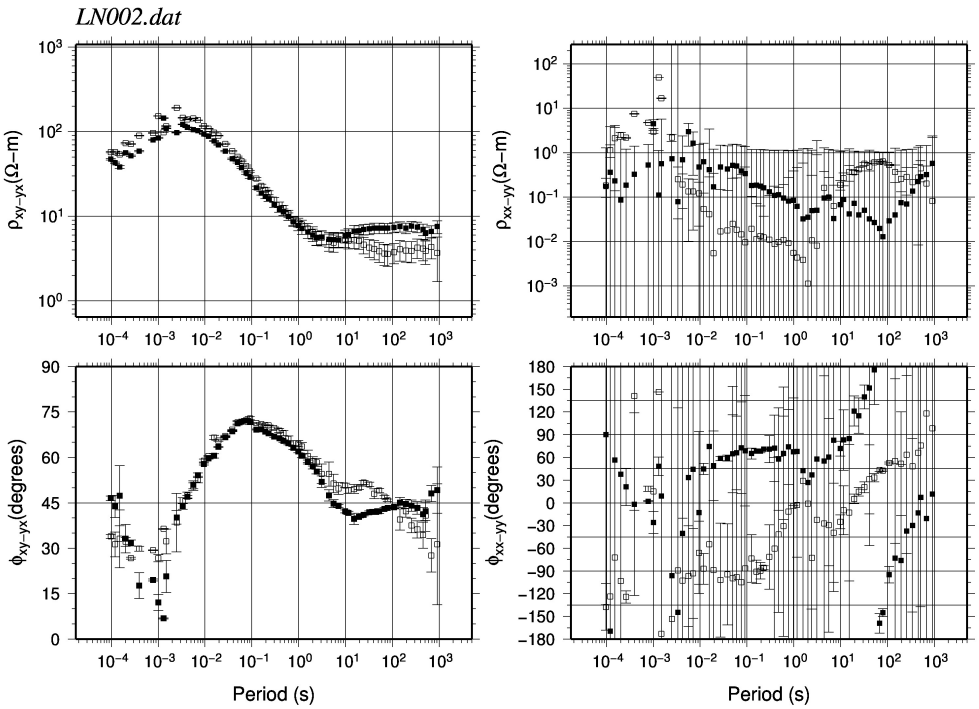

Figure 6.1: Original MT response at site LN002, with the apparent resistivity (top plots) and the impedance phase (bottom plots) plotted as a function of period. The plots on the left show the response functions for the off-diagonal components of the impedance tensor (Z_{xy} and Z_{yx}), while the plots on the right show the response functions for the diagonal components (Z_{xx} and Z_{yy}).

Continuing the processing, a strike angle analysis is carried out in order to determine the best-fitting strike angle and to analyze the dimensionality of the data. The resulting strike angles are used for decomposition of the impedance tensors, using the Groom and Bailey approach as implemented by McNeice & Jones (2001) (section 2.6.2), after which the decomposed data are smoothed using the ρ+ approach (section 2.6.3). When the processing is finished, the decomposed, smoothed data are ready for modeling. Three different 1D inversion codes are used to produce resistivity-depth profiles: Occam, the 1D inversion code implemented in WinGLink, and Minim (section 2.6.4). Of the resulting models the misfit with the MT data is determined using the RMS error. For the models that fit the MT data the best an uncertainty analysis is performed. Finally, the best-fitting models are integrated with borehole wireline log results.

6.1 Strike angle analysis

As explained in section 2.6.2, decomposition is used to remove distortion effects. As the decomposition method assumes as 2D regional structure and in most cases the MT data are not recorded with one of the orthogonal field components parallel to the strike direction, the strike angle must be known in order decompose the data to this angle. Thus when the strike angle is not known, which is the case in this research, a strike angle analysis is performed. Note that when the MT data are 1D they are theoretically insensitive to rotation, since the diagonal components of the impedance tensor will be zero for every rotation angle. Nevertheless, a strike angle can be used for 2D decomposition in order to remove distortion effects. Simultaneously, the strike angle analysis is used to investigate the dimensionality of the data. Since the objective is to produce 1D resistivity-depth profiles for each site, it is important to confirm that the MT data correspond with a subsurface that has a 1D conductivity structure, so that 1D modeling is appropriate. Since in this research only 1D modeling is carried out, no common strike direction for all sites needs to be determined, as would be the case for 2D modeling, and the strike angle can thus be determined for each site individually (single site analysis). However, as the MT sites are located relatively close to each other, similar strike angles for the five sites may be expected.

The strike analysis is carried out using the program STRIKE (McNeice & Jones 2001). This program uses the RMS error, which gives the misfit between the observed impedance tensor and the result from the Groom & Bailey (1989) decomposition, to determine the best-fitting strike angle. A low RMS error indicates a good correlation between the observed impedance tensor and the result from the decomposition,

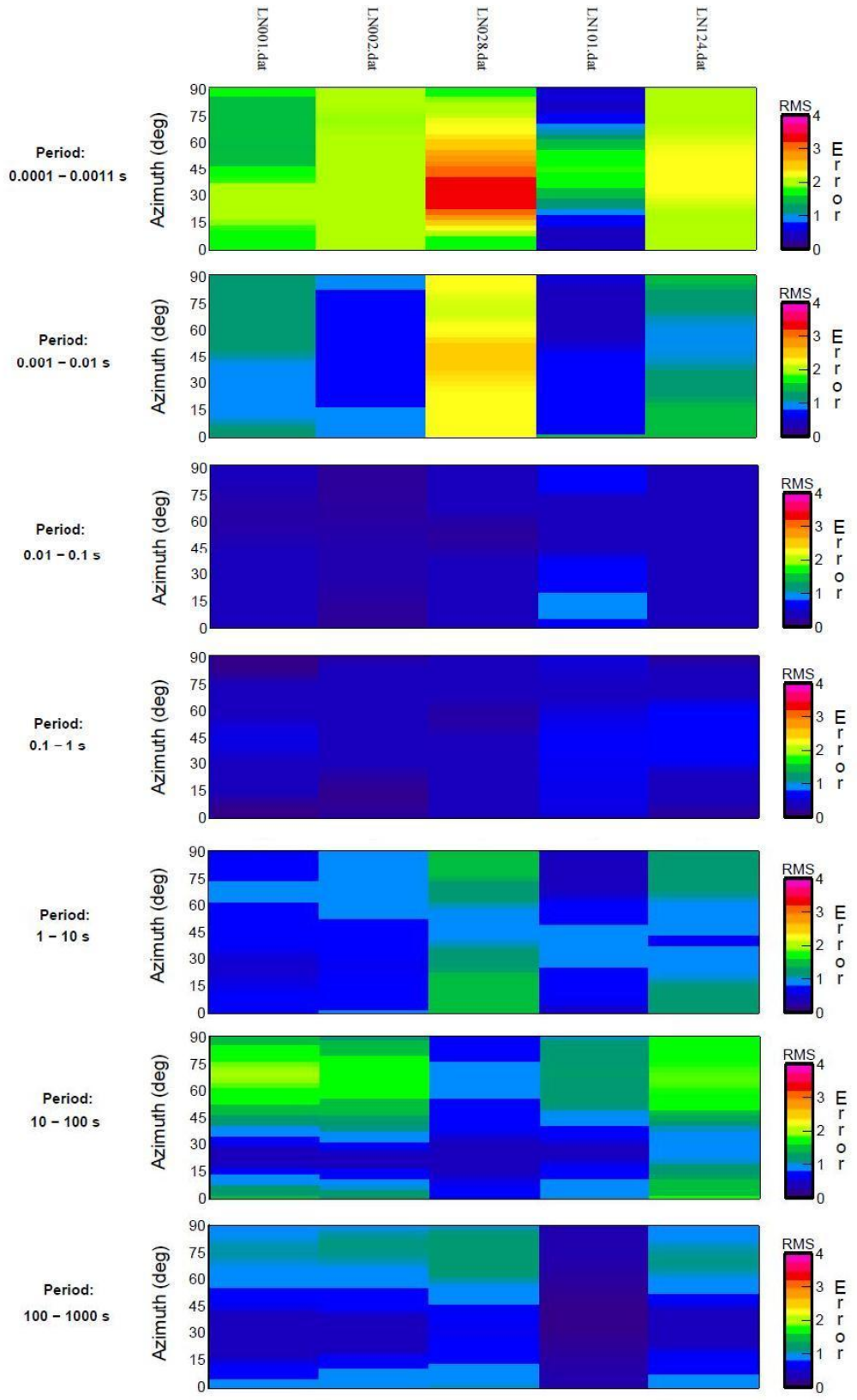

Figure 6.2: Results of the strike angle analysis. The RMS error is determined for every possible strike azimuth (east of True North), in steps of 3 °, for each predefined period band for all sites individually. Note that the sites are labeled at the top of the figure. The RMS error is defined as the misfit between the observed impedance tensor ($\underline{Z}_{obs}$) and the Groom and Bailey model of the data ($\underline{R}_\theta \underline{C} \underline{Z}_{2D} \underline{R}_\theta^T$).

indicating 1D or 2D data. First, STRIKE is used in order to calculate the RMS error for the whole range of possible strike azimuth angles ($0 - 90$ °), utilizing steps of 3 ° and predefined period bands. This is done for every site individually. The results are plotted in figure 6.2. The results show that for the shortest period band ($0.0001 - 0.0011$ s) the RMS errors are relatively high and no common strike direction for all sites can be discovered. A high RMS error may be due to either the observed responses not being 1D or 2D or the distortion being too severe to be adequately captured by the distortion matrices, both of which may result from shallow, small-scale conductivity heterogeneities. These heterogeneities probably also affect, to a lesser extent, the next period band ($0.001 - 0.01$ s). The two following period bands ($0.01 - 0.1$ s and $0.1 - 1$ s) show low RMS errors for all azimuth angles, indicating insensitivity to rotation angle and thus a 1D character of the subsurface. The longer periods show a preference for a specific strike angle, with the lowest RMS errors commonly lying in the range of 15 ° to 40 °, indicating a 2D structure. From this result it can be concluded that the data are 1D, except for the lower periods where 2D regional structures start to influence the MT data.

Next, STRIKE is used for a "free" strike determination, in which the whole frequency range of every site individually is analyzed to determine the best strike angle based on the average RMS error (since the RMS error is different for every frequency). The results are listed in table 6.1, showing a directional trend for all sites with all azimuths lying between 20 ° and 45 °.

MT site	Azimuth (°)	Average RMS error
LN001	25.05	0.770
LN002	23.96	0.867
LN028	42.30	1.088
LN101	34.48	0.831
LN124	36.44	1.321

Table 6.1: Results of the first "free" strike determination, in which the best-fitting strike angle is determined by analyzing the entire frequency range for every site individually. The table gives the best-fitting azimuth for each site and the corresponding RMS errors. Azimuth angles are defined as angles east of True North.

However, in this analysis the shortest periods, which are affected by local conductivity inhomogeneities or are insensitive to rotation angle, also contribute to the determination of the strike angle. Since it is argued that for the shorter periods the MT data are 1D and thus insensitive to rotation angle, a second free strike determination is performed, in which a distinction is made between the shorter periods and the longer periods, in order to find the best-fitting strike angle for the 2D regional structure. The period bands used in this analysis are chosen based on plots of the original data files, in which the response

functions are plotted as a function of period. These plots are examined to determine the period above which the apparent resistivity and phases of each mode diverge, indicating 2D structure. The results of the analysis are listed in table 6.2. The resulting azimuth angles for the shorter periods vary widely, while the azimuth angles for the longer periods are more similar to the results from the first free strike determination, with the azimuths varying between 23.91 ° (LN002) and 32.59 ° (LN124). The best-fitting strike angles for the longer periods thus are in better agreement with each other than the azimuths from the first free strike determination, emphasizing a common directional trend for the five sites. Also, the variation in the azimuth angles determined for the shorter periods shows that no consistent directional trend exists in this period range, which is in accordance with the inference that for the shorter periods (< 1 s) the data are 1D. The average RMS errors are lower in the second free strike determination, which is as expected, since for this analysis the data are separated into period ranges for which the data are 1D and period ranges for which the data are 2D, making it easier to find a single strike direction and distortion matrix to accommodate the data.

Shorter periods			
MT site	**Analyzed period band (s)**	**Azimuth (°)**	**Average RMS error**
LN001	2.5×10^{-3} - 3	82.79	0.308
LN002	3×10^{-3} - 4	12.09	0.322
LN028	5×10^{-3} - 5	50.55	0.396
LN101	3×10^{-3} - 3	62.76	0.370
LN124	5×10^{-3} - 1.25	87.76	0.355
Longer periods			
MT site	**Analyzed period band (s)**	**Azimuth (°)**	**Average RMS error**
LN001	7 - 10^3	24.34	0.485
LN002	4 - 10^3	23.91	0.612
LN028	5 - 10^3	27.49	0.733
LN101	11 - 10^3	28.31	0.350
LN124	10 - 10^3	32.59	0.627

Table 6.2: Results of the second "free" strike determination, in which the best-fitting strike angle (in degrees east of True North) is determined for the shorter periods and the longer periods separately for every site. The table gives the best-fitting azimuths per site for the different period bands and the corresponding RMS errors.

6.2 Decomposition, smoothing and static shift correction

The strike angles determined from the strike angle analysis are used for final decomposition of the data by applying the Groom and Bailey decomposition method (Groom & Bailey 1989). The strike analysis indicates that for the shorter periods (< 1 s) the MT data of the five sites are 1D and does not show a preference towards a certain strike angle. For the longer periods, however, the data show a common

directional trend, indicating 2D data. Therefore, for decomposition the strike angles for the longer periods resulting from the second free strike determination are used, as they are judged to best represent the strike of the regional 2D structure. The period ranges used for decomposition are based on the plots of the original data files. Table 6.3 gives an overview of the strike angles and period ranges used for final decomposition.

MT site	**Strike angle (°)**	**Period range (s)**
LN001	24.34	2.5×10^{-4} - 10^{3}
LN002	23.91	10^{-5} - 10^{3}
LN028	27.49	10^{-4} - 10^{3}
LN101	28.31	10^{-5} - 10^{3}
LN124	32.59	10^{-4} - 10^{3}

Table 6.3: Strike angle (in degrees east of True North) and period range used for final decomposition per site.

As mentioned in section 2.4.2, in the case of 2D structures the EM field is decoupled into two modes (polarizations). Therefore, after decomposition the impedance tensor gives the impedances of the two polarization modes, the TE and the TM mode (for an example, see fig. 6.3 and fig. 6.4). The apparent resistivity and impedance phase thus are also derived for both the TE and the TM modes. Plots of the decomposed MT responses are shown in appendix K. An example of a decomposed response is shown in figure 6.3. For each site the responses show a significant amount of scatter for the shortest periods, most likely caused by local conductivity heterogeneities. Excluding the periods affected by local heterogeneities, the shorter periods (less than about 1 - 10 s) of each site show overlapping TE and TM modes, except for the apparent resistivity curves of site LN001. Following Spratt et al. (2009), who argue that decomposed data can be treated as 1D when the maximum phase difference is less than 10 ° over a broad period range, this overlap between the TE and the TM modes indicates a largely 1D conductivity structure of the subsurface. Although there is no overlap between the two modes of the apparent resistivity for site LN001, the strong agreement between the shape of the two curves indicate that the data from this site are affected by static shift, which is characterized by a shift of the apparent resistivity curves, while the corresponding parts of the impedance phase curves are not affected (section 2.5). For longer periods for all sites the TE and TM modes no longer overlap and deviate from each other, indicating a transition to a 2D conductivity structure of the subsurface.

After decomposition, the response functions are smoothed using the ρ+ approach of Parker & Booker (1996). Using this approach, a consistency check is performed for each site to analyze for inconsistencies

between the apparent resistivity curves and the impedance phase curves. Based on this analysis new, smoothed response function curves are produced. Plots showing the decomposed, smoothed data sets can be found in appendix K. An example of one of these plots is shown in figure 6.3.

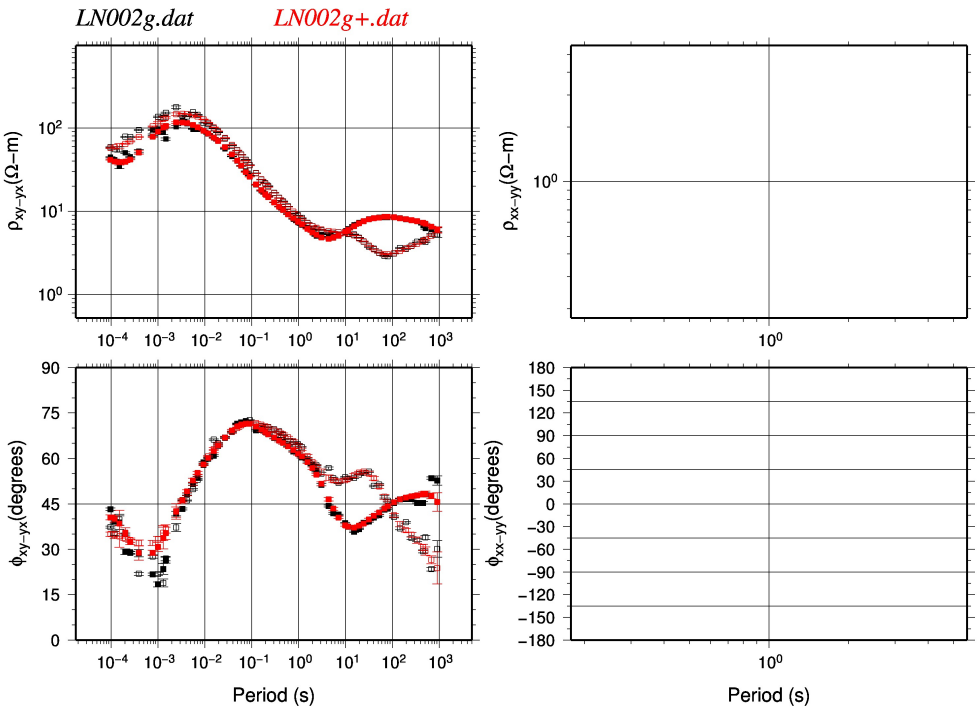

Figure 6.3: Decomposed, smoothed response function at site LN002. The decomposed data are indicated by the black data points, whereas the red data points indicate the decomposed, $\rho+$ smoothed data. Note that after decomposition the diagonal components of the impedance tensor are zero, explaining the absence of data points in the right-hand plots.

As mentioned, the plot of the decomposed data of site LN001 indicates that the data are affected by static shift. Therefore, after smoothing of the curves, the MT data are corrected for static shift in WinGLink. The correction is performed by vertically shifting all data points of the TM curve of the apparent resistivity towards the TE curve, applying a shift of the ρ_{yx} curve by a factor of 0.4407949 (fig. 6.4). Note that the impedance phase curves are not affected by the static shift correction.

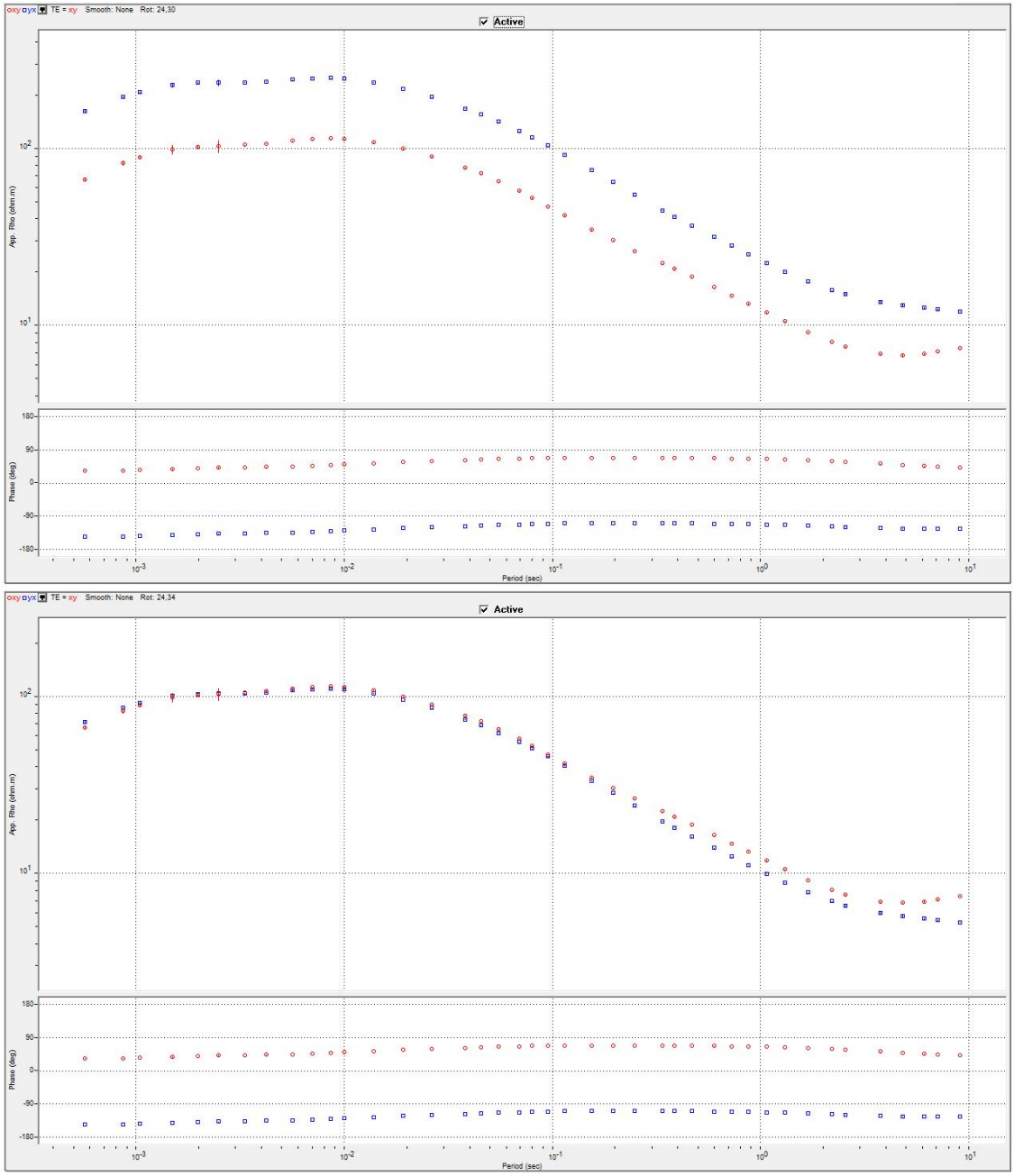

Figure 6.4: Static shift correction applied to the apparent resistivity curves of site LN001 in WinGLink. Based on the other sites, which are characterized by shallow apparent resistivities of about 100 Ωm, all data points of the TM curve (indicated by the blue data points) of the apparent resistivity are shifted downwards towards the TE curve (indicated by the red data points). The top part of the plot shows the curves before the static shift correction, the bottom part shows the curves after the static shift correction. Note that the curves of the impedance phase are not affected by the static shift correction.

6.3 1D modeling

After the data are decomposed, ρ+ smoothed and corrected for static shift they can be used for 1D modeling. Before modeling, the data are edited in WinGLink in order to mask some of the shorter and longer periods that are less reliable and/or are irrelevant, in the sense that they correspond with periods and therefore depths that are greater than the depth of interest, as the aim is to produce resistivity-depth profiles from which the resistivity of the Sherwood Sandstone Group can be derived. Shorter periods describing shallow features and longer periods penetrating significantly deeper than the Sherwood Sandstone Group can therefore be ignored. This means that for all sites nearly all the longer period data characterized by a 2D conductivity structure of the subsurface are masked and not used for modeling.

In WinGLink two different models per site are calculated from the data: a smooth model using the Occam 1D inversion code (Constable et al. 1987) and a sharp boundary model using the WinGLink 1D inversion code. For calculation of the models the invariant curves are used. The invariant apparent resistivity is calculated by taking the geometric mean of the TE and TM modes whereas the invariant phase is calculated as the arithmetic mean of the TE and TM modes. The Occam model is run using 10 iterations and a maximum number of layers of 45 in order to derive the smoothest model. The starting model for the sharp boundary inversion is guessed from the calculated Occam model, using a predefined maximum RMS error of 5 % and defining the maximum number of layers, which is limited to 8. The inversion is then run to establish the best-fitting sharp boundary model. With increasing iterations, the inversion code tends to calculate unrealistically high resistivity values for the resistive layers in the process of finding the model with the lowest RMS error. This is due to the fact that MT responses are primarily sensitive to the minimum resistivity of a resistor. Pushing the resistivity of a resistor upwards has little effect on the MT responses and therefore the inversion code will continue increasing the resistivities if there are no constraints. Therefore the resistivity values of the resistive layers are manually edited and fixed, after which the inversion is run again. Next all layer thicknesses and resistivity values are fixed, except for the thickness and the resistivity of the conductive layer that, with respect to the stratigraphy, can be related to the Sherwood Sandstone Group. The inversion is run again to make sure that the thickness and resistivity of the Sherwood Sandstone layer are the best possible estimates.

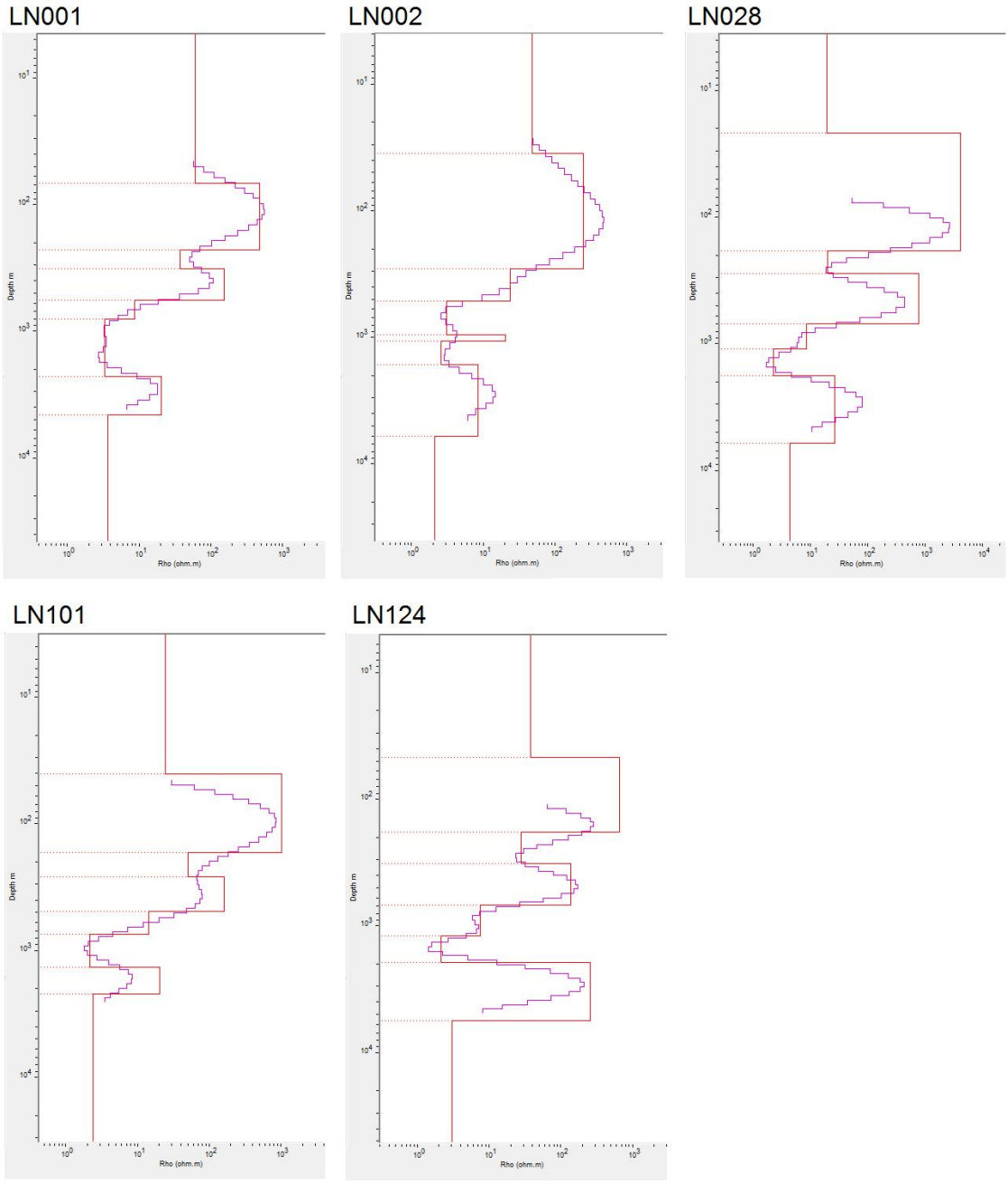

Figure 6.5: Plots of the 1D models calculated in WinGLink for the invariant of the TE and TM modes with the log resistivity (in Ωm) plotted as a function of the log depth (in m). For each site two models are calculated: an Occam model (indicated by the purple lines) and a sharp boundary model (indicated by the red lines).

In figure 6.5, both the smooth model and the sharp boundary models are plotted for each site, with the log resistivity plotted as a function of the log depth. All sites show similar sharp boundary models, with one or two highly resistive, shallow (< 1000 m) layers with resistivities higher than 130 Ωm, followed by a sharp decrease in resistivity, resulting in a conductive zone between 500 and 2000 m depth. The conductive

zone has a resistivity varying between 2.08 Ωm (LN124) and 3.21 Ωm (LN001) and with respect to the stratigraphy of the Lough Neagh Basin can be related to the Sherwood Sandstone Group. The conductive zone is bottomed by a relatively resistive layer of varying resistivity, from 8.21 Ωm (LN002) up to 250 Ωm (LN124). Site LN002 is the only site where the conductive layer is interrupted by a relatively small resistive layer, which is also indicated in the Occam model. A similar interruption of the conductive layer is suggested by the Occam model for site LN001. However, due to the restriction of the maximum number of layers to 8 for the sharp boundary models, this resistive layer is not included in the sharp boundary model of site LN001. See appendix L for the text files of the WinGLink sharp boundary models.

Although Constable et al. (1987) argue that the smoothest possible model is favored as it reduces the temptation of overinterpreting the data and eliminates arbitrary discontinuities in layered models, here the sharp boundary models are assumed to give a more realistic approximation of the layered nature of the sedimentary basin than the Occam models. The sharp boundary models are exported from WinGLink as text files and edited so they can be used as input files for the Minim code (Fischer et al. 1981). The Minim code requires input files containing the number of layers in the model and the resistivity (in Ωm) and the depth of the bottom of each layer (in m). No changes are applied to the exported sharp boundary models, except for site LN001, where the Occam model suggests the presence of a thin resistive layer interrupting the conductive zone, which is not incorporated in the sharp boundary model due to exceeding the maximum number of layers. Therefore, before running the Minim inversion, the sharp boundary model of site LN001 is edited and a relatively thin, resistive layer is added interrupting the conductive zone (fig. 6.6).

```
00008   0.5032E-03  0.4227E-03 LN001G RAV MINIM
  59.2300034  66.6299973
  462.300018  224.650009
  36.6999969  317.497467
  149.41481  557.287476
  8.53131676  792.368164
  3.23257542  2250.62622
  21.6112843  4395.86377
  4.63304424  1.
```

```
00010   0.5032E-03  0.4227E-03 LN001G RAV MINIM
  59.2300034  66.6299973
  462.300018  224.650009
  36.6999969  317.497467
  149.41481  557.287476
  8.53131676  792.368164
  3.23257542  980.3
 20.0         1440.6
  3.23257542  2250.62622
  21.6112843  4395.86377
  4.63304424  1.
```

Figure 6.6: The edited input file for the Minim code for site LN001. The Minim code requires input files containing the number of layers in the model (top left) and the resistivity in Ωm (left column) and the depth of the bottom of each layer in m (right column). The left file shows the original sharp boundary model, while the right file shows the edited sharp boundary model. Note the two extra layers in the right file, facilitating the addition of a resistive layer with a resistivity of 20 Ωm interrupting the conductive zone.

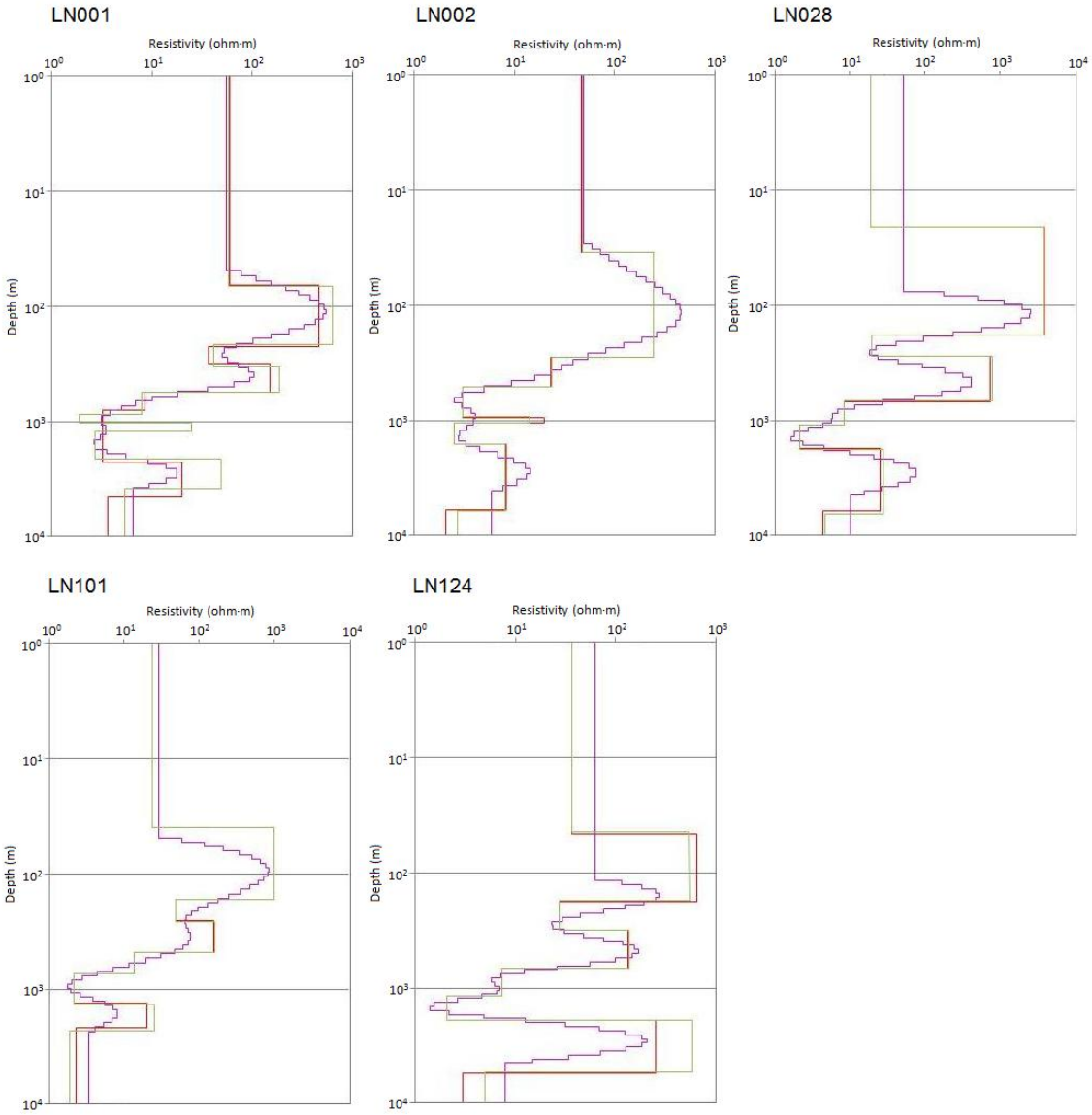

Figure 6.7: Plots of the Occam model (purple lines), the sharp boundary model (red lines) and the Minim model (green lines) for each site, with the log resistivity (in Ωm) plotted as a function of the log depth (in m). Note the difference in the log resistivity scale between sites LN001, LN002 and LN124 and sites LN028 and LN101. Models are all derived from the invariant of the MT responses

To run the inversion, the Minim code requires an MT data set (in this case the decomposed, ρ+ smoothed data sets are used) and an input file which it uses as a starting model. Again, the invariant curves are used for calculation of the models. Figure 6.7 shows a plot of the Occam model, the sharp boundary model and the Minim model for each site, with the log resistivity plotted against the log depth. The Minim models are very similar to the sharp boundary models used as input starting models for the Minim inversion, showing the same overall structure with minor differences in the thicknesses and resistivities of the layers. As mentioned above, two additional layers were added to the sharp boundary model of site

LN001 before being used as an input model for the Minim code. Hence, in contrast to the sharp boundary model the conductive zone of the Minim model of site LN001 consists of two conductive layers, interrupted by a resistive layer. See appendix M for text files of the Minim models.

6.4 Model misfit and uncertainty analysis

In order to determine which model fits the MT data the best, a code called Chi2 is used that determines the RMS error for a model, which is a measure of the differences between the observed MT responses and the MT responses predicted by the model (both apparent resistivity and impedance phase). The RMS error is determined for all three models for each site, the results of which are shown in table 6.4. The table shows that for each site, the Minim model is the best-fitting model showing the lowest RMS error, while the Occam model has the highest RMS error and thus fits the data the worst. Based on these results, it is concluded that the Minim models are the best-fitting models and that they will be used for further research, including an uncertainty analysis and using the resistivity values of the models in order to derive porosity and permeability values for the upper part of the Sherwood Sandstone Group (chapter 7).

MT models	**LN001**	**LN002**	**LN028**	**LN101**	**LN124**
Occam	0.254	0.246	0.865	0.330	0.447
Sharp boundary	0.158	0.215	0.209	0.217	0.321
Minim	0.103	0.167	0.048	0.090	0.195

Table 6.4: RMS errors of the different models for each MT site.

As the aim of the modeling is to determine the resistivity of the upper part of the Sherwood Sandstone Group it is important to know the uncertainty, i.e. the sensitivity to variation of the resistivity and depth values predicted by the Minim models. Therefore, an uncertainty analysis is performed for the conductive layers of the models that, with respect to the stratigraphy, can be related to the Sherwood Sandstone Group. In this analysis, the resistivity and depths of the boundaries of the conductive layers are varied and the Chi2 code is used to analyze the effect of these variations on the RMS error of the models. First, the resistivity and depth of the top boundary of the layer are varied simultaneously. Next, the resistivity and the depth of the bottom boundary of the layer are varied simultaneously. The resistivity of the conductive layer is varied by increasing/decreasing the resistivity values in steps of 0.1 Ωm, while the thickness is varied by increasing/decreasing the depth of the top/bottom of the layer in steps of 1 m. For

each possible variation of the model the Chi2 code is used to determine the RMS error and a variation of the RMS error of 10 % from the best-fitting model is allowed. The results of the uncertainty analysis are listed in table 6.5. The table shows that for each Minim model the resistivity of the conductive layer that comprises (part of) the Sherwood Sandstone Group is well resolved, with no variation of the order of 0.1 Ωm possible except for site LN001, where the resistivity lies between 1.8 and 2 Ωm when allowing a variation of 10 % in the RMS error. The uncertainty ranges for the depths of the top and bottom of the conductive layers vary more widely for the different sites, but in all cases the allowed deviation is less than 2 % of the depth of the boundary.

MT site	**Resistivity (Ωm)**	**Uncertainty range**	**Depth top (m)**	**Uncertainty range**
LN001	1.9	1.8 - 2.0	868.9	859.9 - 879.9
LN002	3.0	-	509.2	507.2 - 511.2
LN028	2.2	-	1089.9	1089.8 - 1091.8
LN101	2.2	-	741.2	740.2 - 743.2
LN124	2.1	-	1177.2	1170.2 - 1186.2
MT site	**Resistivity (Ωm)**	**Uncertainty range**	**Depth bottom (m)**	**Uncertainty range**
LN001	1.9	1.8 - 2.0	1038.7	1021.7 - 1055.7
LN002	3.0	-	934.7	924.7 - 943.7
LN028	2.2	-	1771.8	1767.8 - 1771.8
LN101	2.2	-	1353.2	1343.2 - 1357.2
LN124	2.1	-	1915.2	1904.2 - 1923.2

Table 6.5: Results of the uncertainty analysis for the conductive layer of the Minim models that comprise (part of) the Sherwood Sandstone Group, in which the resistivity and the depth of the top/bottom of the layer and their corresponding uncertainty ranges are determined. The top part of the table shows the results of the first part of the analysis, in which the resistivity and the depth of the top of the formation are varied simultaneously. The bottom part of the table shows the results of the second part of the analysis, in which the resistivity is varied simultaneously with the depth of the bottom of the layer. The RMS error is determined using the code Chi2 for each variation of the model and a variation of the RMS error of 10 % from the best-fitting model is allowed. The dashes in the uncertainty range column indicate that changes of greater than 0.1 Ωm cannot be accommodated without exceeding the 10 % RMS error variation threshold.

6.5 Integration with borehole data

Next, the Minim models are integrated with the borehole geological and wireline logging data in order to verify the models by comparing them with the borehole defined conductivity structure of the subsurface and to relate the models to the stratigraphy. This is done by plotting the Minim models together with the deep induction resistivity (ILD) logs measured in the boreholes. For each MT site, the ILD log from the corresponding borehole is used, i.e. sites LN001 and LN101 correspond with Ballynamullan, site LN002 corresponds with Annaghmore and sites LN028 and LN124 correspond with Ballymacilroy. The ILD logs consist of resistivity measurements made at 0.5 ft intervals. However, for the sake of clarity only one in

every six data points is plotted, which roughly provides one data point per meter.

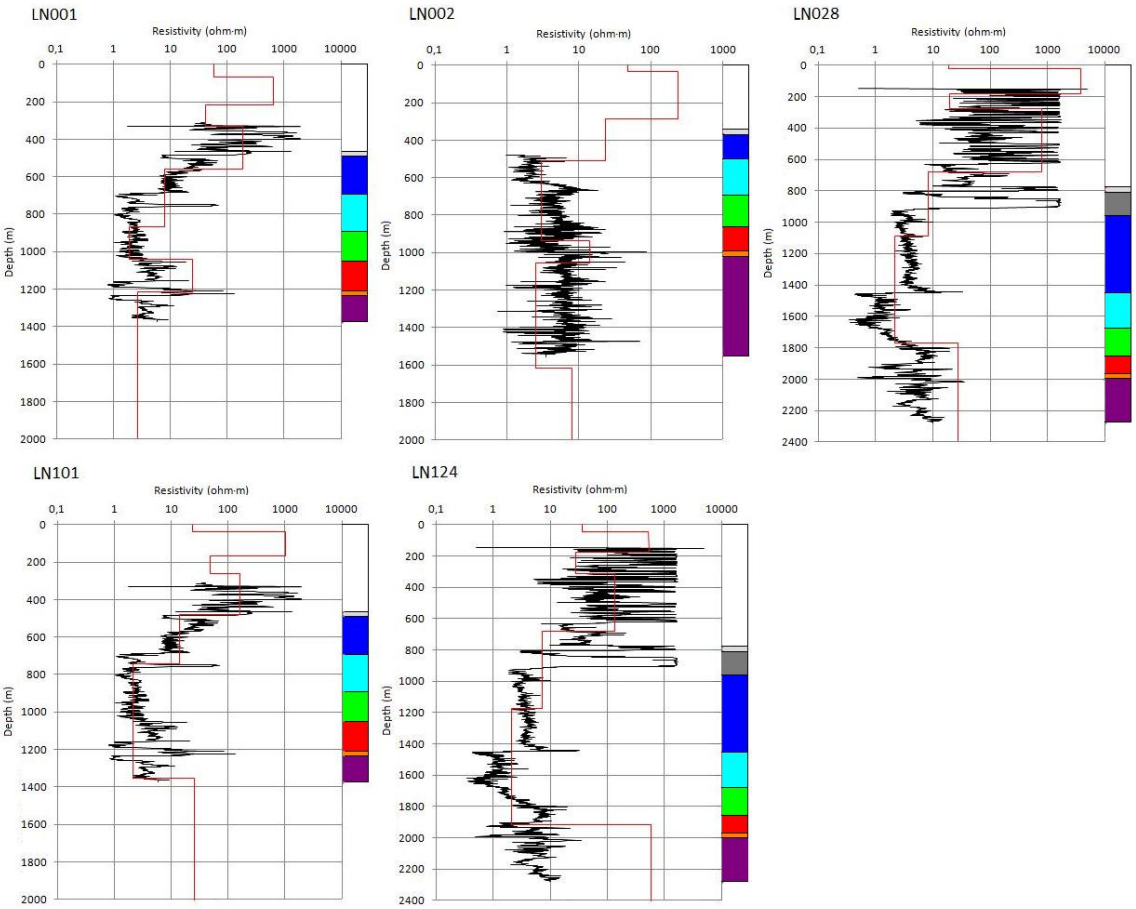

Figure 6.8: For each MT site the Minim model (red lines) is compared with the ILD log (black lines) and the stratigraphy encountered in the boreholes. The log resistivity (in Ωm) is plotted on the y-axis and the depth (in m) is plotted on the y-axis. The following stratigraphic formations are specified: Antrim Lava Group (white), Ulster White Limestone Group (light grey), Lias and Penarth Group (dark grey), Mercia Mudstone Group (dark blue), Upper Sherwood Sandstone Group/Toomebridge Sandstone Formation (light blue), Lower Sherwood Sandstone Group/Drumcullen Formation (green), Permian successions (red), Belfast Harbour Evaporite Formation/Magnesian Limestone (orange) and (Lower) Permian successions (purple).

Figure 6.8 shows a plot of the Minim model and the ILD log per site, with the resistivity plotted as a function of the true vertical depth. The ILD logs indicate that the basalts of the Antrim Lava Group are highly resistive (usually higher than 100 Ωm, sometimes even exceeding 1000 Ωm), whereas the Mercia Mudstone Group is semi-resistive (10-100 Ωm at Ballynamullan, 3-10 Ωm at Ballymacilroy). For each borehole the ILD log shows a significant decrease in resistivity at the stratigraphic boundary between the Mercia Mudstone Group and the Sherwood Sandstone Group, which is highly conductive (1-10 Ωm, occasionally less than 1 Ωm at Ballymacilroy). The dolerite intrusion in the Sherwood Sandstone Group at Ballynamullan is clearly indicated by the ILD log. Compared to the Sherwood Sandstone Group, the

underlying Permian sandstone successions are generally more resistive and the ILD logs show a relatively large amount of variation (from 1 to well over 10 Ωm). At Annaghmore and Ballynamullan, the Belfast Harbour Evaporite Formation is well defined in the resistivity logs, with the resistivity reaching values of about 100 Ωm, in contrast to Ballymacilroy where the Belfast Harbour Evaporite Formation shows resistivity values similar to those of the adjacent sandstone successions.

In general, the resistivity profiles predicted by the Minim models are similar to the conductivity structure measured by the ILD logs, with highly resistive layers representing the Antrim Lava Group and semi-resistive and conductive layers corresponding to the Permian and Triassic successions. Also, each Minim model contains a highly conductive layer that can be related to the Sherwood Sandstone Group. However, there is no clear agreement between the layer depths in the Minim models and the stratigraphy. The Minim model of site LN002 shows a relatively good agreement with the stratigraphy, containing a transition from a semi-resistive layer to a conductive layer that, with respect to the stratigraphy, closely matches the boundary between the Mercia Mudstone Group and the Sherwood Sandstone Group. The conductive layer stratigraphically corresponds to the Sherwood Sandstone Group and the underlying sandstone successions and is bottomed by a semi-resistive layer that can be related to the Belfast Harbour Evaporite Formation. However, this degree of agreement can only be seen for site LN002. For sites LN001 and LN101 a highly resistive dolerite intrusion affects the Minim models, causing the transition from the semi-resistive layer to the conductive layer to be located too deep to match the stratigraphic boundary between the Mercia Mudstone Group and the Sherwood Sandstone Group. For the model of site LN001, the Belfast Harbour Evaporite Formation can roughly be related to a resistive layer, although the top boundary of this resistive layer is affected by relatively high resistivity values of the sandstone successions overlying the Belfast Harbour Evaporite Formation. For site LN101 the resistive Belfast Harbour Evaporite Formation is not present in the Minim model. For sites LN028 and LN124 the transition between the semi-resistive layer and the conducive layer in the Minim models is located well above the stratigraphic boundary between the Mercia Mudstone Group and the Sherwood Sandstone Group, which is likely caused by a relatively low resistivity of the Mercia Mudstone Group at Ballymacilroy. At Ballymacilroy the values of the ILD log for the Mercia Mudstone Group lie between 1 and 10 Ωm, considerably lower than the values measured by the ILD log at Ballynamullan, where the resistivity of the Mercia Mudstone Group varies between 10 - 100 Ωm. A higher resistivity of the Mercia Mudstone Group

at Ballymacilroy would mean that the Minim models of sites LN028 and LN124 would be better able to resolve the stratigraphic boundary between the Mercia Mudstone Group and the Sherwood Sandstone Group. Also, for these two sites there is no good correlation between the resistive layer (that makes up the bottom boundary of the conductive layer) and the Belfast Harbour Evaporite Formation.

Integration of the Minim models with borehole geological and wireline logging data thus indicates that correlating layers of the Minim models with stratigraphic boundaries is highly uncertain. This is confirmed by comparing the results of the uncertainty analysis performed for the conductive layer of the Minim models that can be related to the Sherwood Sandstone Group (table 6.5) with the stratigraphic depths of the Sherwood Sandstone Group determined from the borehole geological and wireline logging data. The comparison shows that for each MT site the depth discrepancies between the Minim models and the stratigraphy in the boreholes are larger than the depth uncertainties resulting from the uncertainty analysis, confirming the high uncertainty associated with correlating layers of the Minim models to the stratigraphy.

6.6 Results

The resistivity of the Sherwood Sandstone Group is derived from the Minim model for each MT site. The results, listed in table 6.6, show that at each site the Sherwood Sandstone Group is highly conductive, with resistivity values varying between 1.9 Ωm and 3.0 Ωm. The results of the uncertainty analysis (table 6.5) indicate that for each Minim model the resistivity and the depths of the conductive layers are well resolved and that the associated uncertainty ranges are small. However, correlating layers of the Minim models with stratigraphic boundaries is highly uncertain, as is shown by the integration of the Minim models with the borehole geological and wireline logging data (section 6.5).

MT site	**Resistivity (Ωm)**
LN001	1.9
LN002	3.0
LN028	2.2
LN101	2.2
LN124	2.1

Table 6.6: Resistivity of the Sherwood Sandstone Group at each MT site, derived from the Minim models.

7 Petrophysical modeling

In the final part of the research petrophysical relations are used to derive porosity and permeability values for the upper part of the Sherwood Sandstone Group from the resistivity values predicted by the Minim models. Archie's first law (section 3.1.1) is used to determine porosity values, while the RGPZ model (section 3.2.1) and the porosity-permeability relationship determined based on the core sample data (section 5.3) are used to calculate permeability values. For all porosity and permeability values the associated uncertainty range is determined. Finally, generalized calibrations of Archie's first law and the RGPZ model are produced.

7.1 Porosity estimation - Archie's first law

For the estimation of the porosity (ϕ) Archie's first law (Archie 1942) can be rewritten as:

$$\phi = \left(\frac{R_w \times a}{R_0} \right)^{1/m}, \tag{68}$$

where R_0 is the bulk effective resistivity and R_w is the water resistivity. For the bulk effective resistivity the resistivity values given by the Minim models for the Sherwood Sandstone Group are used, while for the water resistivity the formation water resistivity values for the upper part of the Sherwood Sandstone Group (or the Toomebridge Sandstone Formation) as determined from the wireline logging data in IP are used (table 7.1). Following Worthington (1993) and Mavko et al. (1998), the tortuosity factor (a) is assumed to be 1. The value of the cementation exponent (m) is determined by fitting Archie's first law to wireline logging data. For each of the three boreholes (Annaghmore, Ballynamullan and Ballymacilroy) a cross-plot is created, combining data from the effective porosity curves determined in IP and deep induction resistivity log data from the upper part of the Sherwood Sandstone Group (or the Toomebridge Sandstone Formation). The value of the cementation exponent is then determined by fitting Archie's first law to the data points of the cross-plots for a variable cementation exponent using the method of least squares (fig. 7.1). This gives values for the cementation exponent of 1.7 (Annaghmore), 1.8 (Ballynamullan) and 2.0 (Ballymacilroy). However, it is argued that for low porosity values Archie's first law is less reliable, which is demonstrated by the plots in figure 7.1. Therefore, the best-fitting cementation exponents are determined a second time, this time excluding data points with porosity values lower than

10 %. The resulting cementation exponent values are 1.8 (Annaghmore), 1.8 (Ballynamullan) and 1.9 (Ballymacilroy). These values fall well within the range expected for arenaceous rocks (1.5 - 2.5) and are comparable to the values found for other sandstone formations (e.g. Gomez et al. (2010)).

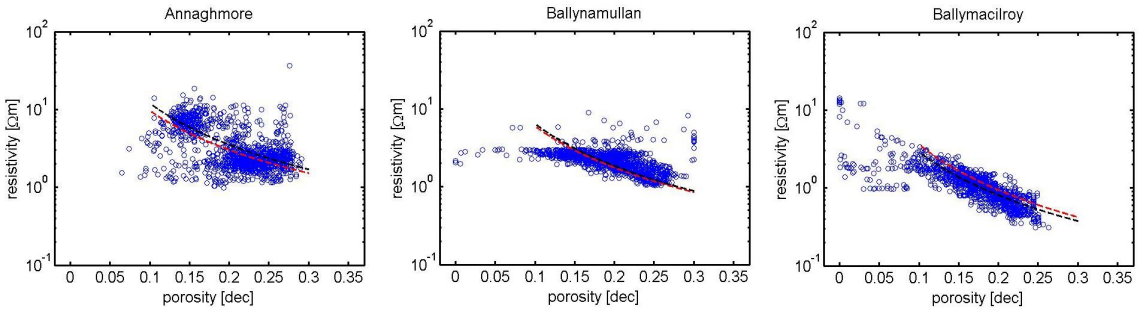

Figure 7.1: Calculation of the cementation exponent (m) for the upper part of the Sherwood Sandstone Group (the Toomebridge Sandstone Formation) for each borehole. The values of the effective porosity curve determined in IP are shown on the x-axis (in decimals), while the y-axis shows the corresponding resistivity values from the deep induction resistivity log (in Ωm). The data points are indicated by the blue circles. The best-fitting cementation exponents are determined twice, first by applying Archie's first law to the entire data sets (red lines) and secondly by applying Archie's first law while excluding data points with a porosity lower than 10 % (black lines).

Then, Archie's first law is used to derive porosity values for the upper part of the Sherwood Sandstone Group from the bulk effective resistivity values following from the Minim models. For each MT site the values of the parameters of Archie's first law are based on the data of the corresponding borehole. Table 7.1 gives the values of the parameters used and the resulting porosity value for each MT site.

Borehole	**MT site**	R_0 (Ωm)	R_w (Ωm)	a	m	ϕ (%)
Annaghmore	LN002	3.0	0.20	1	1.8	22
Ballynamullan	LN001	1.9	0.10	1	1.8	19
	LN101	2.2	0.10	1	1.8	18
Ballymacilroy	LN028	2.2	0.04	1	1.9	12
	LN124	2.1	0.04	1	1.9	12

Table 7.1: Values of the parameters used in Archie's first law and the resulting porosity values for the upper part of the Sherwood Sandstone Group derived from the bulk effective resistivity values predicted by the Minim models.

The results show that for the two MT sites located at Ballymacilroy the porosity has a value of 12 %, which is significantly lower than the porosity determined for the MT sites located at Annaghmore and Ballynamullan, where the porosity ranges from 18 % to 22 %. Additionally, table 7.1 shows that the water resistivity varies significantly per borehole, with the formation water being considerably less resistive at Ballymacilroy (0.04 Ωm) compared to Annaghmore and Ballynamullan (0.2 Ωm and 0.1 Ωm respectively). Comparing the values of the different parameters between the MT sites, it is concluded that the water

resistivity has a significant effect on the resulting porosity values and the low porosity values for the two sites at Ballymacilroy are a consequence of the low water resistivity values at Ballymacilroy compared to Annaghmore and Ballynamullan.

In order to determine the uncertainty associated with the porosity values resulting from Archie's first law, the uncertainty range for each porosity value is calculated. This is done by defining the allowed variations associated with each parameter of Archie's first law. For the bulk effective resistivity the results of the uncertainty analysis performed for the Minim models (section 6.4) are used. The results of this uncertainty analysis (table 6.5) show that the bulk effective resistivity of site LN001 has an associated uncertainty range of 1.8 - 2.0 Ωm. For the other sites, the bulk effective resistivity has no associated uncertainty range, as changes of greater than 0.1 Ωm cannot be accommodated without exceeding the 10 % RMS error variation threshold applied in the uncertainty analysis. For the cementation exponent a variation of 0.2 is accepted, based on the plots in figure 7.1 and the Monte Carlo simulation carried out for the borehole data (section 5.4), in which the uncertainty range of the cementation exponent was also determined at 0.2. The values for the water resistivity and the tortuosity factor are kept constant. Using these allowed variations, the uncertainty ranges associated with the porosity values resulting from Archie's first law are determined for each MT site, showing a maximum deviation from the initial porosity values of of 5 % porosity (table 7.2).

Borehole	**MT site**	**Porosity (%)**	**Uncertainty range**
Annaghmore	LN002	22	18 - 26
Ballynamullan	LN001	19	15 - 24
	LN101	18	14 - 21
Ballymacilroy	LN028	12	9 - 15
	LN124	12	10 - 15

Table 7.2: Uncertainty ranges associated with the porosity values for the upper part of the Sherwood Sandstone Group, derived from the bulk effective resistivity values observed in the Minim models using Archie's first law. The uncertainty ranges are calculated by employing the allowed variations for the bulk effective resistivity as determined from the uncertainty analysis of the Minim models (table 6.5) and using a possible variation of 0.2 for the cementation exponent. The values of the water resistivity and the tortuosity factor, as defined in table 7.1, are kept constant.

7.2 Permeability estimation

7.2.1 The RGPZ model

The permeability (k) of the upper part of the Sherwood Sandstone Group is estimated using the RGPZ model (Glover et al. 2006):

$$k = \frac{d^2 \phi^{3m}}{4pm^2}. \tag{69}$$

First, the value of the effective grain diameter (d) is determined based on core sample data from the upper Sherwood Sandstone Group in the Ballymacilroy borehole, consisting of 28 effective porosity and horizontal intrinsic permeability measurements. The value of the effective grain diameter is determined by fitting the RGPZ model to the core sample data for a variable effective grain diameter using the method of least squares (fig. 7.2). This results in a effective grain diameter of 0.29 mm.

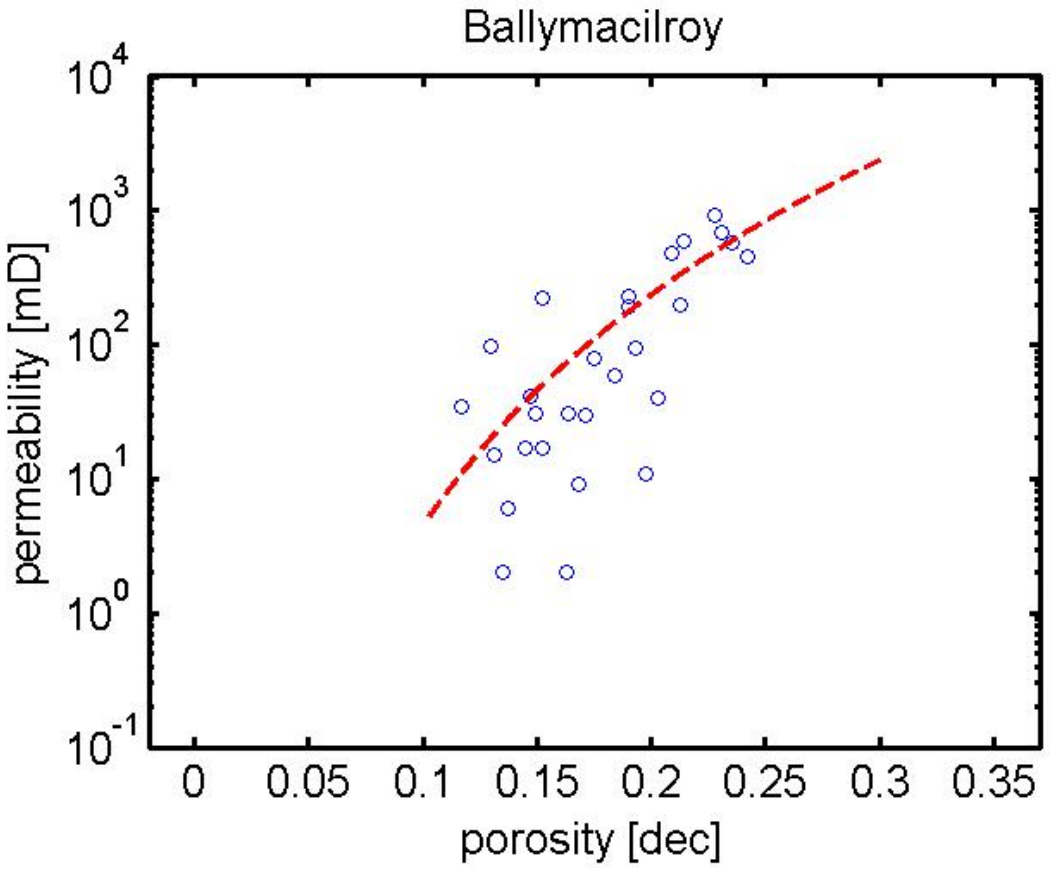

Figure 7.2: Calculation of the effective grain diameter (d) of the RGPZ model for the upper part of the Sherwood Sandstone Group in the Ballymacilroy borehole. The plot, with the porosity (in decimals) on the x-axis and permeability (in mD) on the y-axis, shows core sample data (blue circles) to which the RGPZ model is fitted (red line) for a variable effective grain diameter.

In order to derive permeability values from the resistivity values predicted by the Minim models, the bulk

effective resistivity parameter is introduced in the RGPZ model by applying Archie's first law to the RGPZ model. This gives the following equation:

$$k = \frac{d^2(R_w/R_0)^m}{4pm^2}. \tag{70}$$

Note that the tortuosity factor is left out of this equation, as its value is assumed to be 1. This equation is then used to calculate permeability values for the upper part of the Sherwood Sandstone Group for all five MT sites. For the water resistivity, the bulk effective resistivity and the cementation exponent the previously determined values are used (table 7.1), while the packing parameter (p) has a value of 8/3 (Glover et al. 2006). For lack of core sample data from the Annaghmore and Ballynamullan boreholes, the value for the effective grain diameter of 0.29 mm, determined based on core sample data from the Ballymacilroy borehole, is applied to all MT sites. The resulting permeability values, listed in table 7.3, vary between 13 mD and 741 mD, with the lowest values found at the two MT sites at Ballymacilroy. This is as expected, since a similar trend is observed in the porosity values resulting from applying Archie's first law and thus is a consequence of the low values for the water resistivity at Ballymacilroy compared to Annaghmore and Ballynamullan (table 7.1).

Borehole	**MT site**	**Permeability (mD)**
Annaghmore	LN002	741
Ballynamullan	LN001	365
	LN101	235
Ballymacilroy	LN028	13
	LN124	16

Table 7.3: Permeability values of the upper part of the Sherwood Sandstone Group, derived from the bulk effective resistivity values observed in the Minim models using the RGPZ model for each MT site.

The uncertainty ranges associated with the permeability values resulting from the RGPZ model are determine using the previously established allowed variations for the water resistivity, the bulk effective resistivity and the cementation exponent (section 7.1), while the packing parameter is kept constant. Regarding the effective grain diameter, Naylor et al. (2003) observed that the Toomebridge Sandstone Formation consists mainly of medium grained sandstone, based on borehole reports and the wireline logs. Combining this with the Wentworth scale, the effective grain diameter is assumed to have a maximum value and a minimum value of 0.5 mm and 0.25 mm respectively. Table 7.4 shows that the permeability values resulting from the RGPZ model have large uncertainty ranges, with the uncertainty range

becoming considerably larger with increasing permeability.

Borehole	MT site	Permeability (mD)	Uncertainty range
Annaghmore	LN002	741	438 - 2740
Ballynamullan	LN001	365	185 - 1586
	LN101	235	139 - 868
Ballymacilroy	LN028	13	8 - 49
	LN124	16	9 - 57

Table 7.4: Uncertainty ranges associated with the permeability values for the upper part of the Sherwood Sandstone Group calculated using the RGPZ model based on bulk effective resistivity values following from the Minim models. The uncertainty ranges are calculated employing the previously determined allowed variations for the water resistivity, bulk effective resistivity and the cementation exponent, while for the effective grain diameter a minimum and maximum value of respectively 0.25 and 0.5 mm is used. The packing parameter is kept constant.

7.2.2 The porosity-permeability relationship

In section 5.3, a porosity-permeability relationship is determined based on the core sample data from the upper part of the Sherwood Sandstone Group in the Ballymacilroy borehole. This relationship is given by:

$$Permeability(mD) = exp(-7.67 + 64.782 \times porosity(dec)). \tag{71}$$

Applying Archie's first law, this equation can be related to the bulk effective resistivity, giving:

$$Permeability(mD) = exp(-7.67 + 64.782 \times (R_w/R_0)^{1/m}). \tag{72}$$

This equation can then be used to calculate permeability values from the bulk effective resistivity values predicted by the Minim models. Using the previously determined values for the water resistivity, the bulk effective resistivity, the cementation exponent (table 7.1) and their allowed variations, permeability values and their associated uncertainty ranges are calculated for the upper part of the Sherwood Sandstone Group for each MT site (table 7.5). Again, the results show that the lowest permeability values are found at the two MT sites at Ballymacilroy and that the uncertainty ranges become considerably larger with increasing permeability. Comparing these uncertainty ranges with the uncertainty ranges associated with the permeability values resulting from the RGPZ model (table 7.4) shows that the uncertainty ranges listed in table 7.5 are significantly larger.

Borehole	MT site	Permeability (mD)	Uncertainty range
Annaghmore	LN002	829	70 - 8575
Ballynamullan	LN001	141	10 - 1997
	LN101	51	6 - 465
Ballymacilroy	LN028	1	0 - 7
	LN124	1	0 - 9

Table 7.5: Permeability values and their uncertainty ranges for the upper part of the Sherwood Sandstone Group for each MT site, derived from the bulk effective resistivity values predicted by the Minim models using the porosity-permeability relationship determined based on core sample data from the Ballymacilroy borehole.

7.3 Generalized calibrations of Archie's first law and the RGPZ model

In sections 7.1 and 7.2.1, Archie's first law and the RGPZ model are calibrated three times based on data from three boreholes. However, in order to apply this approach to all MT sites across the Lough Neagh Basin, generalized calibrations of Archie's first law and the RGPZ model will be required. In chapter 8 it is demonstrated that for all five MT sites the RGPZ model performs better than the porosity-permeability relationship of section 7.2.2 and therefore no generalized calibration for the latter is calculated.

Since there is some variation between the three boreholes and there is no indication that one borehole best approximates the average conditions in the Lough Neagh Basin, the three calibrations are used to determine a generalized calibration by taking the average values of the parameters of Archie's first law and the RGPZ model. Archie's first law has three parameters besides the bulk effective resistivity, being the tortuosity factor, the water resistivity and the cementation exponent. As the tortuosity factor has a value of 1 at all three boreholes, this value remains the same. The average value for the water resistivity is determined by taking the geometric average of the three water resistivity values, while the average value for the cementation exponent is determined by taking the arithmetic average. This gives average values of 0.09 Ωm for the water resistivity and 1.83 for the cementation exponent. Additionally, the RGPZ model contains the effective grain diameter. For this parameter a value of 0.29 mm is used for all three boreholes and therefore the same value is used in the generalized calibration. This gives the following generalized calibrations of Archie's first law and the RGPZ model, which can be applied to MT sites across the Lough Neagh Basin:

$$\phi = \left(\frac{0.09}{R_0}\right)^{1/1.83}, \tag{73}$$

$$k = \frac{8.41 \times 10^{-8} \times (0.09/R_0)^3}{35.8518}. \tag{74}$$

These equations are then applied to the resistivity values of the upper part of the Sherwood Sandstone Group predicted by the Minim models. The results are listed in table 7.6.

Borehole	MT site	Porosity (%)	Permeability (mD)
Annaghmore	LN002	15	70
Ballynamullan	LN001	19	267
	LN101	18	178
Ballymacilroy	LN028	18	178
	LN124	18	205

Table 7.6: Porosity and permeability values for each MT site, derived from the resistivity values for the upper part of the Sherwood Sandstone Group predicted by the Minim models using the generalized calibrations of Archie's first law and the RGPZ model.

7.4 Results

Table 7.7 shows an overview of the porosity and permeability values derived from the resistivity observed in the Minim models for each MT site. The results show that at Ballymacilroy the porosity and permeability are significantly lower compared to Annaghmore and Ballynamullan. It is argued that this can be explained by the difference in water resistivity, which is considerably lower at Ballymacilroy (table 7.1). The results of the uncertainty analyses show that the porosity values, calculated using Archie's first law, are reasonably well resolved, with a maximum uncertainty of 5 % porosity (table 7.2). The permeability values, however, have large uncertainty ranges, with the uncertainty ranges associated with the permeability calculated using the porosity-permeability relationship (table 7.5) being significantly larger than the uncertainty ranges associated with the permeability calculated using the RGPZ model (table 7.4). The three calibrations of Archie's first law and the RGPZ model are used to determine generalized calibrations, which can be applied to MT sites across the Lough Neagh Basin (equations 73 and 74). These equations are then applied to the resistivity values of the upper part of the Sherwood Sandstone Group predicted by the Minim models (table 7.6).

Borehole	MT site	Porosity (%) Archie's first law	Permeability (mD) RGPZ model	Permeability (mD) Porosity-permeability relationship
Annaghmore	LN002	22	741	829
Ballynamullan	LN001	19	365	141
	LN101	18	235	51
Ballymacilroy	LN028	12	13	1
	LN124	12	16	1

Table 7.7: Porosity and permeability values for the upper part of the Sherwood Sandstone Group at each MT site, derived from the resistivity values observed in the Minim models. The porosity values are calculated using Archie's first law and the permeability values are calculated using the RGPZ model and the porosity-permeability relationship determined based on core sample data.

8 Summary of results

In this chapter an overview of the results is presented and the results of the MT modeling and the petrophysical modeling are compared with the results of the borehole wireline logging data and core sample data analysis.

In table 8.1 values for the resistivity, the porosity and the permeability of the upper part of the Sherwood Sandstone Group resulting from the borehole data analysis are listed next to the values obtained from the Minim models and the petrophysical models used for each MT site. The table shows that the upper part of the Sherwood Sandstone Group is highly conductive and resistivity values estimated by the Minim models closely match the resistivity values determined based on the wireline logging data, the difference being the largest at MT site LN028 with 1.1 Ωm. The porosity values determined using Archie's first law closely match the porosity values obtained from the borehole logging data analysis for three out of five MT sites (LN001, LN002 and LN101). For sites LN028 and LN124, both located at Ballymacilroy, the porosity determined using Archie's first law is significantly lower than the porosity obtained from the borehole logging data analysis. This is a consequence of the resistivity values predicted by the Minim models being higher than the resistivity values determined based on the wireline logging data at Ballymacilroy. Comparing the permeability values resulting from the borehole data analysis and the petrophysical models shows that the permeability values estimated using the RGPZ model are good approximations of the permeability values resulting from the borehole data analysis. Again, the difference between the permeability values is the largest for the MT sites located at Ballymacilroy, which can be explained by the resistivity values predicted by the Minim models being higher than the resistivity values determined based on the wireline logging data. The comparison also demonstrates that the RGPZ model performs better than the porosity-permeability relationship for all five MT sites. Furthermore, table 8.1 shows that based on the Minim models, the upper part of the Sherwood Sandstone Group has the highest resistivity at site LN002. Simultaneously, the porosity and permeability values resulting from the petrophysical models also are highest at site LN002. A similar trend was observed in the results of the borehole data analysis, which show that the resistivity as well as the porosity and permeability are highest at Annaghmore (section 5.5). This is contrary to expectations, as theoretically a higher resistivity would indicate a lower porosity and a lower permeability.

Borehole	MT site	Resistivity (Ωm)		Porosity (%)		Permeability (mD)		
		Borehole data	Minim models	Borehole data	Archie's first law	Borehole data	RGPZ model	Porosity-permeability relationship
Annaghmore	LN002	3.1	3.0	21	22	723	741	829
Ballynamullan	LN001	2.1	1.9	20	19	303	365	141
	LN101	2.1	2.2	20	18	303	235	51
Ballymacilroy	LN028	1.1	2.2	18	12	83	13	1
	LN124	1.1	2.1	18	12	83	16	1

Table 8.1: Values for the resistivity, the porosity and the permeability of the upper part of the Sherwood Sandstone Group at each MT site, resulting from the borehole data analysis, the Minim models and the petrophysical models.

Table 8.2 shows the porosity and permeability values derived from the resistivity values for the upper part of the Sherwood Sandstone Group predicted by the Minim models, using the generalized calibrations of Archie's first law and the RGPZ model respectively. These values are compared with the porosity and permeability values resulting from the borehole data analysis and the porosity and permeability values derived using the petrophysical models calibrated for each borehole separately. Obviously, the values calculated using the petrophysical models calibrated for each borehole separately agree better with results from the borehole data analysis than the values determined using the generalized calibrations (except for the porosity values determined for the sites located at Ballymacilroy). At Annaghmore the difference between the results of the generalized calibrations and the results of the petrophysical models calibrated for each borehole separately are the largest, followed by the MT sites located at Ballymacilroy. These relatively large differences are explained by the difference between the values for the water resistivity at these locations (table 7.1) and the average value for the water resistivity (0.09 Ωm). At Ballynamullan, the value for the water resistivity closely matches the average value for the water resistivity (0.1 Ωm), and thus the differences between the values resulting from the generalized calibrations and the petrophysical models calibrated for each borehole separately are small. The results suggest that applying the generalized calibrations of Archie's first law and the RGPZ model to MT sites across the Lough Neagh Basin, away from borehole control, may not produce reliable results.

Borehole	MT site	Porosity (%)			Permeability (mD)		
		Borehole data	Archie's first law	Archie's first law generalized calibration	Borehole data	RGPZ model	RGPZ model generalized calibration
Annaghmore	LN002	21	22	15	723	741	70
Ballynamullan	LN001	20	19	19	303	365	276
	LN101	20	18	18	303	235	178
Ballymacilroy	LN028	18	12	18	83	13	178
	LN124	18	12	18	83	16	205

Table 8.2: Porosity and permeability values for the upper part of the Sherwood Sandstone Group determined for each MT site. The table shows the porosity and permeability values resulting from the borehole data analysis, as well as the porosity and permeability values derived from the resistivity values predicted by the Minim models using Archie's first law and the RGPZ model calibrated for each borehole separately and the generalized calibrations of Archie's first law and the RGPZ model.

PART 3

DISCUSSION, SUMMARY AND CONCLUSIONS

9 Discussion

In this chapter the data quality, the effectiveness and limitations of the applied methods and the results are discussed for each part of the research. Furthermore, the results are used in order to verify the method for porosity and permeability estimation introduced in this thesis and to continue the assessment of the geothermal energy potential of the Sherwood Sandstone Group in the Lough Neagh Basin.

9.1 Borehole data analysis

Data quality

The wireline logging data used in this research are very complete and overall the data are of good quality. However, there are two zones in the Ballymacilroy borehole where the data quality is of such a low quality that it is decided that interpretation in these zones is unreliable and thus no porosity and permeability curves are determined for these zones. The nature of the wireline logs in these zones indicate that the bad quality is due to technical errors and not due to a change in the stratigraphy. One of these zones is located in the upper part of the Sherwood Sandstone Group and thus affects the results of this study. As this zone makes up less than 10 % of the total thickness of the upper part of the Sherwood Sandstone Group and there are no indications that the zone is significantly different from the surrounding stratigraphy, the effect of this zone on the final results is assumed to be negligible and is not considered in further discussion. In addition to the wireline logging data a number of reports are available, containing information on the zone tops and borehole deviation data. However, no information is available for the drilling mud properties (i.e. temperature and resistivity), which is a big limitation as these parameters are necessary for calculating the porosity in IP. Since no information is available, default values for these parameters are used. The effect of varying these values on the final results is included in the Monte Carlo uncertainty analysis.

Methodology

The wireline log values and the values of the petrophysical parameters employed in IP all fall within the expected range. The resulting porosity curves are checked by comparing them with porosity curves based on different porosity models and using the core sample data as a QC. The results of these checks are satisfactory and confirm the validity of the porosity curves. Permeability curves are produced by applying a

porosity-permeability relation that is calculated based on the core sample data. Although the core sample data show a substantial amount of scatter, a satisfactory porosity-permeability relation is produced (fig. 5.7).

9.2 Processing and modeling of MT data

Data quality and methodology

The MT data of the five sites used in this study are not significantly affected by noise or the MT dead-band and the MT responses of the sites are very similar (appendix J), which is as expected since all five MT sites are located relatively close to each other within the Lough Neagh Basin, a maximum distance of 14 km apart. For processing and modeling of the MT data widely used methods are applied. The MT models used to derive resistivity values for the Sherwood Sandstone Group are produced using the Minim inversion code. It has been shown here that models produced using the Minim code are very similar to the sharp boundary models produced by the 1D inversion code incorporated in WinGLink. The resulting Minim models demonstrate that there is a strong agreement between the five sites (fig. 6.7), showing that the final MT models can be considered robust.

Note that the Minim models in this study are produced by running unconstrained inversions (i.e. not constrained by known depths to stratigraphic boundaries). When using the depths of stratigraphic boundaries known from the borehole data analysis to run constrained inversions, in most cases the resulting Minim models do not fit the MT data better than the unconstrained Minim models. Also, the unconstrained Minim models do not necessarily predict the depth of stratigraphic boundaries better than the constrained Minim models. Due to the inconsistent performances of the constrained models it was decided to use the unconstrained Minim models.

Uncertainty analysis

A problem involved in analyzing the uncertainty of an MT model is the trade-off between the conductivity and the thickness of the layer of interest, which is caused by the fact that MT models resolve the conductance (the product of the conductivity and the thickness) of the layers of the subsurface. As a result, layers of an MT model with different conductivity values and thicknesses can fit the MT data equally well. Therefore, in order to determine the sensitivity of the model to variation both conductivity and thickness of the layer should be varied simultaneously. This leads to another problem, as the thickness of a layer

can be varied by increasing or decreasing the depth of the top boundary of the layer, the bottom boundary of the layer or both. However, changing the depths of both the top boundary and the bottom boundary simultaneously gives an extremely large amount of possibilities for varying the thickness of the layer. Therefore, in this study the uncertainties associated with the depths of the top boundary and the bottom boundary are analyzed separately (table 6.5). Also, in this uncertainty analysis the resistivity values and thicknesses of the layers adjacent to the conductive layer are kept constant. However, changing the thickness of the conductive layer also changes the thickness of the adjacent layer and thus the conductance, causing the RMS error to increase. When the resistivity of the adjacent layer is allowed to vary, its value can be adjusted in order to accommodate the varying thickness of the layer. As a result the uncertainty ranges determined in this study are relatively conservative. Varying the depths of the top and bottom boundaries simultaneously and allowing the resistivity of the layers adjacent to the conductive layer to vary would produce broader uncertainty ranges.

Integration with borehole data

When integrating MT models with borehole data it is important to understand the differences between the two methods for measuring the resistivity. MT images the conductivity structure of the subsurface based on surface measurements and thus detects relatively large-scale features. This in contrast to wireline log measurements made in the boreholes, which detect variations in the resistivity on a very small scale. Also, MT measurements yield volume soundings and the MT response functions thus are volumetric averages of the sampled medium. Wireline logging measurements, on the other hand, provide 1D resistivity profiles. Lateral variations in stratigraphy and resistivity can therefore significantly affect the MT models compared to the wireline log measurements. The results of integrating the Minim models with the borehole data (fig. 6.8) show that generally the MT models succeed in defining the larger-scale conductivity structure of the subsurface and for each site the Minim model contains a conductive layer that can be related to the Sherwood Sandstone Group. However, the results also indicate that correlating layers in the MT models with stratigraphic boundaries is highly uncertain.

Besides the aforementioned differences between MT and wireline logging measurements, this can partly be explained by the fact that the resolution of MT models is relatively low and MT models thus are not capable of resolving small-scale features. These small-scale features (e.g. highly resistive intrusions, high resistivity peaks in (semi-)conductive formations), however, significantly affect the MT models, as

is shown in section 6.5. Also, there is the possibility that the MT responses of the five sites suffer from static shift, which may account for all or some of the depth discrepancies between the Minim models and the stratigraphic depths in the boreholes. Note that the the static shift correction applied to the response functions of MT site LN001 (section 6.2) consists of correcting for the shift between the TE and the TM modes. The static shift that is not corrected for (and referred to above) is a potential static shift between both TE and TM modes at one site with respect to both TE and TM modes at another site. However, as no independent means of assessing this static shift in the MT responses are available (e.g., using coincident TDEM soundings) it is not possible to determine whether any of the MT responses suffer from static shift.

Another inference is that the conductive layers of the Minim models do not solely relate to the Sherwood Sandstone Group but also incorporate (parts of) the overlying and underlying formations. The resistivity values determined for the Sherwood Sandstone Group based on the Minim models thus are averages of the resistivities of all the formations incorporated in the conductive layer of the models.

9.3 Petrophysical modeling

Methodology

Archie's first law assumes a fully saturated, clean (i.e. clay-free) medium. Therefore, it is assumed that the upper part of the Sherwood Sandstone Group is fully saturated, which is confirmed by the borehole data analysis. Also, the results of the borehole data analysis show that for the upper part of the Sherwood Sandstone Group the mean clay volume is less than 20 % (section 5.2.1), which is assumed to be low enough to allow the use of Archie's first law. The plots resulting from the calculation of the cementation exponent (fig. 7.1) demonstrate a strong agreement between Archie's first law and the borehole data. The plots also show that when the porosity is less than 10 % Archie's first law is significantly less reliable. However, since the results of both the borehole data analysis and the petrophysical modeling indicate that the average porosity of the upper part of the Sherwood Sandstone Group is larger than 10 % this does not affect the results of this study.

The RGPZ model is modified by applying Archie's first law, in order to introduce the bulk effective resistivity parameter into the RGPZ model. The main advantage of this approach, compared to using other permeability models, is that the number of parameters in the RGPZ model is limited and all variable parameters of the RGPZ model follow directly from Archie's first law and the MT models, with the exception

of the effective grain size parameter. The effective grain size, however, can accurately be estimated using borehole geological data. The limited number of parameters of the RGPZ model and the fact that values for these parameters can be estimated accurately reduces the uncertainty associated with the resulting permeability values. Additionally, extensive testing of different permeability models (including the RGPZ model, the Kozeny-Carman model, Berg, Schwartz, Katz and Thompson and the SSJ model) has been performed by Glover et al. (2006) and Walker & Glover (2010), using theoretical and experimental data. In these tests the values predicted by the different permeability models were compared. In all cases it was concluded that the RGPZ model performed well with respect to the true measured permeability and performed better than the other permeability models. Note that, despite a number of limitations (section 3.2.1), the RGPZ model can be applied to a wide range of reservoir rocks, including the Sherwood Sandstone Group. However, the effects of the clay content and the degree of saturation were not included in the tests performed by Glover et al. (2006) and Walker & Glover (2010) and might affect the performance of the RGPZ model. As the average clay volume of the upper part of the Sherwood Sandstone Group is less than 20 % and the formation is fully saturated, it is assumed that in this study the performance of the RGPZ model is not affected.

Finally, the porosity-permeability relationship, determined based on the core sample data from the upper part of the Sherwood Sandstone Group in the Ballymacilroy borehole, is used to derive permeability values. Obviously, this approach relies on the availability of core sample data and the relationship can only be applied to a specific stratigraphic formation.

Uncertainty analyses

The results of the uncertainty analysis performed for the porosity values calculated using Archie's first law (table 7.2) show that the porosity is reasonably well resolved. However, in this case values for the water resistivity and the cementation exponent are accurately determined based on wireline logging data. Tables 7.1 and 7.3 show that varying the values of the cementation exponent and specifically the water resistivity significantly affect the resulting porosity values. Therefore, in order to reliably derive the porosity from resistivity values predicted by MT models using Archie's first law, additional geological data (in complement to the MT data) from which these parameters can accurately be determined is essential. The same is true for reliably estimating the permeability using the RGPZ model and the porosity-permeability relationship, since in both approaches the porosity parameter is replaced by Archie's first law. Addition-

ally, the RGPZ model contains the effective grain diameter, for which additional geological data are necessary in order to give an accurate estimation of its value. The results of the uncertainty analyses performed for the permeability values calculated using the RGPZ model (table 7.4) and the porosity-permeability relationship (table 7.5) show large uncertainty ranges associated with the permeability values. However, the results of the Monte Carlo simulation (section 5.4) show that the uncertainty ranges associated with the permeability values determined in the borehole data analysis are equally large. It can be argued that large degrees of uncertainty are inherent in estimating the permeability, due to the many parameters involved and the wide variability in permeability at different scales.

9.4 Results

Porosity and permeability values for the Sherwood Sandstone Group

In previous studies, average porosity and permeability values for the Sherwood Sandstone Group are determined. McCann (1990) mentions an average porosity of 18 %, measured at Ballymacilroy, while Illing & Griffith (1986) mention an average porosity of 20 %. Note that the value mentioned by Illing & Griffith (1986) is measured in the Larne No. 2 borehole in the Larne Basin. Previously determined average permeability values for the upper part of the Sherwood Sandstone Group, measured in the Larne Basin and at Ballymacilroy in the Lough Neagh Basin, lie between 200 mD and 306 mD (Bennett 1986, Illing & Griffith 1986, McCann 1990). Table 8.1 shows that, with the exception of the porosity values determined using Archie's first law for the MT sites located at Ballymacilroy (LN028 and LN124), the porosity values calculated in this study are comparable to previously determined average porosity values for the upper part of the Sherwood Sandstone Group. Most of the permeability values determined in this study are substantially higher or lower than the permeability values found in the literature, except for the values determined for the MT sites located at Ballynamullan (LN001 and LN101).

The water resistivity and the deep induction resistivity (ILD) log

Table 7.1 shows that at Ballymacilroy the value for the water resistivity, determined based on wireline logging data, is considerably lower compared to Annaghmore and Ballynamullan. This is contrary to expectations and possibly indicates distinct and compartmentalized waters in the Lough Neagh Basin. Additionally, comparing the deep induction resistivity (ILD) log of the different boreholes shows that at Ballymacilroy the ILD log values for the upper part of the Sherwood Sandstone Group are substantially

lower than the values of the ILD log at Annaghmore and Ballynamullan (section 6.5). Too low values of the ILD log could explain the low water resistivity values at Ballymacilroy, as well as the fact that the average permeability value resulting from the borehole data analysis is substantially lower (83 mD) than the average permeability values for the Sherwood Sandstone Group at Ballymacilroy found in the literature (212 mD) (McCann 1990). However, there are no indications that the ILD log at Ballymacilroy is flawed, and as no water sample analysis data are available the values for the water resistivity cannot be confirmed.

Relation between the resistivity, the porosity and the permeability

In the results displayed in table 8.1, a trend can be observed in which the highest resistivity values for the upper part of the Sherwood Sandstone Group are associated with the highest porosity and permeability values. This is contrary to expectations, as theoretically a higher resistivity would indicate a lower porosity and a lower permeability. However, the resistivity values determined for the upper part of the Sherwood Sandstone Group (based both on the borehole data analysis and the Minim models) range from 1.1 to 3.1 Ωm, indicating a highly conductive formation. This is an extremely small variation in resistivity values, especially considering the fact that resistivity values can vary over many orders of magnitude. The results therefore imply that, while on a larger scale high resistivity values can still be related to low porosity and permeability values, this relation does not apply to variations in resistivity on a smaller scale.

9.5 An alternative method for porosity and permeability estimation

An alternative method is introduced for porosity and permeability estimation of (potential) geothermal reservoirs. In this approach, MT data are used to determine the resistivity of the reservoir. Then, petrophysical models (i.e. Archie's first law and the RGPZ model) are applied to the resistivity values predicted by the MT models in order to derive porosity and permeability values. In this study, wireline logging data and core sample data from three boreholes are used for calibration of the petrophysical models.

In chapter 8 it has been shown that using this approach the resistivity, the porosity and the permeability can accurately be estimated. Furthermore, the values for the resistivity, the porosity and the permeability determined utilizing this approach have satisfactory associated uncertainty ranges. It must be noted, however, that in cases where the resistivity predicted by the MT models deviates more than

1 Ωm from the actual resistivity (here the actual resistivity refers to the average resistivity determined based on wireline logging data), the porosity and permeability values estimated using the petrophysical models are significantly less accurate. Additionally, it has been demonstrated that in order to reliably define values for the parameters of Archie's first law and the RGPZ model the availability of additional geological data (in complement to the MT data) is essential. Without additional geological data that can be used for calibration, porosity and permeability values estimated using the petrophysical models will be inaccurate with large associated uncertainty ranges. Additional geological data would also be necessary in order to accurately determine the depth and thickness of the (potential) geothermal reservoir, as it has been shown that correlating layers in the MT models with stratigraphic boundaries is highly uncertain.

Therefore, for a successful implementation of the method introduced here this approach is best utilized in combination with additional geological data from a reference point. As argued by Niwas & Singhal (1985) and Soupios et al. (2007), when at a reference point surface measurements can be combined with additional geological data (e.g. wireline logging data, core sample data, water sample analysis data), correlations between the resistivity, the porosity and the permeability can be established. In this case, wireline logging data and core sample data are used to calibrate Archie's first law and the RGPZ model. These calibrations can then be used to estimate the hydraulic properties of the reservoir rocks or the aquifer for the entire MT survey area. However, note that for this approach a homogeneous character of the target formation is favorable, as for a heterogeneous character of the formation the values for the parameters of the petrophysical models will vary significantly per MT site, compromising the use of this approach.

Finally, the assumptions and limitations of Archie's first law and the RGPZ model need to be considered. None of the limitations of the RGPZ model seriously affects its application to many sedimentary reservoir rocks. In cases where the reservoir rocks contain a significant amount of clay minerals and/or are not fully saturated, Archie's first law is invalid. However, multiple methods and modifications of Archie's first law are available to correct for these effects. The effects of a significant clay content and partial saturation on the performance of the RGPZ model are uncertain and should be taken into account when necessary.

9.6 Geothermal energy potential assessment of the Sherwood Sandstone Group in the Lough Neagh Basin

In previous studies, temperatures were modeled for the Lough Neagh basin and the geothermal gradient was determined. This resulted in temperatures between 40 °C and 85 °C for the depth range between 1000 m and 2500 m and a geothermal gradient of approximately 30 °C/km (Pasquali et al. 2010). Also, the conductivity structure of the basin was analyzed, showing that the Sherwood Sandstone Group is the main conductive feature, and the total energy stored in the Sherwood Sandstone Group was estimated. The results, together with the obtained temperatures and geothermal gradient in the basin, indicated that the Sherwood Sandstone Group is a low-enthalpy reservoir with a high potential for geothermal energy exploitation (Pasquali et al. 2010, Loewer 2011). However, this potential only exists if it can be supported by adequate hydraulic properties of the reservoir rocks.

In this thesis, the average porosity and the average permeability of the upper part of the Sherwood Sandstone Group is determined using wireline logging data and core sample data from three boreholes in the Lough Neagh Basin: Annaghmore, Ballynamullan and Ballymacilroy. The average porosity varies between 18 % to 21 %, while the average permeability varies between 83 mD to 723 mD. Figure 9.1 shows that these values indicate a good/excellent quality of the reservoir. Additionally, the wireline logging data analysis indicates that the upper part of the Sherwood Sandstone Group is fully saturated. This, in combination with the results from previous studies, indicates a high potential for geothermal exploitation of the Sherwood Sandstone Group in the Lough Neagh Basin. It should be noted that, as mentioned before, the northeastern and southwestern areas of Lough Neagh have been identified as the main depocentres in the Lough Neagh Basin (Pasquali et al. 2010). However, no data are available for these areas and the boreholes and the MT sites used in this research are located away from the main depocentres. In the boreholes studied here the Sherwood Sandstone Group reaches a maximum depth of 1850 m at Ballymacilroy, with a temperature of approximately 70 °C. At the main depocentres, however, the Sherwood Sandstone Group is expected to be located at higher depths, providing higher temperatures. Additionally, it is likely these areas contain thicker sedimentary sequences. This, together with the higher temperatures, indicates a higher potential for geothermal exploitation at the main depocentres than the areas that have been investigates so far.

Future work on geothermal energy exploration of the Sherwood Sandstone Group in the Lough Neagh Basin should focus on identifying the areas in the basin with the highest geothermal potential. Theoretically, the method for porosity and permeability estimation introduced in this thesis can be utilized for this purpose, provided that there are sufficient MT data available. In section 7.3, generalized calibrations of Archie's first law and the RGPZ model have been calculated, which can be applied to MT sites across the Lough Neagh Basin. However, two problems arise when applying this method to the Sherwood Sandstone Group. First, as mentioned in section 9.5, for this approach a homogeneous character of the target formation is favorable. Since the Sherwood Sandstone Group was deposited in a braided fluviatile setting (Cowan 1993, Mitchell 2004a), a heterogeneous character can be assumed, which should be taken into account when utilizing the generalized calibrations of Archie's first law and the RGPZ model. Secondly, table 8.2 shows that the generalized calibrations may not produce reliable results, which in this case is due to varying values for the water resistivity of the upper part of the Sherwood Sandstone Group. The water resistivity values, determined based on the wireline logging data, vary significantly per borehole, with values ranging from 0.04 Ωm (Ballymacilroy) to 0.2 Ωm (Annaghmore). This might indicate distinct and compartmentalized waters in the Lough Neagh Basin, which would have a significant effect on potential geothermal energy exploitation of the Sherwood Sandstone Group. Therefore, it is recommended that the water resistivity values of the upper part of the Sherwood Sandstone Group in the Lough Neagh Basin determined in this study are

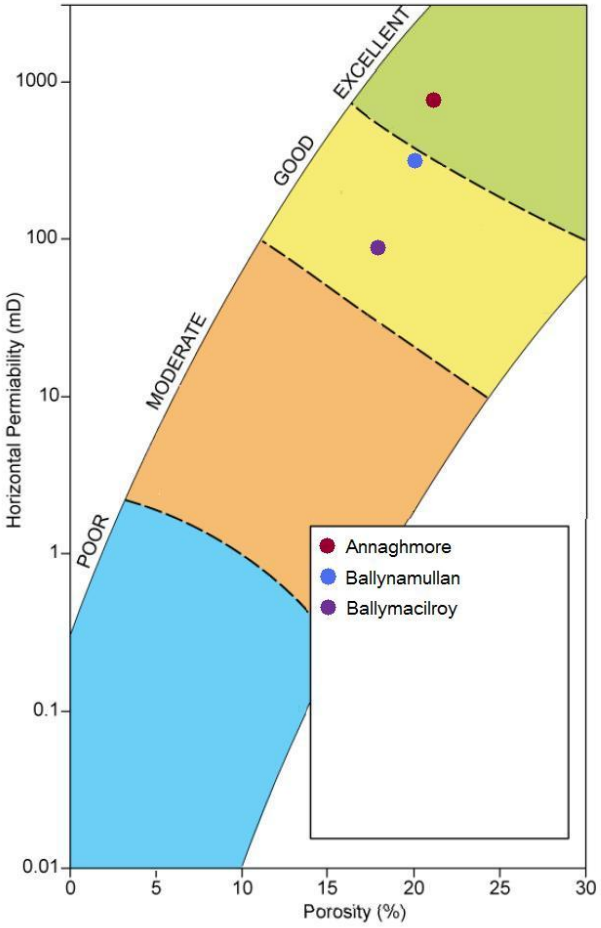

Figure 9.1: Porosity-permeability cross-plot showing the reservoir quality of the upper part of the Sherwood Sandstone Group. The data points show the average porosity and permeability values for each borehole (Annaghmore, Ballynamullan and Ballymacilroy), resulting from the borehole data analysis performed in this thesis. Modified from Reay (2004).

verified (for example using water sample analysis), in order to determine the applicability of the proposed approach on the Sherwood Sandstone Group in the Lough Neagh Basin. If the water resistivity values prove correct, it is recommended to investigate the cause of these large variations in water resistivity in order to determine the consequences for geothermal energy exploitation of the Sherwood Sandstone Group.

10 Summary and conclusions

An alternative method is introduced for estimating the porosity and the permeability of (potential) geothermal reservoirs based on MT data. First, MT data are used to determine the resistivity of the reservoir. Then, porosity and permeability values are derived from the resistivity values predicted by the MT models using petrophysical models (i.e. Archie's first law and the RGPZ model). In this study, this approach is applied to a case study of the Sherwood Sandstone Group in the Lough Neagh Basin, Northern Ireland. MT data from five MT sites are utilized in conjunction with wireline logging data and core sample data of three boreholes located in the Lough Neagh Basin. Archie's first law and the RGPZ model are calibrated using the borehole data. The results are used to advance the assessment of the geothermal energy potential of the Sherwood Sandstone Group.

The research is subdivided into three different parts: borehole data analysis, processing and modeling of MT data and petrophysical modeling. In the first part, the wireline logging data of the three boreholes (Annaghmore, Ballynamullan and Ballymacilroy) are evaluated using Interactive Petrophysics (IP) software. In IP, standard deterministic evaluation techniques are applied in order to produce porosity curves. Using the core sample measurements, a porosity-permeability relationship is determined based on reduced major axis regression (RMA). This relationship is applied to the porosity curves to produce permeability curves. Using the deep induction resistivity (ILD) logs and the estimated porosity and permeability curves, average values for the resistivity, the porosity and the permeability of the upper part of the Sherwood Sandstone Group are determined for each borehole. A Monte Carlo simulation is run to investigate the impact of uncertainties on the calculated results. The second part of the research concerns the processing and modeling of MT data. A strike angle and dimensionality analysis is carried out using the STRIKE program, which utilizes the extended Groom-Bailey decomposition method. The results of this analysis demonstrate a 1D character of the data for the period range used for modeling. Using the best-fitting strike angles determined in the strike angle analysis, the MT data are decomposed by applying the extended Groom-Bailey decomposition method. The decomposed data are corrected for static shift between the TE and TM modes where necessary and the response functions are smoothed by applying the ρ+ approach. Then, 1D modeling is performed using three different inversion codes: Occam, the 1D inversion code implemented in WinGLink and Minim. The misfit between the resulting MT models and the MT

data is determined using the Chi2 code, showing that the Minim models fit the MT data the best. An uncertainty analysis is performed for the Minim models and the Minim models are integrated with wireline logging data. Based on the Minim models, average resistivity values are determined for the Sherwood Sandstone Group. In the third part, Archie's first law, the RGPZ model and the porosity-permeability relationship determined based on the core sample measurements are used to derive the porosity and the permeability for the upper part of the Sherwood Sandstone Group from the resistivity values predicted by the Minim models. The petrophysical models are calibrated for each borehole separately, using the wireline logging data and the core sample data. The wireline logging data are used to define values for the cementation and the water resistivity parameter of Archie's first law, while the core sample data are used to define a value for the effective grain diameter parameter of the RGPZ model. For all porosity and permeability values resulting from the petrophysical models the associated uncertainty range is determined. Finally, generalized calibrations of Archie's first law and the RGPZ model are determined by taking the average values of the parameters of Archie's first law and the RGPZ model.

Comparing the average values for the resistivity, the porosity and the permeability resulting from the borehole wireline logging data and core sample data analysis with the resistivity, porosity and permeability values resulting from the MT models and the petrophysical models shows that the values estimated by the MT models and the petrophysical models are good approximations of the values resulting from the borehole data analysis. The resistivity values resulting from the wireline logging data analysis indicate that the upper part of the Sherwood Sandstone Group is highly conductive, with the resistivity varying between 1.1 and 3.1 Ωm. The resistivity values estimated by the Minim models closely match these values, with the difference being the largest at MT site LN028 with 1.1 Ωm. The porosity values determined using Archie's first law closely match the porosity values obtained from the wireline logging data analysis for three out of five MT sites (LN001, LN002 and LN101), with a maximum difference of 2 % porosity. For the MT sites located at Ballymacilroy (LN028 and LN124), the porosity determined using Archie's first law is significantly lower than the porosity obtained from wireline logging data analysis, with a difference of 6 % porosity, which is caused by the difference between the resistivity values predicted by the Minim models and the resistivity values determined based on the wireline logging data. The RGPZ model performs better than the porosity-permeability relationship determined based on the core sample measurements for all five MT sites and the permeability values estimated using the RGPZ model are good

approximations of the permeability values resulting from the borehole data analysis. Furthermore, the resistivity values predicted by the MT models and the porosity values estimated using Archie's first law are well resolved with small degrees of uncertainty. The permeability values estimated using the RGPZ model have relatively large associated uncertainty ranges. However, it is argued that large degrees of uncertainty are inherent in estimating the permeability.

Using the method for porosity and permeability estimation introduced in this thesis accurate estimates of the resistivity, the porosity and the permeability of a potential geothermal reservoir are obtained. It is demonstrated that for effective implementation of this approach the resistivity determined based on the MT models should not deviate from the actual average resistivity of the target formation more than 1 Ωm. Furthermore, for a successful implementation of this approach, the availability of additional geological data in complement to the MT data (e.g. wireline logging data, core sample data, water sample analysis data) is essential, in order to reliably define values for the parameters of Archie's first law and the RGPZ model and to determine the depth and thickness of the reservoir. Therefore, this approach is best utilized in combination with additional geological data from a reference site. Using the additional geological data, Archie's first law and the RGPZ model can be calibrated. The calibrated models can then be applied to MT sites throughout the entire investigation area. This approach is a time-saving, noninvasive and less expensive alternative to traditional methods for estimating the hydraulic properties of a (potential) geothermal reservoir and can be applied to many sedimentary reservoir rocks. However, the effects of a significant clay content and partial saturation of the reservoir rocks should be taken into account when necessary.

In previous studies temperatures between 40 °C and 85 °C were found for the depth range between 1000 m and 2500 m in the Lough Neagh Basin, which corresponds to a geothermal gradient of approximately 30 °C/km. Also, it was found that the Sherwood Sandstone Group is the main conductive feature in the basin. These results indicate that the Sherwood Sandstone Group is a low-enthalpy reservoir with a high potential for geothermal energy exploitation, provided that the reservoir rocks have adequate hydraulic properties. The results of the borehole data analysis conducted in this research show that the average porosity varies between 18 % and 21 %, while the average permeability ranges from 83 mD to 723 mD. These values indicate a good to excellent quality of the Sherwood Sandstone Group as a geothermal reser-

voir. Future work on geothermal energy exploration of the Sherwood Sandstone Group in the Lough Neagh Basin should focus on identifying the areas in the basin with the highest geothermal potential. It is expected that the northeastern and southwestern areas of Lough Neagh have a higher geothermal potential, as these areas have been identified as the main depocentres in the Lough Neagh Basin. In theory, the method for porosity and permeability estimation introduced in this thesis can be used for identifying the areas with the highest geothermal potential. However, two problems arise when applying this method, being (1) the heterogeneous character of the Sherwood Sandstone Group and (2) the large variation in water resistivity of upper part of the Sherwood Sandstone Group. It is recommended that the water resistivity values of the Sherwood Sandstone Group determined in this study are verified and that the possible causes for the large variations in water resistivity in the basin are investigated.

11 References

Anderson, T., Johnston, T., Mitchell, W. (2004): Chapter 1: Basement structure and the terrane model. *In:* Mitchell, W. (Ed.): The Geology of Northern Ireland; Our Natural Foundation 2. Geological Survey of Northern Ireland, 1–8.

Archie, G. (1942): The electrical resistivity log as an aid in determining some reservoir characteristics. Petroleum Transactions of AIME 146, 54–62.

Bahr, K. (1988): Interpretation of the magnetotelluric impedance tensor; regional induction and local telluric distortion. Journal of Geophysics 62, 119–127.

Barbier, E. (2002): Geothermal energy technology and current status: an overview. Renewable and Sustainable Energy Reviews 6, 3–65.

Bennett, J. (1986): Investigation of the geothermal potential of the UK. The sedimentary basins of Northern Ireland. Environmental and Deep Geology Division, Institute of Geological Sciences and Geological Survey of Northern Ireland, 35.

Berdichevsky, M., Dmitriev, V. (2008): Models and methods of magnetotellurics. Springer-Verlag, Berlin Heidelberg, Germany.

Berg, R. (1970): Method for determining permeability from reservoir rock properties. GCAG Transactions 20, 303–335.

Berg, R. (1975): Capillary pressures in stratigraphic traps. AAPG Bulletin 59, 929–956.

Bohonak, A. (2004): RMA - Software for Reduced Major Axis Regression. San Diego State University, San Diego, USA.

Bostick, F. (1977): A simple almost exact method of MT analysis. Workshop on electrical methods in geothermal exploration, U.S. Geological Survey.

Bruggeman, D. (1935): Berechnung verschiedener physikalischer Konstanten von heterogenen Substanzen. Annales Physik 24, 636–664.

Bussian, A. (1983): Electrical conductance in a porous medium. Geophysics 49, 1258–1268.

Cagniard, L. (1953): Basic theory of the magnetotelluric method of geophysical prospecting. Geophysics 18, 605–635.

Caldwell, T., Bibby, H., Brown, C. (2004): The magnetotelluric phase tensor. Geophysical Journal International 158, 457–469.

Carman, P. (1937): Fluid flow through granular beds. Transactions, Institution of Chemical Engineers 15, 150–167.

Chandra, S., Ahmed, S., Ram, A., Dewandel, B. (2008): Estimation of hard rock aquifers hydraulic conductivity from geoelectrical measurements: A theoretical development with field application. Journal of Hydrology 357, 218–227.

Clavier, C., Coates, G., Dumanoir, J. (1977): The theoretical and experimental bases for the "dual water" model for the interpretation of shaly sands. 52^{nd} Annual Fall Technical Conference and Exhibition of the Society of Petroleum Engineers of the AIME.

Constable, S., Parker, R., Constable, C. (1987): Occam's inversion: A practical algorithm for generating smooth models from electromagnetic sounding data. Geophysics 52, 289–300.

Cooper, M. (2004): Chapter 14: Palaeogene extrusive igneous rocks. *In:* Mitchell, W. (Ed.): The Geology of Northern Ireland; Our Natural Foundation 2. Geological Survey of Northern Ireland, 167–178.

Cowan, G. (1993): Identifaction and significance of aeolian deposits within the dominantly fluvial Sherwood Sandstone Group of the East Irish Sea Basin UK. *In:* North, C., Prosser, D. (Eds.): Characterization of Fluvial and Aeolian Reservoirs. Geological Socieity Special Publication 73, 231–245.

Devarajan, S., Toumelin, E., Torres-Verdin, C. (2006): Pore-scale analysis of the Waxman-Smits shaly sand conductivity model. SPWLA 47^{th} Annual Logging Symposium 2006.

Erkan, K., Holdmann, G., Benoit, W., Blackwell, D. (2008): Understanding the Chena Hot Springs, Alaska, geothermal system using temperature and pressure data from exploration boreholes. Geothermics 37, 565–85.

Fischer, G., Schnegg, P., Peguiron, M., Le Quang, B. (1981): An analytic one-dimensional magnetotelluric inversion scheme. Geophysical Journal. Royal Astronomical Society 67, 257–278.

Friedman, S. (2005): Soil properties influencing apparent electrical conductivity: a review. Computers and Electronics in Agriculture 46, 45–70.

Friedman, S., Seaton, N. (1998): Critical path analysis of the relationship between permeability and electrical conductivity of three-dimensional pore networks. Water Resources Research 34, 1703–1710.

Gamble, T., Goubau, W., Clarke, J. (1979): Magnetotellurics with a remote magnetic sounding. Geophysics 67, 53–68.

Glover, P. (2009): What is the cementation exponent? A new interpretation. The Leading Edge 28, 82–85.

Glover, P. (2010): A generalized Archie's law for n phases. Geophysics 75, 247–265.

Glover, P., Zadjali, I., Frew, K. (2006): Permeability prediction from MICP and NRM data using an electrokinetic approach. Geophysics 71, 49–60.

Gomez, C., Dvorkin, J., Vanorio, T. (2010): Laboratory measurements of porosity, permeability, resistivity and velocity on Fontainebleau sandstones. Geophysics 75, 191–204.

Goodman, R., Jones, G., Kelly, J., Slowey, E., O'Neill, N. (2004): Geothermal Energy Resource Map of Ireland; Final Report. Online publication at www.seai.ie.

Goubau, W., Gamble, T., Clarke, J. (1978): Magnetotelluric data analysis: removal of bias. Geophysics 43, 1157–1169.

Groom, R., Bailey, R. (1989): Decomposition of magnetotelluric impedance tensors in the presence of local three-dimensional galvanic distortion. Journal of Geophysical Research (Solid Earth) 94, 1913–1925.

Hanai, T. (1960): Theory of the dielectric dispersion due to the interfacial polarization and its application to emulsions. Kolloid-Zeitschrif 171, 23–31.

Hanai, T. (1961): Dielectric on the interfacial polarization for two-phase mixtures. Bulletin of the Institute of Chemical Research of Kyoto University 39, 341–367.

Herweijer, J. (1997): Sedimentary heterogeneity and flow towards a well; Assessment of flow through heterogeneous formations. Ph.D. thesis, University of Amsterdam, Amsterdam, The Netherlands.

IFTechnology (2012): Kennisdocument IP. Internal corporate document.

Illing, L., Griffith, A. (1986): Gas prospects in the 'Midland Valley' of Northern Ireland. *In:* Brooks, J., Goff, J., van Hoorn, B. (Eds.): Habitat of Palaeozoic Gas in N.W. Europe. Geological Society Special Publication 23, 73–84.

Jiracek, G. (1990): Near-surface and topographic distortions in electromagnetic induction. Surveys in Geophysics 11, 163–203.

Johnson, D., Koplik, J., Schwartz, L. (1986): New pore-size parameter characterizing transport in porous media. Physical Review Letters 57, 2564–2567.

Johnson, D., Sen, P. (1988): Dependence of the conductivity of a porous medium on electrolyte conductivity. Physics Review B 37, 3502–3510.

Johnston, T. (2004): Post-Variscan deformation and basin formation. *In:* Mitchell, W. (Ed.): The Geology of Northern Ireland; Our Natural Foundation 2. Geological Survey of Northern Ireland, 205–210.

Jones, A., Chave, A., Egbert, G., Auld, D., Bahr, K. (1989): A comparison of techniques for magnetotelluric response function estimation. Journal of Geophysical Research (Solid Earth) 94, 14201–14213.

Juhasz, I. (1986): Conversion of routine air-permeability data into stressed brine-permeability data. Society of Professional Well Log Analysts, Aberdeen Chapter, 10^{th} European Formation Evaluation Symposium Transactions, paper Y, 1-15.

Katz, A., Thompson, A. (1986): Quantitative prediction of permeability in porous rock. Physical Review B 34, 8179–8181.

Kearey, P., Brooks, M., Hill, I. (2002): An introduction to geophysical exploration. Blackwell Science Ltd., Oxford, UK.

Khalil, M., Santos, F. (2009): Influence of degree of saturation in the electric resistivity-hydraulic conductivity relationship. Survey in Geophysics 30, 601–615.

Kozeny, J. (1927): Ueber kapillare leitung des wassers im boden. Situngsberichte Wiener Akademie 136, 271–306.

Lesmes, D., Friedman, S. (2005): Relationships between the electrical and hydrogeological properties of rocks and soils. *In:* Rubin, Y., Hubbard, S. (Eds.): Hydrogeophysics. Springer, 87–128.

Loewer, M. (2011): Investigation of the geothermal energy potential of the Lough Neagh Basin, Northern Ireland, using magnetotelluric and gravity modelling. Unpubl. msc thesis, Swiss Federal Institute of Technology, Zurich, Switzerland.

Lund, J., Freeston, D. (2000): World-wide direct uses of geothermal energy 2000. Proceedings World Geothermal Congress 2000, Japan.

Mavko, G., Mukerji, T., Dvorkin, J. (1998): The rock physics handbook. Cambridge University Press, Cambridge, UK.

McCaffrey, R., McCann, N. (1992): Post-Permian basin history of northeast Ireland. *In:* Parnell, J. (Ed.): Basins on the Atlantic Seaboard: Petroleum Geology, Sedimentology nd Basin Evolution. Geological Society Special Publication 62, 277–290.

McCann, N. (1990): The subsurface geology between Belfast and Larne, Northern Ireland. Irish Journal of Earth Sciences 10, 157–173.

McCann, N. (1991): Subsurface geology of the Lough Neagh - Larne Basin, Northern Ireland. Irish Journal of Earth Sciences 11, 53–64.

McKinley, J., Worden, R., Ruffell, A. (2001): Contact diagenesis: the effect of an intrusion on reservoir quality in the Triassic Sherwood Sandstone Group, Northern Ireland. Journal of Sedimentary Research 71, 484–495.

McNeice, G., Jones, A. (2001): Multisite, mutlifrequency tensor decomposition of magnetotelluric data. Geophysics 66, 158–173.

Mitchell, W. (2004a): Chapter 10: Triassic. *In:* Mitchell, W. (Ed.): The Geology of Northern Ireland; Our Natural Foundation 2. Geological Survey of Northern Ireland, 133–144.

Mitchell, W. (2004b): Chapter 11: Jurassic. *In:* Mitchell, W. (Ed.): The Geology of Northern Ireland; Our Natural Foundation 2. Geological Survey of Northern Ireland, 145–148.

Mitchell, W. (2004c): Chapter 12: Cretaceous. *In:* Mitchell, W. (Ed.): The Geology of Northern Ireland; Our Natural Foundation 2. Geological Survey of Northern Ireland, 149–160.

Mitchell, W. (2004d): Chapter 16: Late Paleogene (Oligocene) sedimentary basins. *In:* Mitchell, W. (Ed.): The Geology of Northern Ireland; Our Natural Foundation 2. Geological Survey of Northern Ireland, 199–204.

Mitchell, W. (2004e): Chapter 7: Carboniferous. *In:* Mitchell, W. (Ed.): The Geology of Northern Ireland; Our Natural Foundation 2. Geological Survey of Northern Ireland, 79–116.

Mitchell, W. (2004f): Chapter 8: Variscan (Hercynian) orogenic cycle. *In:* Mitchell, W. (Ed.): The Geology of Northern Ireland; Our Natural Foundation 2. Geological Survey of Northern Ireland, 117–124.

Mitchell, W. (2004g): Chapter 9: Permian. *In:* Mitchell, W. (Ed.): The Geology of Northern Ireland; Our Natural Foundation 2. Geological Survey of Northern Ireland, 125–132.

Muffler, L., Cataldi, R. (1978): Methods for regional assessment of geothermal resources. Geothermics 7, 53–89.

Naylor, D., Philcox, M., Clayton, G. (2003): Annaghmore-1 and Ballynamullan-1 wells, Larne-Lough Neagh Basin, Northern Ireland. Irish Journal of Earth Sciences 21, 47–69.

Naylor, D., Shannon, P. (1999): The Irish Sea region: Why the general lack of exploration success? Journal of Petroleum Geology 22, 363–370.

Niblett, C., E.R. nd Sayn-Wittgenstein (1960): Variation of electrical conductivity with depth b magnetotelluric method. Geophysics 25, 998–1008.

Niwas, S., de Lima, O. (2003): Aquifer parameter estimation from surface resistivity data. Groundwater 41, 94–99.

Niwas, S., Singhal, D. (1985): Aquifer transmissivity of porous media from resistivity data. Journal of Hydrology 82, 143–153.

Noetinger, B. (1994): The effective permeability of a heterogeneous medium. Transport in Porous Media 15, 99.

Parker, R. (1980): The inverse problem of electromangetic induction: Existence and construction of solutions based on incomplete data. Journal of Geophysical Research 85, 4421–4428.

Parker, R. (1982): The existence of a region inaccessible to magnetotelluric sounding. Geophysical Journal of the Royal Astronomical Society 68, 165–170.

Parker, R., Booker, J. (1996): Optimal one-dimensional inversion and bounding of magnetotelluric apparent resistivity and phase measurements. Physics of the Earth and Planetary Interiors 98, 269–282.

Parker, R., Whaler, K. (1981): Numerical methods for establishing solutions for the inverse problem of electromagnetic induction. Journal of Geophysical Research 86, 9574–9584.

Pasquali, R., O'Neill, N., Reay, D., Waugh, T. (2010): The geothermal potential of Northern Ireland. Proceedings World Geothermal Congress 2010.

Reay, D. (2004): Chapter 22: Oil and gas. *In:* Mitchell, W. (Ed.): The Geology of Northern Ireland; Our Natural Foundation 2. Geological Survey of Northern Ireland, 273–290.

Salem, H., Chillingarian, G. (1999): The cementation factor of Archie's equation for shaly sandstone reservoirs. Journal of Petroleum Science and Engineering 23, 83–93.

Sen, P., Scala, C., Cohen, M. (1981): A self-similar model for sedimentary rocks with application to the dielectric constant of fused glass beads. Geophysics 45, 781–795.

Shelton, R. (1997): Tectonic evolution of the Larne Basin. *In:* Meadows, N., Trueblood, S., Hardman, M., Cowan, G. (Eds.): Petroleum Geology of the Irish Sea and Adjacent Areas. Geological Society Special Publications 2, 113–133.

Simpson, F., Bahr, K. (2005): Practical Magnetotellurics. Cambridge University Press, Cambridge, UK.

Sleeman, A., McConnell, B., Gatley, S. (2004): Understanding Earth processes, rocks and the geological history of Ireland. Geological Survey of Ireland, Dublin, Ireland.

Soupios, P., Kouli, M., Vallinatos, F., Vafidis, A., Stavroulakis, G. (2007): Estimation of aquifer hydraulic parameters from surficial geophysical methods. Journal of Hydrology 338, 122–131.

Spratt, J., Jones, A., Jackson, V., Collins, L., Avdeeva, A. (2009): Lithospheric geometry of the Wopmay orogen from a Slave craton to Bear Province magnetotelluric transect. Journal of Geophysical Research 114.

Swift, C. (1967): A magnetotelluric investigation of an electrical conductivity anomaly in the Southwestern United States. Ph.D. thesis, Massachusetts Institute of Technology, Cambridge, USA.

Telford, W., Geldart, L., Sheriff, R. (1990): Applied Geophysics. Cambridge University Press, Cambridge, UK.

Tikhonov, A. (1950): On determining electrical characteristics of the deep layers of the Earth's crust. Doklady Nauk SSSR 73, 295–297.

Unsworth, M., Soyer, W., Tuncer, V. (2005): Magnetotelluric measurements for determining the subsurface salinity and porosity structure of Amchitka Island, Alaska. Online publication at www.cresp.org.

Walker, E., Glover, P. (2010): Permeability models of porous media; Characteristic length scales, scaling constants and time-dependent electrokinetic coupling. Geophysics 75, 235–246.

Waxman, M., Smits, L. (1968): Electrical conductivities in oil-bearing shaly sands. Society of Petroleum Engineers Journal 8, 107–122.

Weaver, J., Agarwal, A., Lilley, F. (2000): Characteristics of the magnetotelluric tensor in terms of its invariants. Geophysical Journal International 141, 321–336.

WesternGeco (2009): Magnetotelluric Survey Lough Neagh, Northern Ireland - Final Report: 3D inversion modeling. WesternGeco SDI, Milan, 1, 2009.

Worthington, P. (1993): The uses and abuses of the Archie equations; 1: The formation factor-porosity relationship. Journal of Applied Geophysics 30, 215–228.

A Appendix - Stratigraphy for each borehole as defined in IP

Annaghmore

Zone #	Zone Name	Zone Top	Zone Bottom	Zone Color
1	Mercia Mudstone Gp	364	491.64	
2	Mercia Mudstone Gp	491.64	497.4	
3	Toomebridge Sandstone Fm	497.4	688.8	
4	Drumcullen Fm	688.8	862.6	
5	Drumderg House Fm	862.6	968.3	
6	Gallagh Bridge Fm	968.3	995.2	
7	Belfast Harbour Evaporite Fm	995.2	1011.9	
8	Carlane Fm	1011.9	1031.7	
9	Ballina Bridge Fm	1031.7	1406.6	
10	Annaghmore Fm	1406.6	1554.5	

Ballynamullan

Zone #	Zone Name	Zone Top	Zone Bottom	Zone Color
1	Mercia Mudstone Gp	486.2	659.7	
2	Mercia Mudstone Gp	659.7	700.4	
3	Toomebridge Sandstone Fm	700.4	763.4	
4	Dolerite intrusion	763.4	779.7	
5	Toomebridge Sandstone Fm	779.7	926.6	
6	Drumcullen Fm	926.6	1109.5	
7	Drumderg House Fm	1109.5	1229.2	
8	Dolerite intrusion	1229.2	1230.8	
9	Gallagh Bridge Fm	1230.8	1271	
10	Gallagh Bridge Fm	1271	1287.5	
11	Belfast Harbour Evaporite Fm	1287.5	1295.4	
12	Belfast Harbour Evaporite Fm	1295.4	1317.3	
13	Carlane Fm	1317.3	1347.2	
14	Ballina Bridge Fm	1347.2	1450	

Ballymacilroy

Zone #	Zone Name	Zone Top	Zone Bottom	Zone Color
1	Mercia Mudstone Gp	1221	1447	
2	Upper Sherwood Sandstone Gp	1447	1474.9	
3	Anomaly	1474.9	1495.4	
4	Upper Sherwood Sandstone Gp	1495.4	1673	
5	Lower Sherwood Sandstone Gp	1673	1822	
6	Lower Sherwood Sandstone Gp	1822	1850	
7	Permian Marls	1850	1876.9	
8	Permian Marls	1876.9	1902	
9	(Upper) Permian Sandstone	1902	1912.4	
10	Anomaly	1912.4	1939.6	
11	(Upper) Permian Sandstone	1939.6	1967	
12	Magnesian Limestone	1967	1995	
13	(Lower) Permian Sandstone & Conglomerate	1995	2241	

Figure A.1: Overview of the stratigraphy for each borehole as defined in IP. All depths are in measured depth. The Ballymacilroy borehole contains two zones where the logs are nullified due to bad data quality. These zones are named 'Anomaly'.

B Appendix - Clay volume module interactive plots

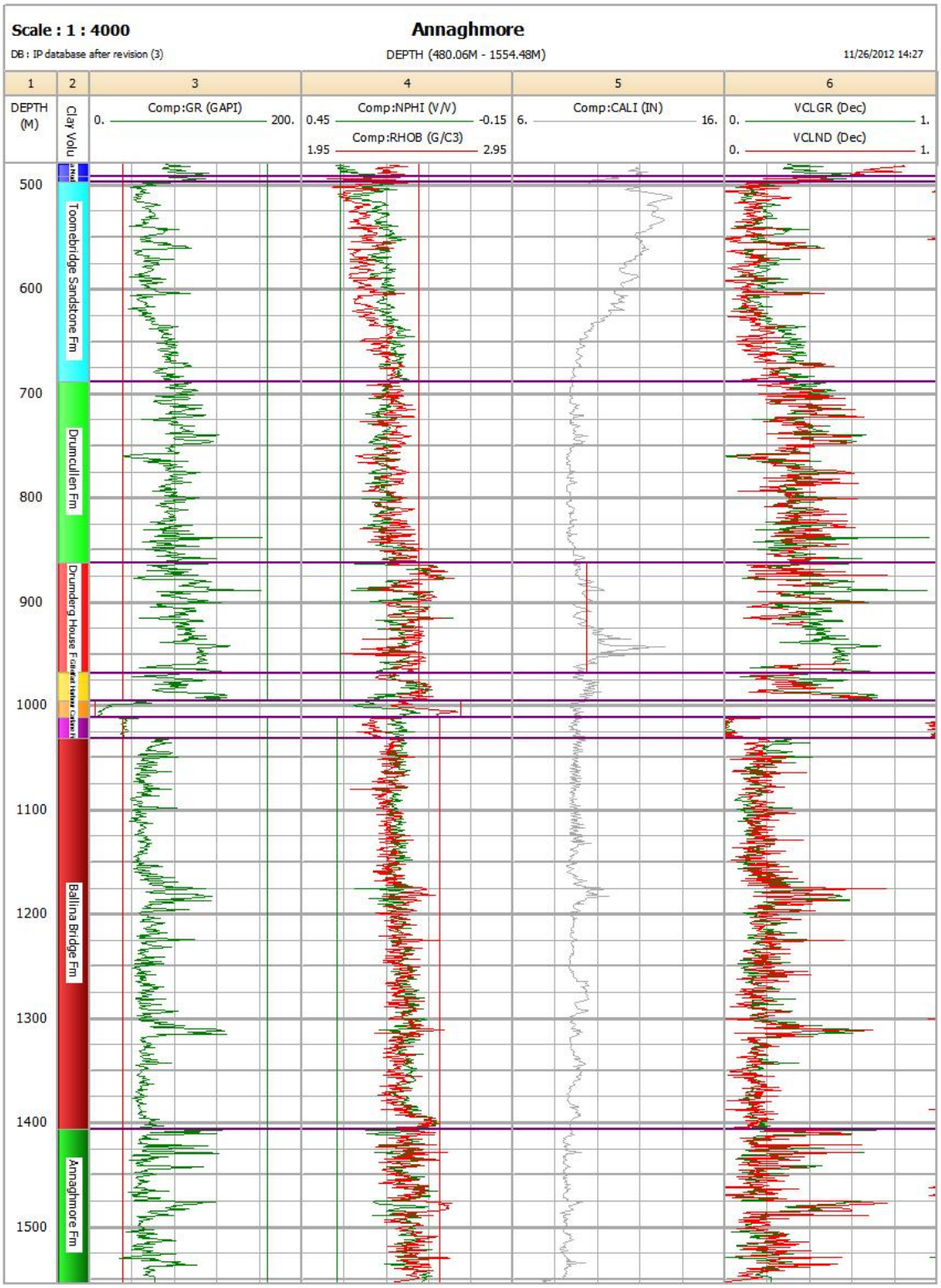

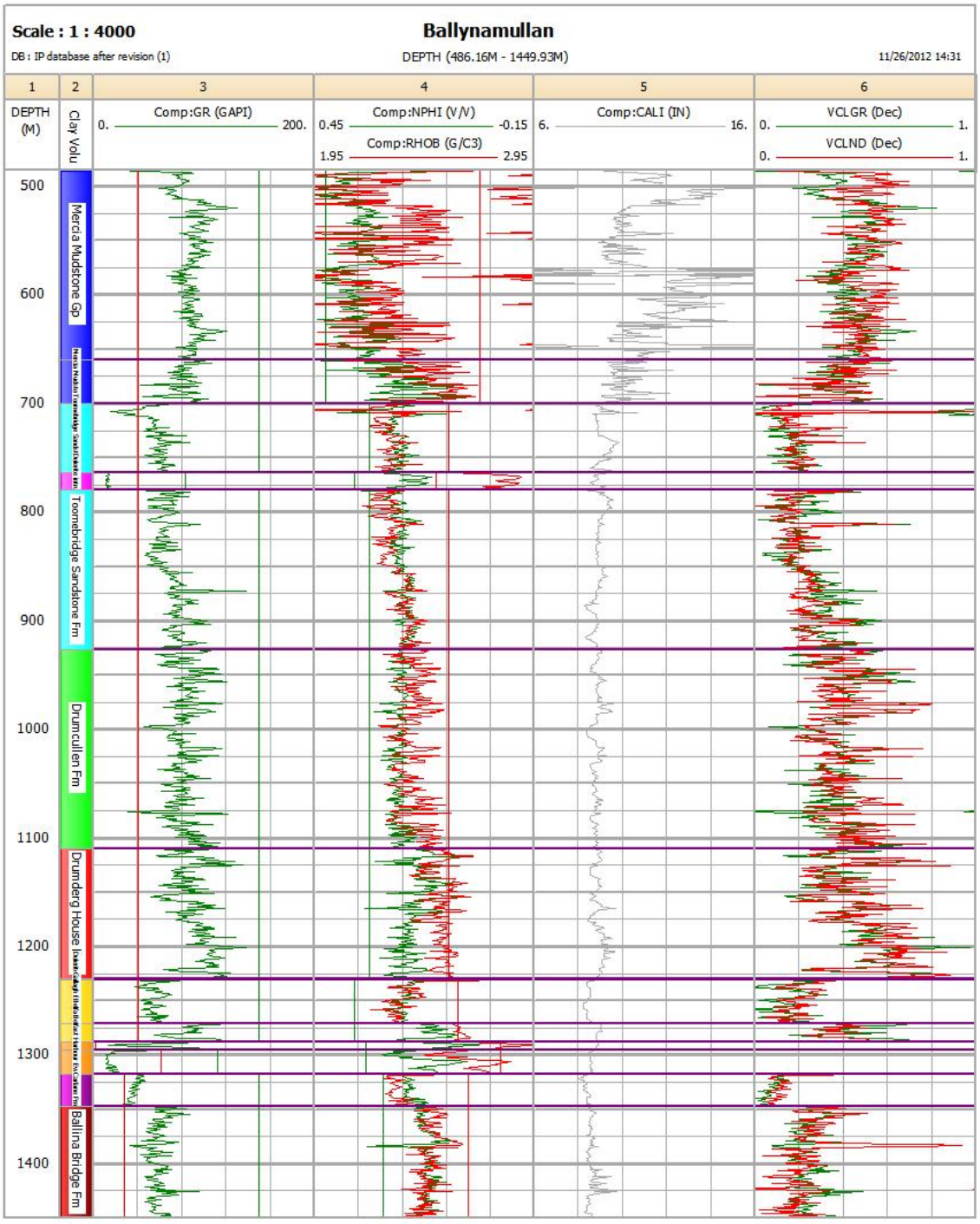
Scale : 1 : 4000
Ballynamullan
DB : IP database after revision (1)
DEPTH (486.16M - 1449.93M)
11/26/2012 14:31
1
2
3
4
5
6
DEPTH (M)
Clay Volu
Comp:GR (GAPI)
0.
200.
Comp:NPHI (V/V)
0.45
-0.15
Comp:RHOB (G/C3)
1.95
2.95
Comp:CALI (IN)
6.
16.
VCLGR (Dec)
0.
1.
VCLND (Dec)
0.
1.
500
600
700
800
900
1000
1100
1200
1300
1400
Mercia Mudstone Gp
Toomebridge Sandstone Fm
Drumcullen Fm
Drumderg House
Ballina Bridge Fm

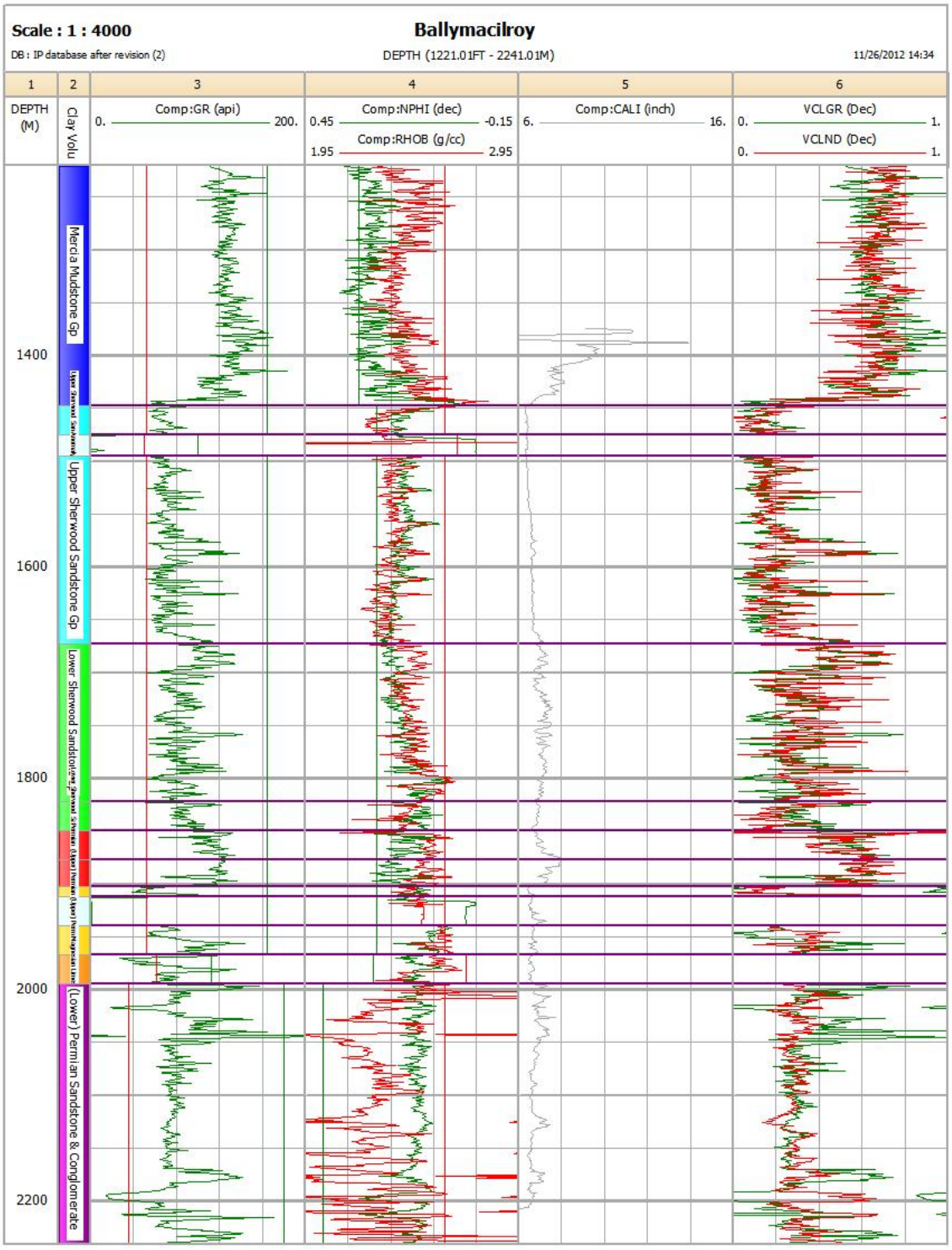

Figure B.1: Clay volume module interactive plot for each borehole. The first track shows the measured depth, the second track shows the stratigraphy, the third track is the single clay indicator track showing the gamma ray (GR) log, the fourth track is the double clay indicators track showing the neutron (NPHI) and the density (RHOB) logs, the fifth track shows the caliper (CALI) log and the sixth track shows the clay volume curves calculated from the single clay indicator ($VCLGR$; green line) and the double clay indicators ($VCLND$; red line). For each log/curve the units are specified in the figure.

C Appendix - Clay volume module parameter values

CLAY VOLUME PARAMETERS

Input Curves

Gamma Ray	: Comp:GR	Neu/Den Density	: Comp:RHOB
Neu/Den Neutron	: Comp:NPHI	Bad Hole 1	: Comp:CALI

Output Curves

Vclay Gamma Ray	: VCLGR	Vclay Neu/Den	: VCLND
Vclay minimum	: VCL	Vclay average	: VCLAV
Vclay mixed	: VCLmix		

Well : Annaghmore

Zone number 3 Toomebridge Sandstone Fm Top : 497.40 Bottom : 688.80

Gr Use	: Yes	Gr Clean	: 31	Gr Clay	: 168
Gr Method	: Linear	ND Use	: Yes	ND Neu Clay	: 0.34
ND Den Clay	: 2.5	ND Den Clean1	: 2.65	ND Den Clean2	: 2.05
ND Neu Clean1	: -0.03	ND Neu Clean2	: 0.28	BadH1 Use	: No
BadH1 Min	:	BadH1 Max	:	Link PhiSw Clay	: Yes
Vcl Av Method	: Mean	Vcl Mix Method	: Minimum		

Well : Ballynamullan

Zone number 3 Toomebridge Sandstone Fm Top : 700.40 Bottom : 763.40

Gr Use	: Yes	Gr Clean	: 41	Gr Clay	: 150
Gr Method	: Linear	ND Use	: Yes	ND Neu Clay	: 0.3
ND Den Clay	: 2.56	ND Den Clean1	: 2.65	ND Den Clean2	: 2.09
ND Neu Clean1	: -0.02	ND Neu Clean2	: 0.27	BadH1 Use	: No
BadH1 Min	:	BadH1 Max	:	Link PhiSw Clay	: Yes
Vcl Av Method	: Mean	Vcl Mix Method	: Minimum		

Zone number 4 Dolerite intrusion Top : 763.40 Bottom : 779.70

Zone number 5 Toomebridge Sandstone Fm Top : 779.70 Bottom : 926.60

Gr Use	: Yes	Gr Clean	: 41	Gr Clay	: 150
Gr Method	: Linear	ND Use	: Yes	ND Neu Clay	: 0.3
ND Den Clay	: 2.56	ND Den Clean1	: 2.65	ND Den Clean2	: 2.09
ND Neu Clean1	: -0.02	ND Neu Clean2	: 0.27	BadH1 Use	: No
BadH1 Min	:	BadH1 Max	:	Link PhiSw Clay	: Yes
Vcl Av Method	: Mean	Vcl Mix Method	: Minimum		

Well : Ballymacilroy

Zone number 2 Upper Sherwood Sandstone Gp Top : 1447.00 Bottom : 1474.90

Gr Use	: Yes	Gr Clean	: 52	Gr Clay	: 165
Gr Method	: Linear	ND Use	: Yes	ND Neu Clay	: 0.25
ND Den Clay	: 2.6	ND Den Clean1	: 2.65	ND Den Clean2	: 2.14
ND Neu Clean1	: -0.03	ND Neu Clean2	: 0.24	BadH1 Use	: No
BadH1 Min	:	BadH1 Max	:	Link PhiSw Clay	: Yes
Vcl Av Method	: Mean	Vcl Mix Method	: Minimum		

Zone number 3 Anomaly Top : 1474.90 Bottom : 1495.40

Zone number 4 Upper Sherwood Sandstone Gp Top : 1495.40 Bottom : 1673.00

Gr Use	: Yes	Gr Clean	: 52	Gr Clay	: 165
Gr Method	: Linear	ND Use	: Yes	ND Neu Clay	: 0.25
ND Den Clay	: 2.6	ND Den Clean1	: 2.65	ND Den Clean2	: 2.14
ND Neu Clean1	: -0.03	ND Neu Clean2	: 0.24	BadH1 Use	: No
BadH1 Min	:	BadH1 Max	:	Link PhiSw Clay	: Yes
Vcl Av Method	: Mean	Vcl Mix Method	: Minimum		

Figure C.1: Clay volume module parameter values for the Upper Sherwood Sandstone Group/Toomebridge Sandstone Formation in each borehole.

D Appendix - Equations porosity and water saturation module

D.1 Automatically calculated parameters

Before the iterative process is started, the following parameters are calculated automatically.

Mud filtrate salinity ($SalinSxozone$):

$$SalinSxozone = Alog\left(\frac{3.562 - log(Rmf75 - 0.0123)}{0.955}\right) \quad \text{(ppm)} \tag{75}$$

Mud filtrate density ($RhoSxozone$):

$$RhoSxozone = 1.0 + 7 \times SalinSxozone \times 10^{-7} - (Temp - 80)^2 \times 10^{-6} \quad \text{(gm/cc)} \tag{76}$$

Hydrocarbon hydrogen index ($NeuHcHI$):

$$NeuHcHI = 9 \times HcDen \times \frac{4 - 2.5 \times HcDen}{16 - 2.5 \times HcDen} \tag{77}$$

Apparent hydrocarbon density ($DenHcapp$):

$$DenHcapp = 2 \times HcDen \times \frac{10 - 2.5 \times HcDen}{16 - 2.5 \times HcDen} \tag{78}$$

Where $Rmf75$ is the mud filtrate resistivity converted to 75 °F, $Temp$ is the input from the temperature log and $HcDen$ is the hydrocarbon density.

D.2 Sonic porosity model

When the sonic porosity model is selected the porosity can be calculated using the Wyllie equation or the Raymer equation.

Wyllie equation:

$$\phi = \frac{Dt - Dtma - VCL \times (Dtcl - Dtma)}{(Dtfl \times Sxo + Dthy \times (1 - Sxo) - Dtma) \times Cp} \tag{79}$$

Where Dt: input from the sonic log, $Dtma$: sonic matrix value, $Dtcl$: sonic clay value, $Dtfl$: sonic filtrate value, $Dthy$: sonic hydrocarbon value, VCL: clay volume, Sxo: flushed zone water saturation and Cp: compaction factor.

Raymer equation:

$$\phi_{clay} = \frac{(2 \times Vma - Vf) - \sqrt{(2 \times Vma - Vf)^2 - 4 \times Vma \times (Vma - Vclay)}}{2 \times Vma} \tag{80}$$

$$Vfc = \frac{1}{Dtfl \times Sxo + Dthy \times (1 - Sxo)} \tag{81}$$

$$\phi_{son} = \frac{(2 \times Vma - Vfc) - \sqrt{(2 \times Vma - Vfc)^2 - 4 \times Vma \times (Vma - Vlog)}}{2 \times Vma} \tag{82}$$

$$\phi = \phi_{son} - \phi_{clay} \times VCL \tag{83}$$

Where $Vma = 1/Dtma$, $Vf = 1/Dtfl$, $Vclay = 1/Dtclay$ and $Vlog = 1/Dt$.

D.3 $PHIlimit$ and m

For intervals where the value of the minimum clay volume (VCL) curve is larger than the cutoff value (VCL_{cutoff}) of 0.4 a maximum $PHIE$ value is determined ($PHIlimit$). For these intervals $PHIE$ is less than or equal to$PHIlimit$ and the cementation exponent (m) is recalculated:

$$PHIlimit = (PHIE_{max} + \Delta PHIE_{max}) \times (1 - VCL) \times 10^{-10(VCL - VCL_{cutoff})^{1.6}} \tag{84}$$

$$m = m \times 10^{VCL - VCL_{cutoff}} \tag{85}$$

Where $\Delta PHIE_{max}$ is a parameter with a value of 0.05.

D.4 BVW and $VSILT$

When the iteration is finished, the bulk water volume (BVW) curve and the silt volume ($VSILT$) curve are calculated:

$$BVW = PHIE \times Sw \tag{86}$$

$$VSILT = \frac{1 - PHIE}{PHIE_{max} - VCL} \tag{87}$$

Where Sw is the effective water saturation.

E Appendix - Porosity and water saturation module interactive plots

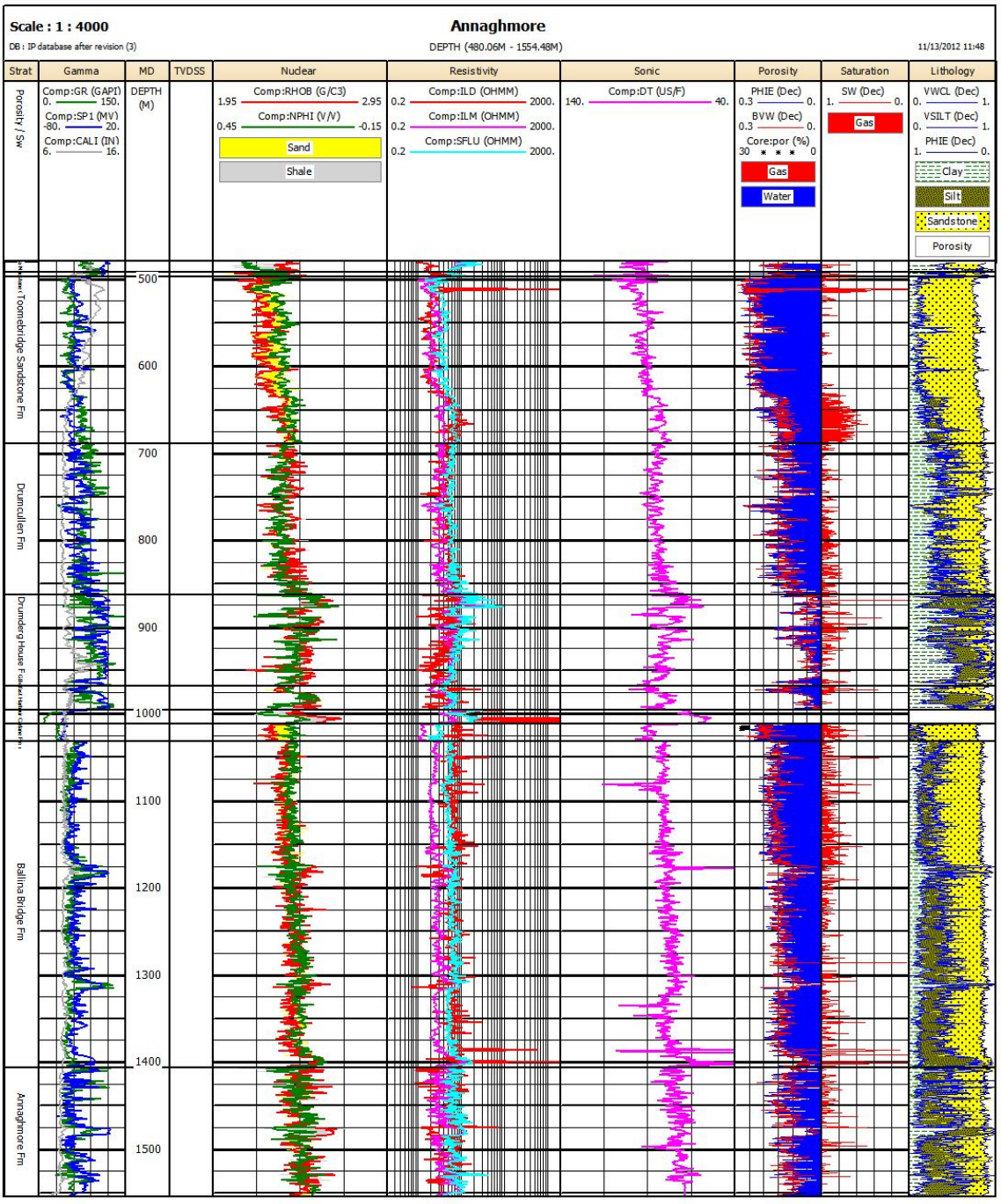

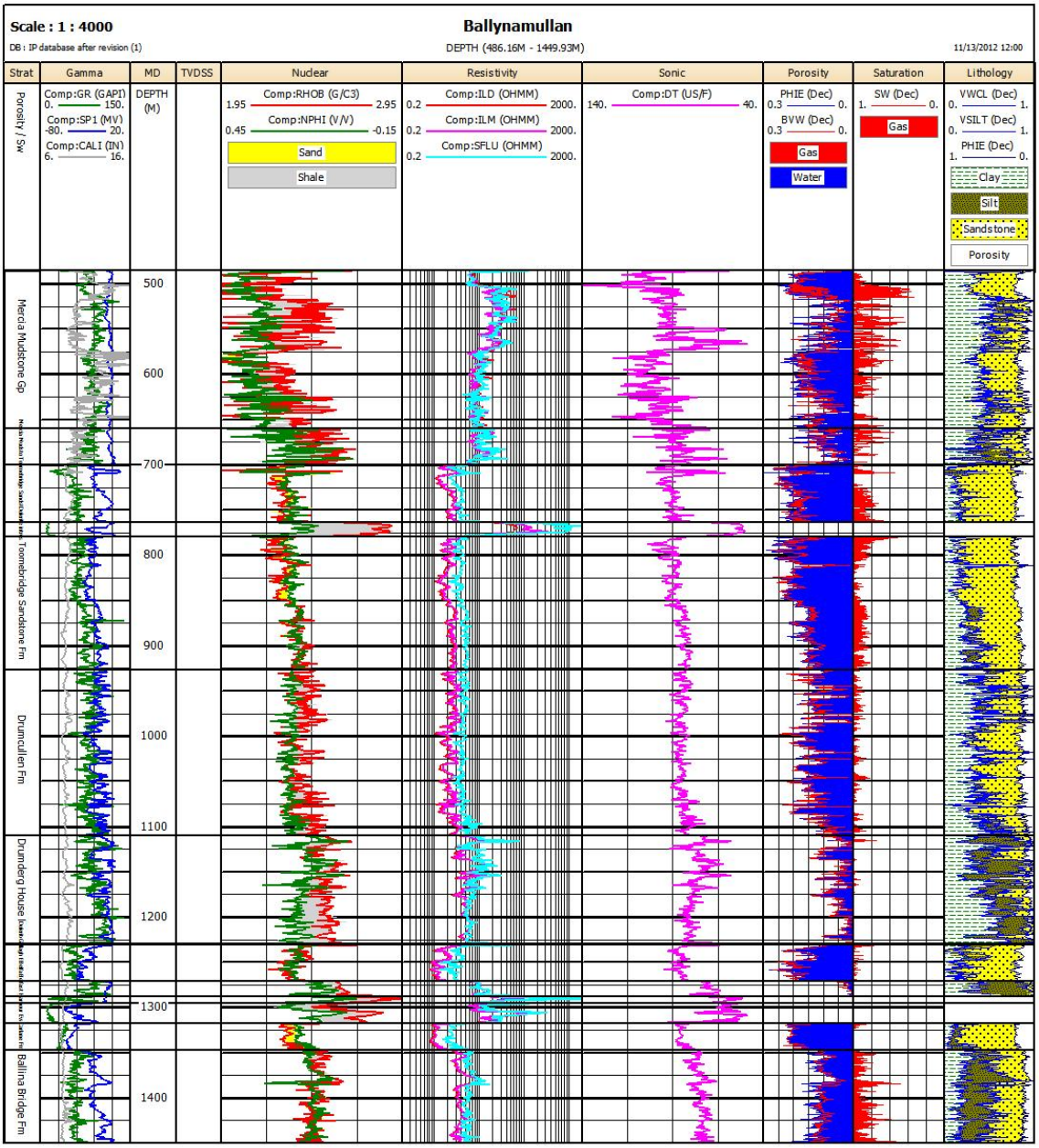
Scale : 1 : 4000
Ballynamullan
DB : IP database after revision (1)
DEPTH (486.16M - 1449.93M)
11/13/2012 12:00
Strat
Gamma
MD
TVDSS
Nuclear
Resistivity
Sonic
Porosity
Saturation
Lithology
Porosity / Sw
Comp:GR (GAPI)
0. 150.
Comp:SP1 (MV)
-80. 20.
Comp:CALI (IN)
6. 16.
DEPTH (M)
Comp:RHOB (G/C3)
1.95 2.95
Comp:NPHI (V/V)
0.45 -0.15
Sand
Shale
Comp:ILD (OHMM)
0.2 2000.
Comp:ILM (OHMM)
0.2 2000.
Comp:SFLU (OHMM)
0.2 2000.
Comp:DT (US/F)
140. 40.
PHIE (Dec)
0.3 0.
BVW (Dec)
0.3 0.
Gas
Water
SW (Dec)
1. 0.
Gas
VWCL (Dec)
0. 1.
VSILT (Dec)
0. 1.
PHIE (Dec)
1. 0.
Clay
Silt
Sandstone
Porosity
Mercia Mudstone Gp
Tremebridge Sandstone Fm
Drumcullen Fm
Drumderg House
Ballina Bridge Fm
500
600
700
800
900
1000
1100
1200
1300
1400

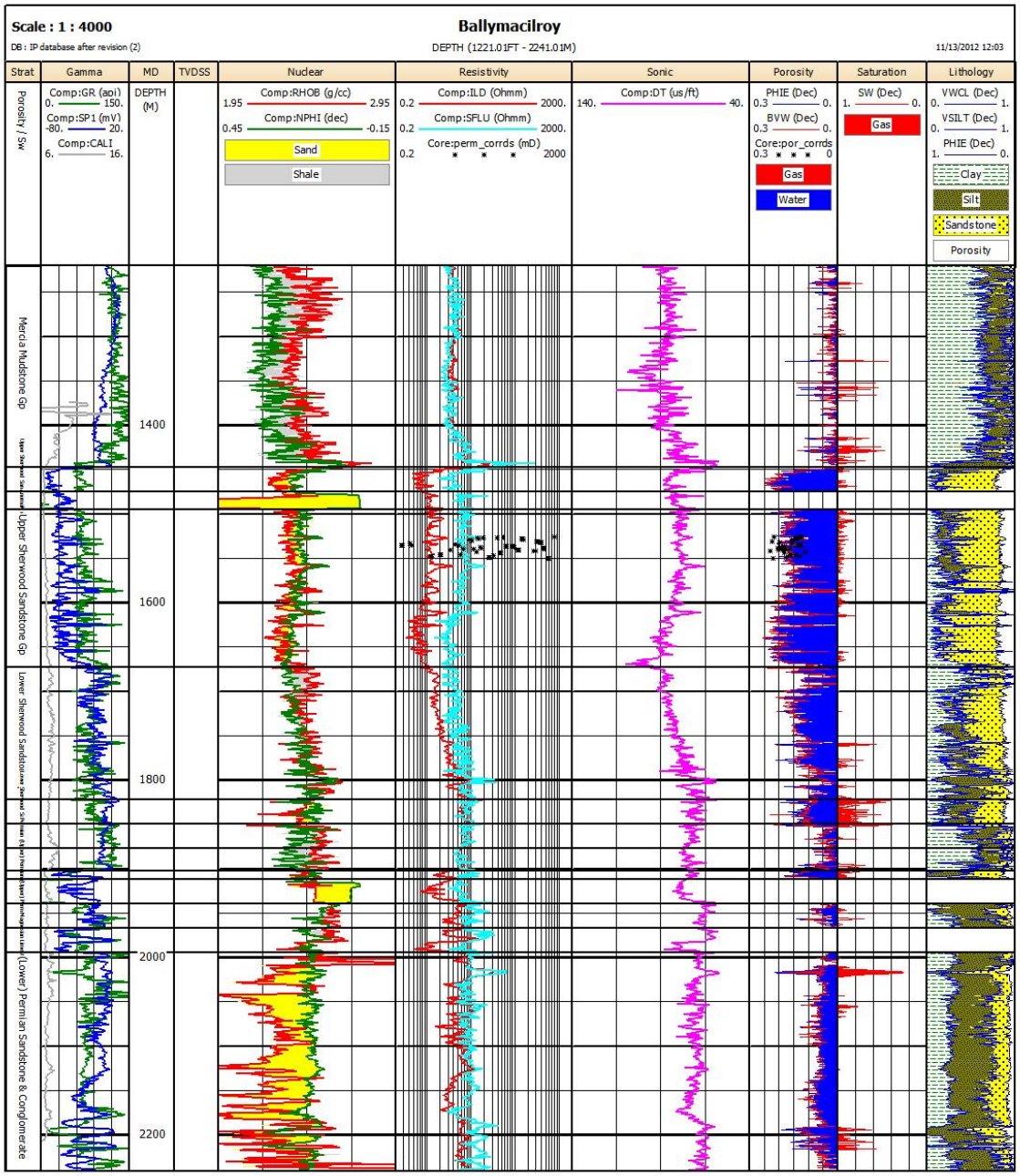

Figure E.1: Porosity and water saturation module interactive plot for each borehole. The interactive plot displays the following wireline logs: the gamma ray (GR) log, the spontaneous potential (SP1) log, the caliper (CALI) log, the density (RHOB) log, the neutron (NPHI) log, the deep induction resistivity (ILD) log, the medium induction (ILM) log, the spherically focused resistivity (SFLU) log and the sonic (DT) log. The following output curves are displayed in the interactive plot: the effective porosity ($PHIE$) curve, the bulk volume water (BVW) curve, the effective water saturation (SW) curve, the wet clay volume ($VWCL$) curve and the silt volume ($VSILT$) curve. For each log/curve the units are specified in the figures. The output curves can be used for interpretation, as can be seen in the lithology track of the interactive plot, where the clay volume curve, the silt volume curve and the effective porosity curve are used to display the proportion of clay, silt, sandstone and porosity of the total rock.

F Appendix - Porosity and water saturation module parameter values

POROSITY WATER SATURATION PARAMETERS

Input Curves

Neutron	: Comp:NPHI	Density	: Comp:RHOB
Sonic	: Comp:DT	Clay Volume	: VCL
Rt	: Comp:ILD	Temperature	: Temp
Bad hole	: Comp:RHOB		

Output Curves

Phi Total	: PHIT	Phi effective	: PHIE
Sw	: SW	Sw unlimited	: SWU
Bulk vol water	: BVW	Wet clay volume	: VWCL
Dry Clay volume	: VDCL	Volume silt	: VSILT
Logic flag	: PHIFLAG	Matrix density	: RHOMA
Sonic matrix	: DTMA	Coal Volume	: VCOAL
Salt volume	: VSALT	Hydrocarbon den	: RHOHY
Density Porosity	: PhiDen	Sonic Porosity	: PhiSon
Kill Anal. Flag	: KillFlag		

Well : Annaghmore

Zone number 3 Toomebridge Sandstone Fm Top : 497.40 Bottom : 688.80

Rw	: 0.2	Rw Temp	: 37	Rmf	: 0.1
Rmf Temp	: 23.9	Rho Sxo zone	:	Salin Sxo zone	:
Rho Wet Clay	: 2.5	Neu Wet Clay	: 0.34	Sonic Wet Clay	: 90
Res Clay	: 2	Hc Den	: 0.2	Neu Hc HI	:
Den Hc app	:	GD source	: Param	Rho GD	: 2.65
Rho GD max	: 2.85	Rho GD min	: 2.6	Sonic matrix	: 55.5
Sonic Equ	: Raymer	Sonic water	: 189	Neu Form Sal	: Yes
Neu Log Cont	: Schlumb	Neu Tool Type	: CNL	Porosity Method	: Neu Den
Variable Hc Den	: No	Variable GD	: Yes	Variable Vcl	: No
Mineral Model	: ss/ls/dol	OBM ?	: No	Phi max	: 0.25
Delta Phi max	: 0.05	m vari wth Vcl	: Yes	Vcl cutoff	: 0.4
Bad Hole Disc ?	: Yes	Disc Min	:	Disc Max	: 2.2
Sat Equation	: Indon	a factor	: 1	m exponent	: 2
n exponent	: 2	Invasion factor	: 1	Sxo Method	: Inv Fac
m source	: Param	n source	: Param	Coal Logic	: No
Salt Logic	: No	PhiT Clay	: 0.1	Phie Sw Limit	: 0
Phie Limit	: 0	Vcl Limit	: 1	Kill Logic	: No
Link Clay Vol	: Yes	Swi Limit	: 0		

Well : Ballynamullan

Zone number 3 Toomebridge Sandstone Fm Top : 700.40 Bottom : 763.40

Rw	: 0.1	Rw Temp	: 40	Rmf	: 0.1
Rmf Temp	: 25	Rho Sxo zone	:	Salin Sxo zone	:
Rho Wet Clay	: 2.56	Neu Wet Clay	: 0.3	Sonic Wet Clay	: 90
Res Clay	: 2	Hc Den	: 0.2	Neu Hc HI	:
Den Hc app	:	GD source	: Param	Rho GD	: 2.65
Rho GD max	: 2.85	Rho GD min	: 2.6	Sonic matrix	: 55.5
Sonic Equ	: Raymer	Sonic water	: 190	Neu Form Sal	: Yes
Neu Log Cont	: Schlumb	Neu Tool Type	: CNL	Porosity Method	: Neu Den
Variable Hc Den	: No	Variable GD	: Yes	Variable Vcl	: No
Mineral Model	: ss/ls/dol	OBM ?	: No	Phi max	: 0.25
Delta Phi max	: 0.05	m vari wth Vcl	: Yes	Vcl cutoff	: 0.4
Bad Hole Disc ?	: Yes	Disc Min	:	Disc Max	: 2.2
Sat Equation	: Indon	a factor	: 1	m exponent	: 2
n exponent	: 2	Invasion factor	: 1	Sxo Method	: Inv Fac
m source	: Param	n source	: Param	Coal Logic	: No
Salt Logic	: No	PhiT Clay	: 0.1	Phie Sw Limit	: 0
Phie Limit	: 0	Vcl Limit	: 1	Kill Logic	: No
Link Clay Vol	: Yes	Swi Limit	: 0		

Zone number 4 Dolerite intrusion Top : 763.40 Bottom : 779.70

Zone number 5 Toomebridge Sandstone Fm Top : 779.70 Bottom : 926.60

Rw	: 0.1	Rw Temp	: 40	Rmf	: 0.1
Rmf Temp	: 25	Rho Sxo zone	:	Salin Sxo zone	:
Rho Wet Clay	: 2.56	Neu Wet Clay	: 0.3	Sonic Wet Clay	: 90
Res Clay	: 2	Hc Den	: 0.2	Neu Hc HI	:
Den Hc app	:	GD source	: Param	Rho GD	: 2.65
Rho GD max	: 2.85	Rho GD min	: 2.6	Sonic matrix	: 55.5
Sonic Equ	: Raymer	Sonic water	: 190	Neu Form Sal	: Yes
Neu Log Cont	: Schlumb	Neu Tool Type	: CNL	Porosity Method	: Neu Den
Variable Hc Den	: No	Variable GD	: Yes	Variable Vcl	: No
Mineral Model	: ss/ls/dol	OBM ?	: No	Phi max	: 0.25
Delta Phi max	: 0.05	m vari wth Vcl	: Yes	Vcl cutoff	: 0.4
Bad Hole Disc ?	: Yes	Disc Min	:	Disc Max	: 2.2
Sat Equation	: Indon	a factor	: 1	m exponent	: 2
n exponent	: 2	Invasion factor	: 1	Sxo Method	: Inv Fac
m source	: Param	n source	: Param	Coal Logic	: No
Salt Logic	: No	PhiT Clay	: 0.1	Phie Sw Limit	: 0
Phie Limit	: 0	Vcl Limit	: 1	Kill Logic	: No
Link Clay Vol	: Yes	Swi Limit	: 0		

Well : Ballymacilroy

Zone number 2 Upper Sherwood Sandstone Gp Top : 1447.00 Bottom : 1474.90

Rw	: 0.04	Rw Temp	: 65	Rmf	: 0.1
Rmf Temp	: 25	Rho Sxo zone	:	Salin Sxo zone	:
Rho Wet Clay	: 2.6	Neu Wet Clay	: 0.25	Sonic Wet Clay	: 94
Res Clay	: 5	Hc Den	: 0.8	Neu Hc HI	:
Den Hc app	:	GD source	: Param	Rho GD	: 2.65
Rho GD max	: 2.85	Rho GD min	: 2.6	Sonic matrix	: 55.5
Sonic Equ	: Raymer	Sonic water	: 190	Neu Form Sal	: Yes
Neu Log Cont	: Schlumb	Neu Tool Type	: CNL	Porosity Method	: Neu Den
Variable Hc Den	: No	Variable GD	: Yes	Variable Vcl	: No
Mineral Model	: ss/ls/dol	OBM ?	: No	Phi max	: 0.25
Delta Phi max	: 0.05	m vari wth Vcl	: Yes	Vcl cutoff	: 0.4
Bad Hole Disc ?	: Yes	Disc Min	:	Disc Max	: 2.2
Sat Equation	: Indon	a factor	: 1	m exponent	: 2
n exponent	: 2	Invasion factor	: 1	Sxo Method	: Inv Fac
m source	: Param	n source	: Param	Coal Logic	: No
Salt Logic	: No	PhiT Clay	: 0.1	Phie Sw Limit	: 0
Phie Limit	: 0	Vcl Limit	: 1	Kill Logic	: No
Link Clay Vol	: Yes	Swi Limit	: 0		

Zone number 3 Anomaly Top : 1474.90 Bottom : 1495.40

Zone number 4 Upper Sherwood Sandstone Gp Top : 1495.40 Bottom : 1673.00

Rw	: 0.04	Rw Temp	: 65	Rmf	: 0.1
Rmf Temp	: 25	Rho Sxo zone	:	Salin Sxo zone	:
Rho Wet Clay	: 2.6	Neu Wet Clay	: 0.25	Sonic Wet Clay	: 94
Res Clay	: 5	Hc Den	: 0.8	Neu Hc HI	:
Den Hc app	:	GD source	: Param	Rho GD	: 2.65
Rho GD max	: 2.85	Rho GD min	: 2.6	Sonic matrix	: 55.5
Sonic Equ	: Raymer	Sonic water	: 190	Neu Form Sal	: Yes
Neu Log Cont	: Schlumb	Neu Tool Type	: CNL	Porosity Method	: Neu Den
Variable Hc Den	: No	Variable GD	: Yes	Variable Vcl	: No
Mineral Model	: ss/ls/dol	OBM ?	: No	Phi max	: 0.25
Delta Phi max	: 0.05	m vari wth Vcl	: Yes	Vcl cutoff	: 0.4
Bad Hole Disc ?	: Yes	Disc Min	:	Disc Max	: 2.2
Sat Equation	: Indon	a factor	: 1	m exponent	: 2
n exponent	: 2	Invasion factor	: 1	Sxo Method	: Inv Fac
m source	: Param	n source	: Param	Coal Logic	: No
Salt Logic	: No	PhiT Clay	: 0.1	Phie Sw Limit	: 0
Phie Limit	: 0	Vcl Limit	: 1	Kill Logic	: No
Link Clay Vol	: Yes	Swi Limit	: 0		

Figure F.1: Porosity and water saturation module parameter values for the Upper Sherwood Sandstone Group/Toomebridge Sandstone Formation in each borehole.

G Appendix - Core sample measurements

Depth (m)	Porosity (%)	Permeability (mD)
1524	22.8	919
1524.9	13	98
1525.2	14.7	41
1525.8	14.9	31
1526.7	15.2	226
1527.7	16.4	31
1529.5	23.5	580
1530.4	20.9	488
1531.6	16.3	2
1532.2	13.1	15
1533.1	14.5	17
1533.4	13.5	2
1534.1	19	233
1535	19	192
1535.9	20.3	40
1536.8	21.4	588
1537.7	17.1	30
1538	19.8	11
1538.6	21.3	196
1539.5	24.2	455
1540.5	11.7	35
1541.4	19.3	95
1543.2	15.2	17
1544.1	16.8	9
1545	17.5	80
1545.9	13.7	6
1546.9	18.4	59
1547.8	23.1	692

Table G.1: Core sample measurements for the upper part of the Sherwood Sandstone Group in the Ballymacilroy borehole, consisting of 28 effective porosity and horizontal intrinsic permeability values.

H Appendix - Permeability curves

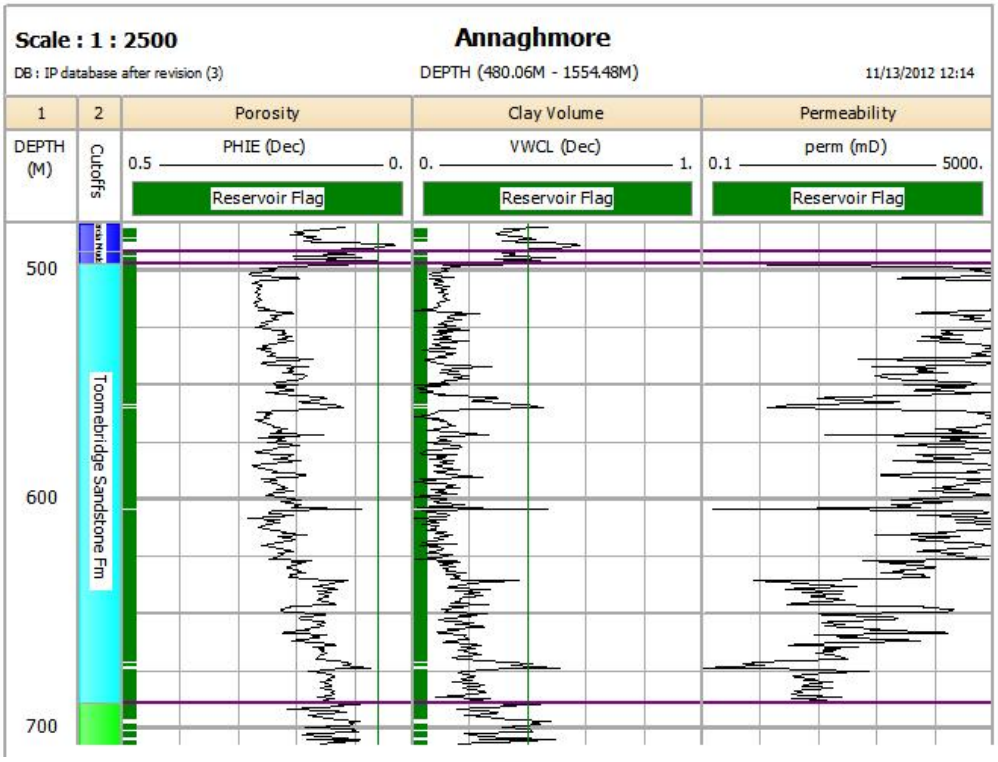

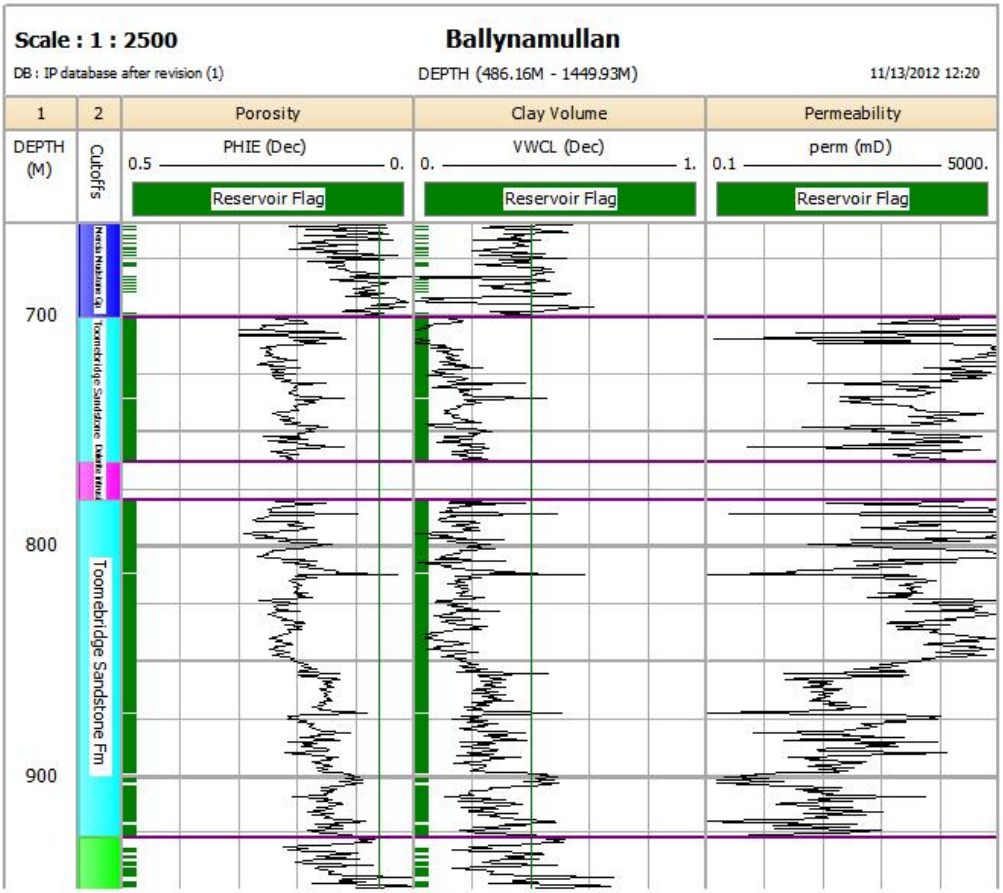

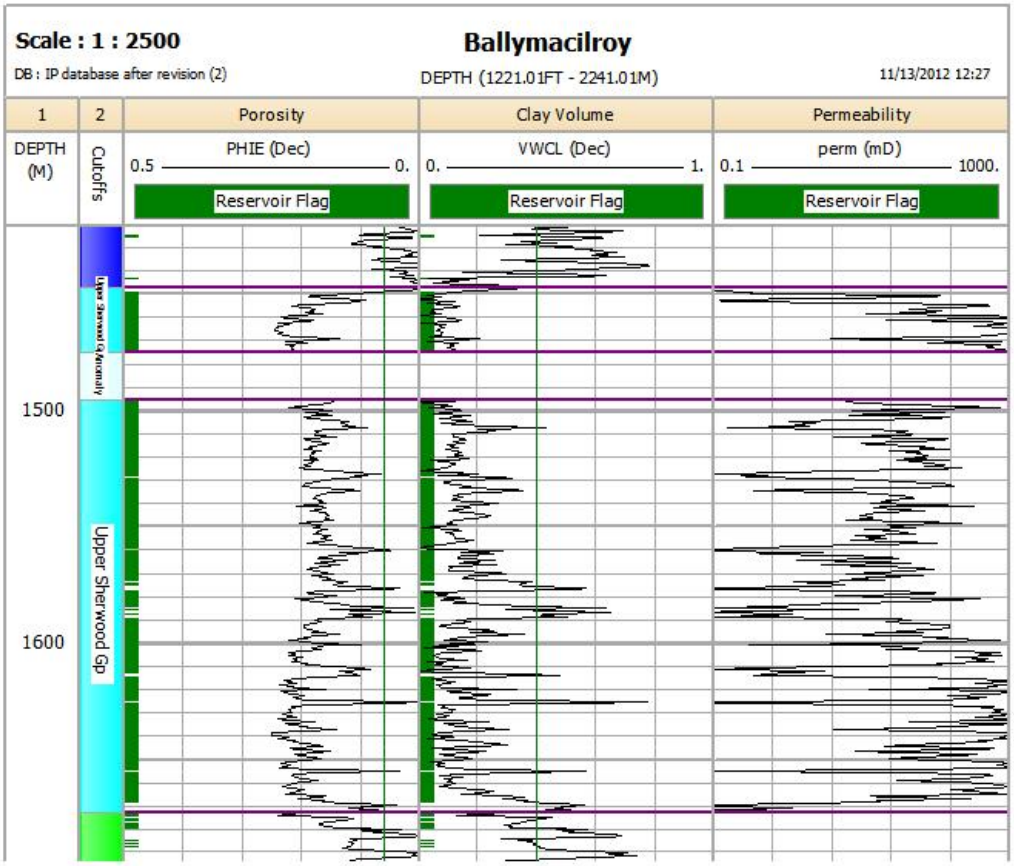

Figure H.1: Plot showing the calculated effective porosity ($PHIE$), wet clay volume ($VWCL$) and permeability curves ($perm$) for each borehole. For each curve the units are specified in the figure.

I Appendix - Monte Carlo simulation results

MONTE CARLO SUMMARY RESULTS

Well : Annaghmore

Zn #	Zone Name	Top	Bottom	Gross	Net	N/G	Av Phi	Av Sw	Av Vcl Ari	Av Perm Ari	Av Perm Geo	Phi*H	PhiSo*H
3	Toomebridge Sandston	497.40	688.80	191.40	187.33	0.979	0.210	0.920	0.135	2274.574	581.729	39.38	3.14
	Mean				187.53	0.980	0.210	0.915	0.134	1795.313	569.139	39.43	3.34
	10				185.62	0.970	0.200	0.947	0.171	148.737	19.792	37.37	2.09
	50				187.63	0.980	0.211	0.922	0.135	1717.027	289.920	39.39	3.09
	90				189.46	0.990	0.219	0.874	0.099	3437.685	1548.926	41.29	4.83

Well : Ballynamullan

3	Toomebridge Sandston	-685.28	-741.38	56.15	55.65	0.991	0.213	0.890	0.133	1491.852	405.868	11.84	1.31
	Mean				55.61	0.990	0.214	0.885	0.125	1567.585	757.205	11.90	1.37
	10				55.11	0.981	0.205	0.946	0.166	151.709	28.152	11.34	0.65
	50				55.65	0.991	0.214	0.889	0.127	1258.198	314.689	11.92	1.31
	90				55.79	0.994	0.222	0.822	0.078	3841.314	2555.567	12.40	2.12
4	Dolerite intrusion	-741.38	-755.68	14.29	0.09	0.006	0.265	0.422	0.013	5000.000	5000.000	0.02	0.01
5	Toomebridge Sandston	-755.68	-885.29	129.61	123.02	0.949	0.188	0.917	0.200	746.437	83.771	23.13	1.92
	Mean				122.02	0.941	0.189	0.909	0.193	915.951	244.882	23.10	2.10
	10				117.17	0.904	0.180	0.975	0.234	59.322	5.824	21.27	0.56
	50				122.95	0.949	0.190	0.915	0.195	610.852	55.406	23.29	1.89
	90				125.71	0.970	0.197	0.838	0.149	2347.724	787.449	24.64	3.63

Well : Ballymacilroy

2	Upper Sherwood Gp	1447.00	1474.90	27.90	25.76	0.923	0.194	0.974	0.085	766.675	377.241	5.00	0.13
	Mean				25.77	0.924	0.194	0.972	0.080	421.007	152.006	5.01	0.14
	10				25.76	0.923	0.187	0.997	0.115	32.027	6.112	4.81	0.02
	50				25.76	0.923	0.195	0.981	0.079	434.137	95.949	5.02	0.09
	90				25.76	0.923	0.201	0.938	0.041	751.414	367.139	5.19	0.31
3	Anomaly	1474.90	1495.40	20.50	0.07	0.003	0.146	0.786	0.253	116.656	116.656	0.01	0.00
4	Upper Sherwood Gp	1495.40	1673.00	177.60	164.96	0.929	0.178	0.951	0.149	626.754	341.187	29.36	1.43
	Mean				164.67	0.927	0.179	0.967	0.140	261.334	105.986	29.43	0.98
	10				160.80	0.905	0.171	0.999	0.175	11.344	2.425	27.65	0.04
	50				164.96	0.929	0.179	0.981	0.141	184.243	39.681	29.49	0.55
	90				168.00	0.946	0.185	0.915	0.101	600.986	294.691	30.96	2.36

Figure I.1: Results of the Monte Carlo uncertainty analysis for the upper part of the Sherwood Sandstone Group/Toomebridge Sandstone Formation. The results show the determined values, the mean values and P90, P50 and P10 averages for, amongst others, the porosity (Av Phi), water saturation (Av Sw), clay volume (Av Vcl) and permeability (Av Perm).

J Appendix - Original MT responses

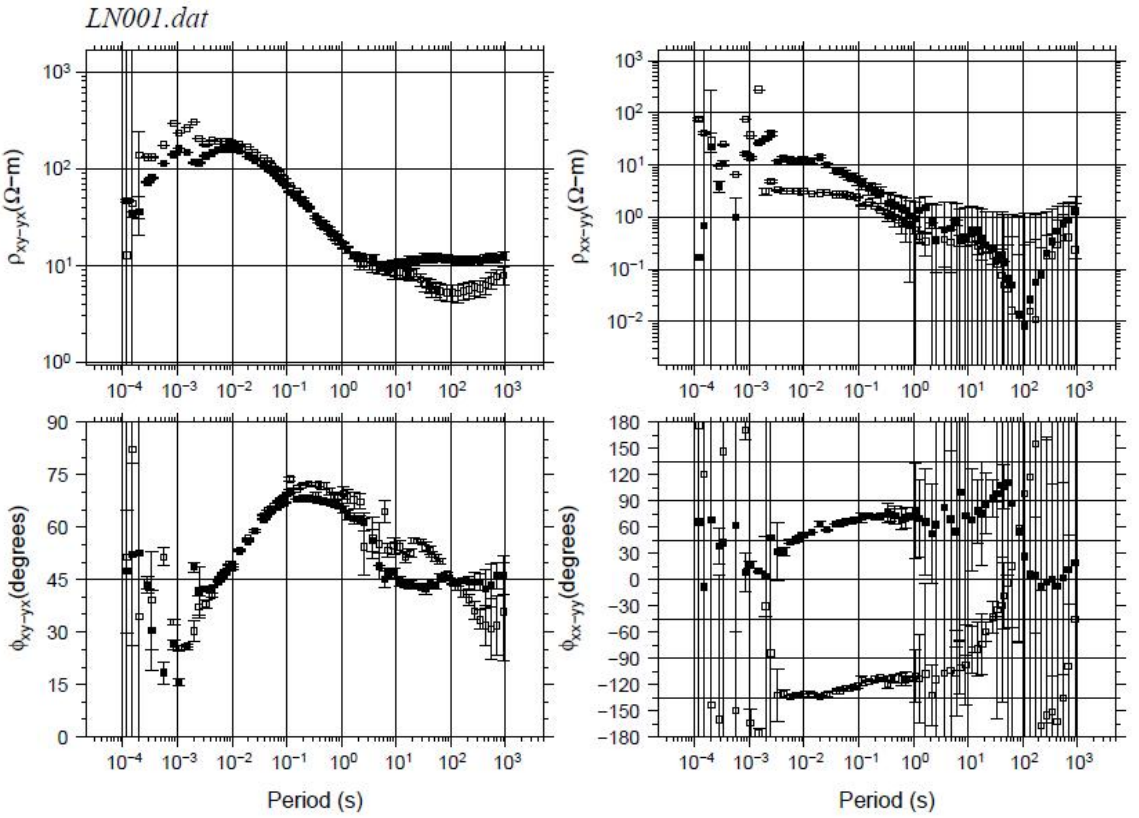

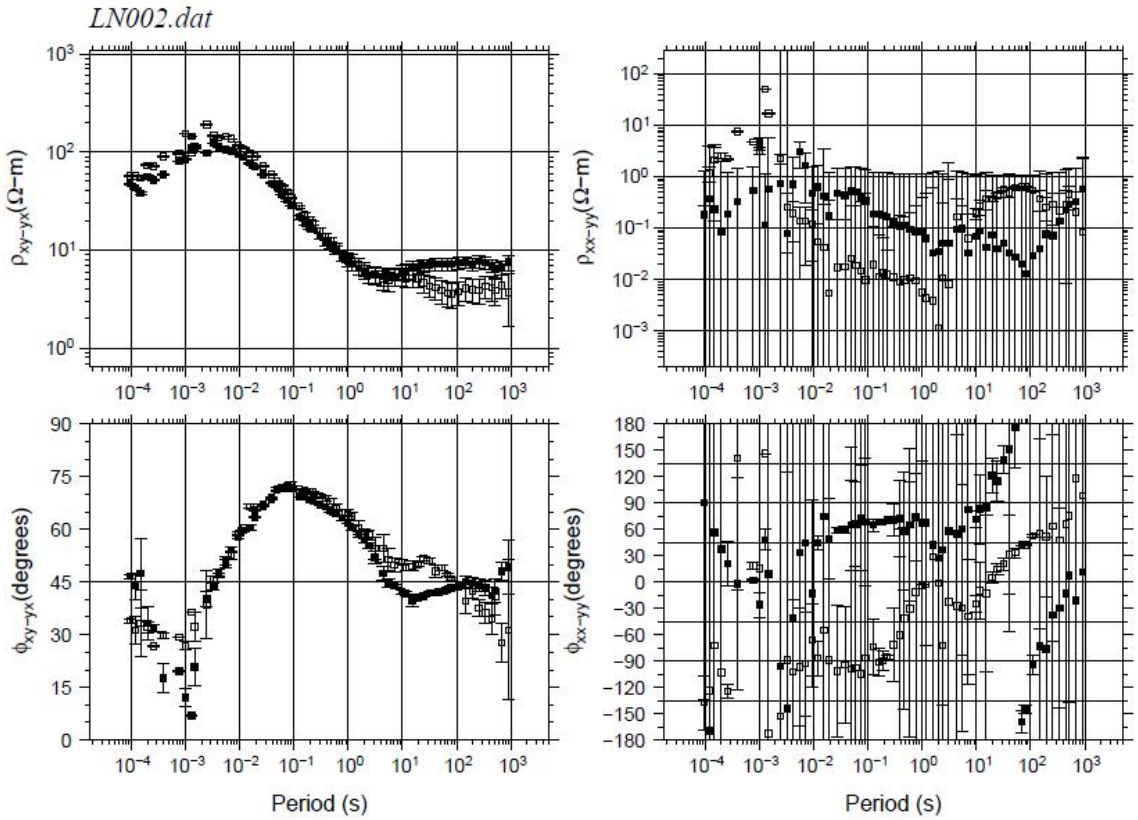

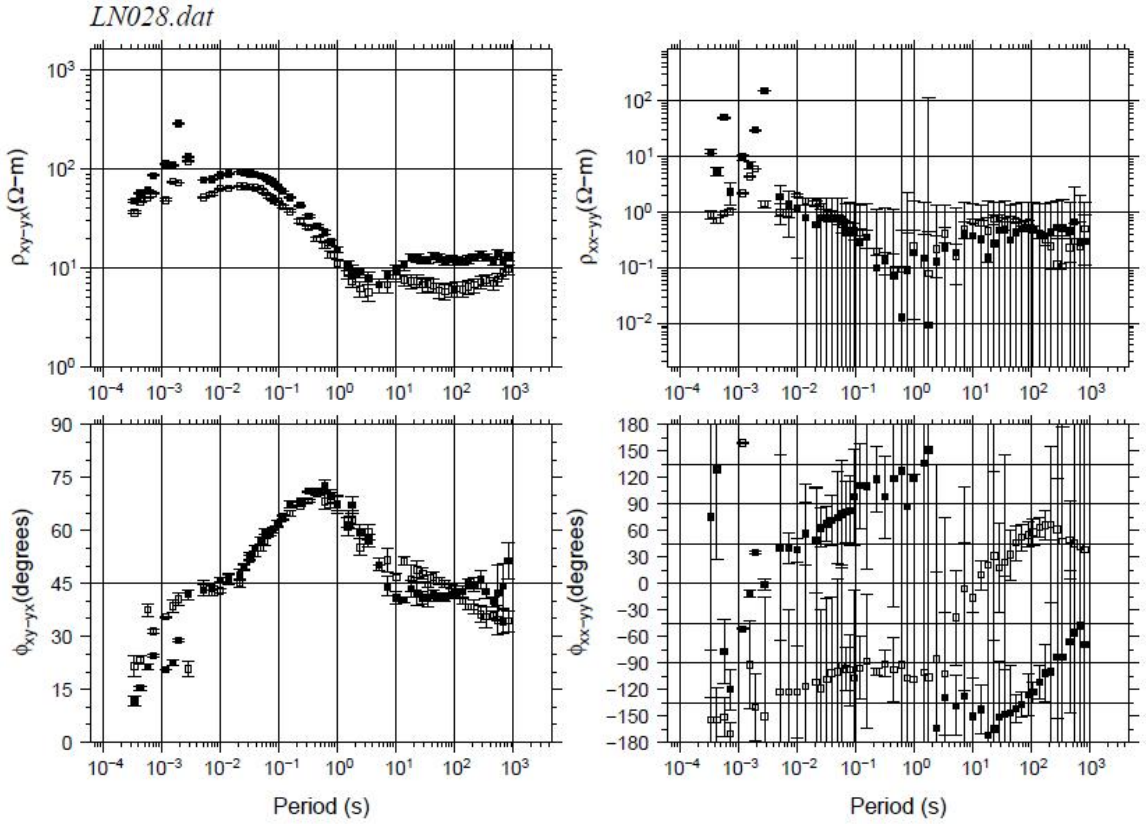
LN028.dat
ρxy-yx(Ω-m)
ρxx-yy(Ω-m)
φxy-yx(degrees)
φxx-yy(degrees)
Period (s)
Period (s)

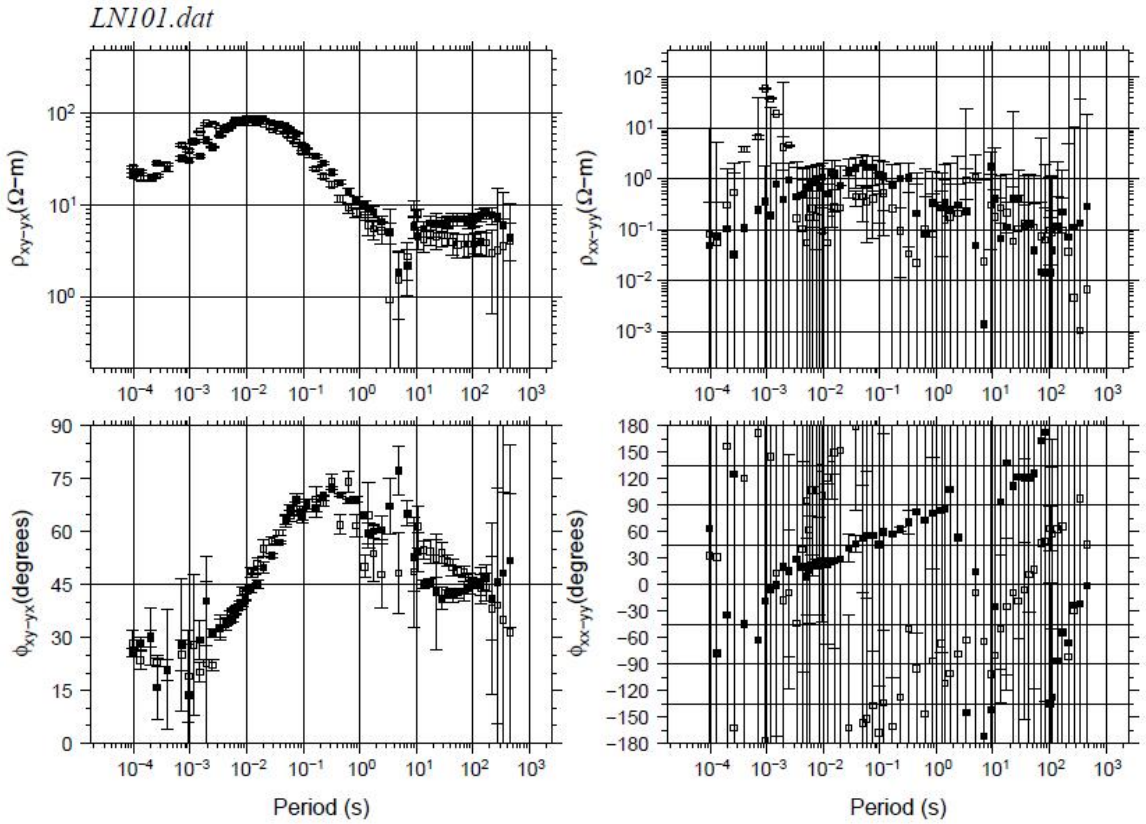
LN101.dat
ρxy-yx(Ω-m)
ρxx-yy(Ω-m)
φxy-yx(degrees)
φxx-yy(degrees)
Period (s)
Period (s)

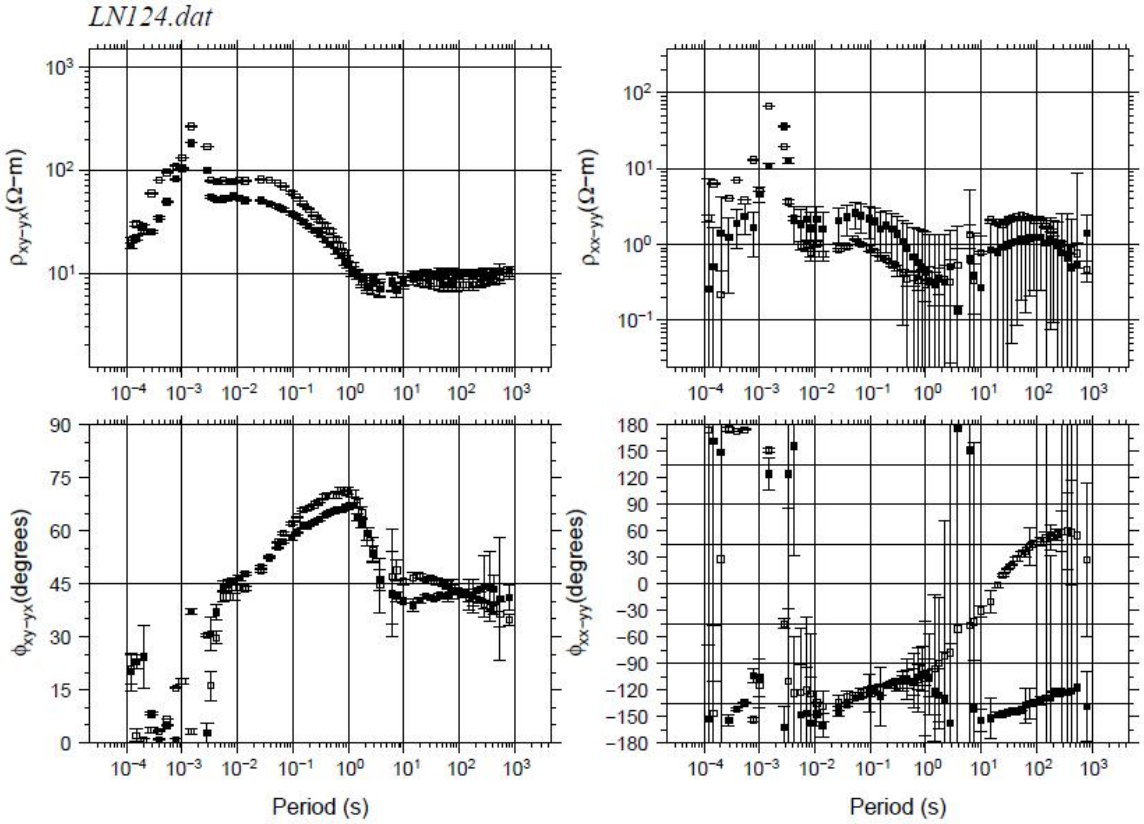

Figure J.1: Original MT responses for each MT site. Plotted are the apparent resistivity (top plots) and the impedance phase (bottom plots) plotted as a function of period. The plots on the left show the response functions for the off-diagonal components of the impedance tensor, while the plots on the right show the response functions for the diagonal components.

K Appendix - Decomposed, smoothed MT responses

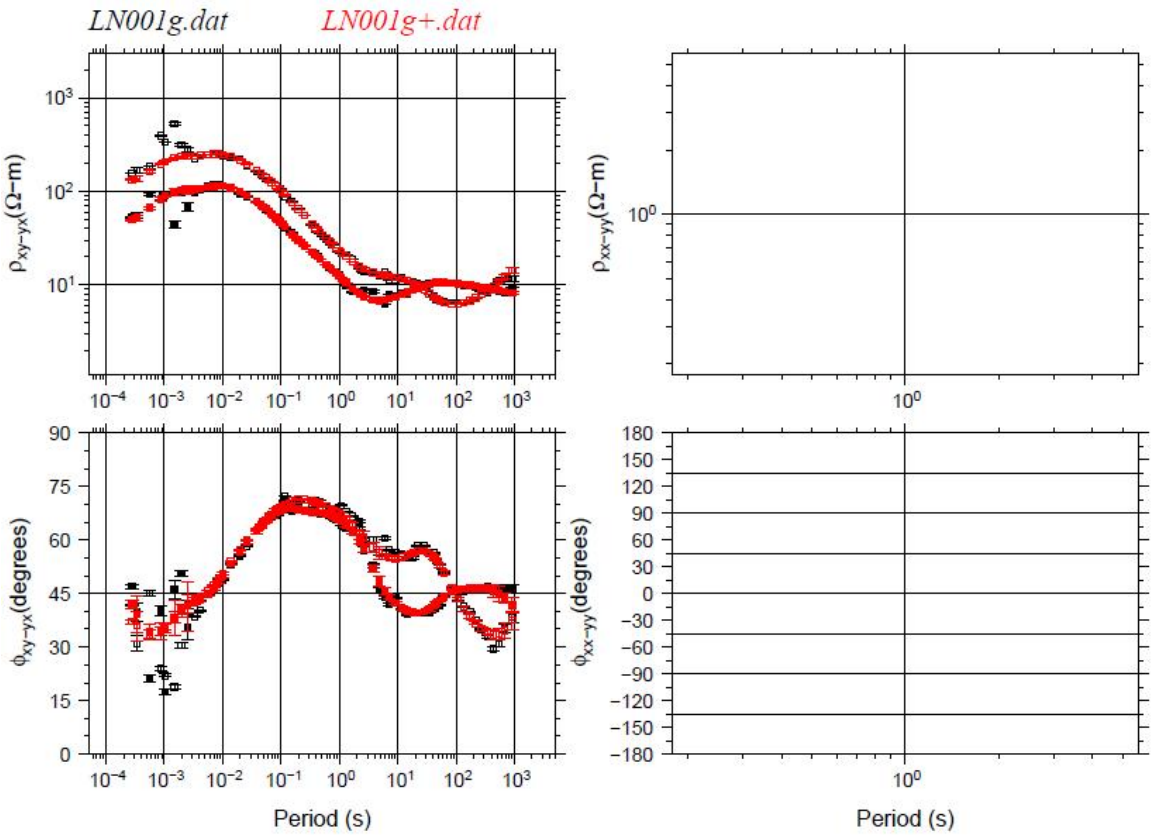

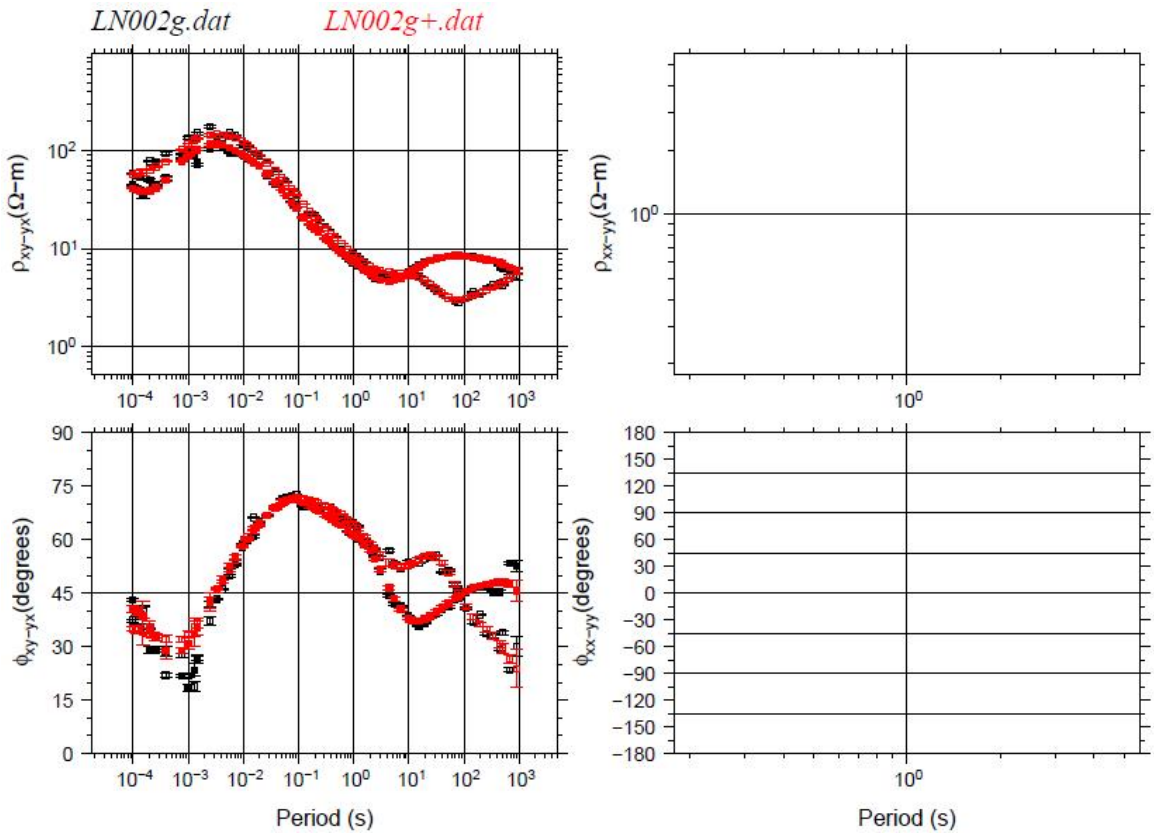

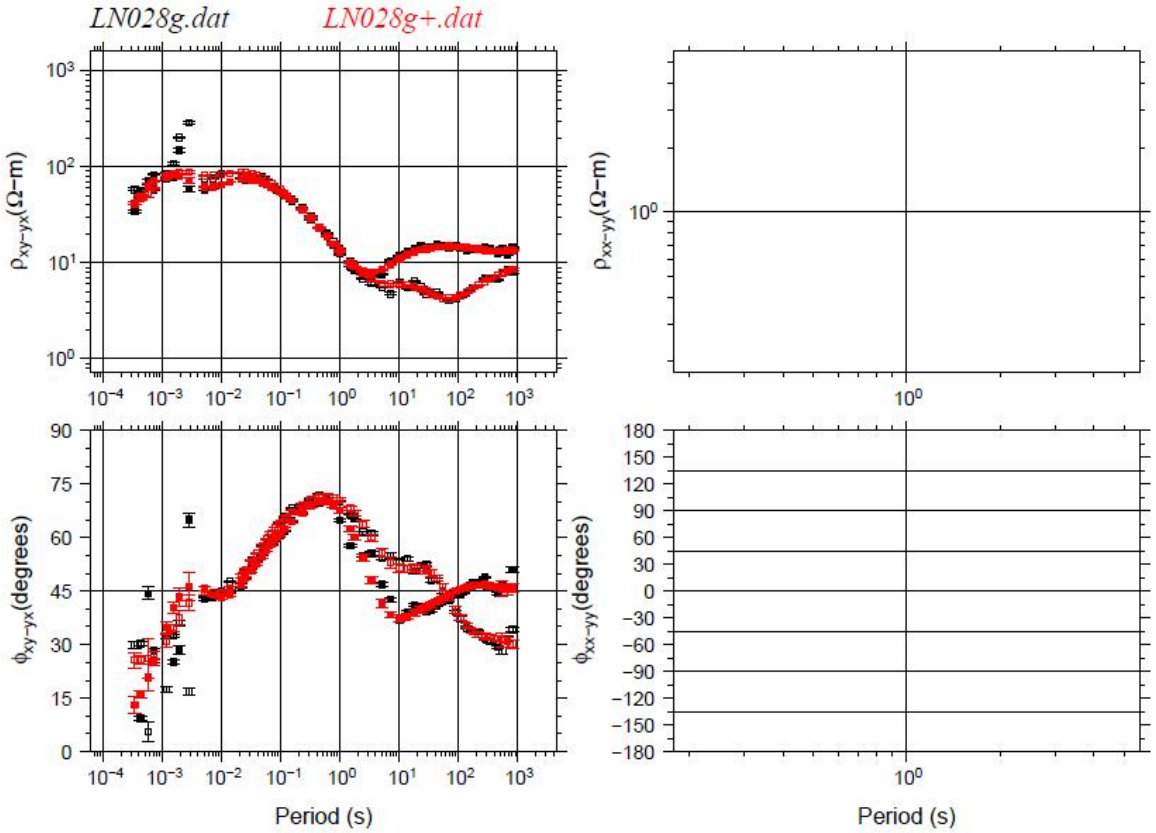
LN028g.dat
LN028g+.dat
ρxy-yx(Ω-m)
ρxx-yy(Ω-m)
ϕxy-yx(degrees)
ϕxx-yy(degrees)
Period (s)
Period (s)

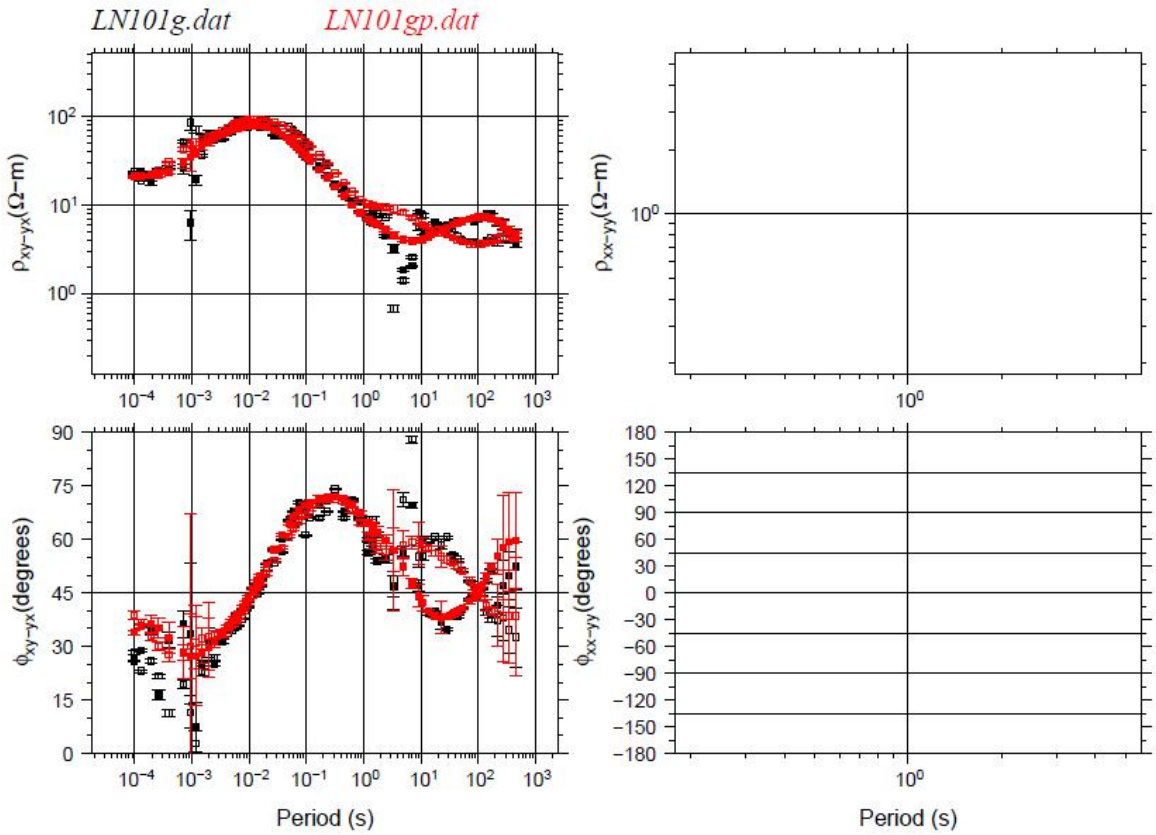
LN101g.dat
LN101gp.dat
ρxy-yx(Ω-m)
ρxx-yy(Ω-m)
ϕxy-yx(degrees)
ϕxx-yy(degrees)
Period (s)
Period (s)

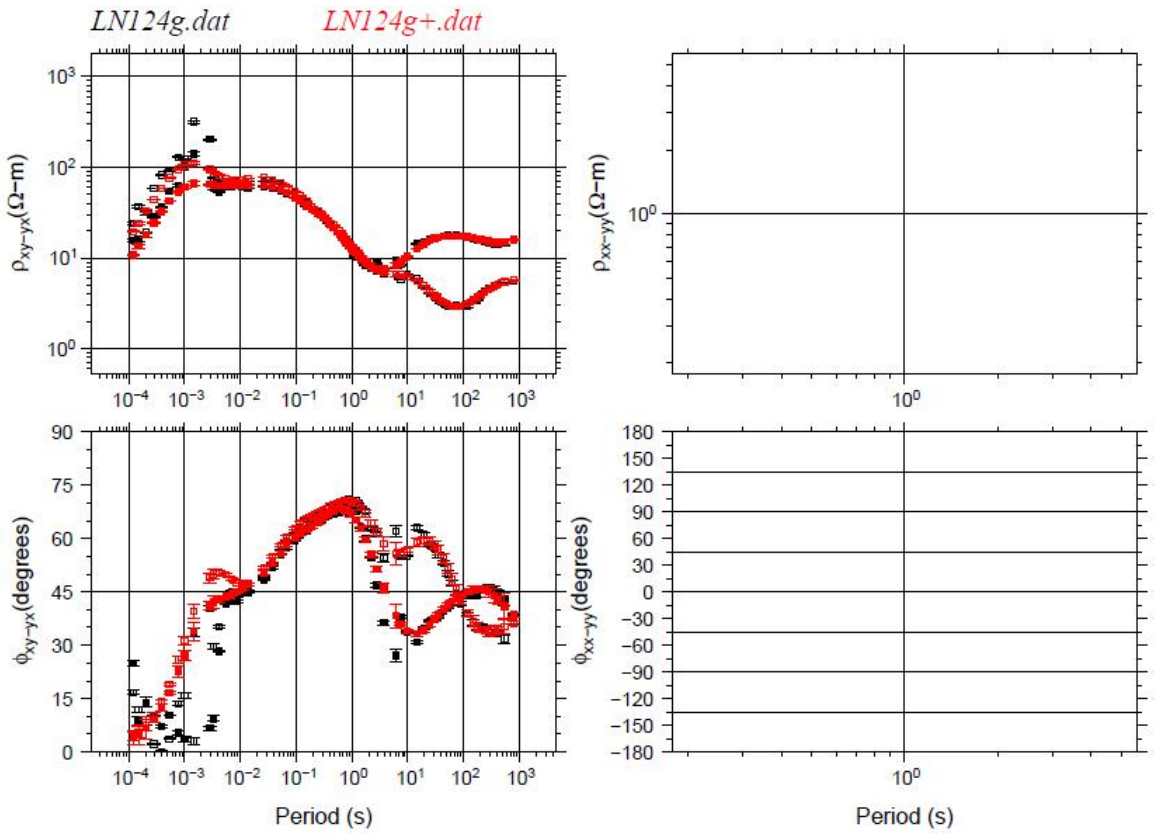

Figure K.1: Decomposed, smoothed MT responses for each MT site. The decomposed data are indicated by the black data points, whereas the red data points indicate the decomposed, smoothed data.

L Appendix - WinGLink sharp boundary models

LN001

Name	Resistivity (Ωm)	Thickness (m)
LN001ge	59.23	66.63
LN001ge	462.30	158.02
LN001ge	36.70	93.39
LN001ge	150.00	239.79
LN001ge	8.50	234.89
LN001ge	3.21	1456.97
LN001ge	20.00	2247.23
LN001ge	3.62	

LN002

Name	Resistivity (Ωm)	Thickness (m)
LN002g+	46.85	34.78
LN002g+	245.00	250.77
LN002g+	22.95	223.62
LN002g+	3.03	431.65
LN002g+	20.00	118.35
LN002g+	2.53	564.92
LN002g+	8.21	4312.29
LN002g+	2.08	

LN028

Name	Resistivity (Ωm)	Thickness (m)
LN028g+	18.85	21.22
LN028g+	3942.17	160.69
LN028g+	19.34	94.28
LN028g+	758.85	407.65
LN028g+	8.32	406.43
LN028g+	2.16	674.53
LN028g+	25.44	4272.11
LN028g+	4.31	

LN101

Name	Resistivity (Ωm)	Thickness (m)
LN101gp	23.79	39.82
LN101gp	1000.00	126.28
LN101gp	48.85	92.08
LN101gp	157.64	223.00
LN101gp	13.80	255.39
LN101gp	2.12	597.40
LN101gp	20.00	833.21
LN101gp	2.31	

LN124

Name	Resistivity (Ωm)	Thickness (m)
LN124g+	37.02	46.29
LN124g+	642.79	131.73
LN124g+	27.28	137.13
LN124g+	133.76	364.22
LN124g+	7.30	496.03
LN124g+	2.08	741.94
LN124g+	250.00	3588.44
LN124g+	2.96	

Table L.1: Text file of the WinGLink sharp boundary model for each Mt site, giving the resistivity and thickness of each layer of the model.

M Appendix - Minim models

LN001

Resistivity (Ωm)	Depth (m)
58.7453308	67.7629318
638.016602	215.597443
40.9723053	332.9198
185.628357	560.939209
7.8272953	868.906982
1.88144147	1038.72815
24.5309162	1216.6438
2.69055295	2137.75415
48.9404755	3833.52734
5.41384697	1.

LN002

Resistivity (Ωm)	Depth (m)
47.4102058	34.8059921
241.649612	285.575989
23.4528694	509.203156
3.04264832	934.730652
14.0219488	1055.3374
2.53301907	1614.54907
8.07295132	6028.67139
2.69455481	1.

LN028

Resistivity (Ωm)	Depth (m)
18.8500004	21.2200012
3855.66162	181.910004
19.4150391	276.427063
792.713989	682.805847
8.32707024	1089.79443
2.16493177	1771.75806
27.655592	6484.34766
4.62936401	1.

LN101

Resistivity (Ωm)	Depth (m)
23.7900028	39.8199959
1011.55804	166.358856
48.8922462	260.001984
162.471619	482.498383
13.7694426	741.221191
2.15313053	1353.16199
25.0692616	2306.38403
1.8986845	1.

LN124

Resistivity (Ωm)	Depth (m)
37.0199966	44.5590515
530.428711	176.289062
27.5302429	314.541138
137.437469	678.761169
7.30282164	1177.15564
2.06442785	1915.16931
589.069336	5372.73828
5.01376534	1.

Table M.1: Text file of the Minim model for each Mt site, giving the resistivity and the depth of each layer of the model.